Part I

LATENT HEAT OF VAPORIZATION OF 1-PENTENE

Part II

THERMAL TRANSFER FROM A SMALL WIRE IN ISOTHERMAL AND NONISOTHERMAL BOUNDARY FLOWS ABOUT A CYLINDER

Thesis by

Robert Fredrick Cuffel

In Partial Fulfillment of the Requirements

For the Degree of

Doctor of Philosophy

California Institute of Technology

Pasadena, California

1964

(Submitted May 15, 1964)

ACKNOWLEDGMENTS

The author wishes to express his gratitude to Professor B. H. Sage, under whose direction this research was conducted, for his most helpful advice and guidance.

At this time, the author also wishes to express his appreciation for the encouragement and assistance given him by others in his research. Dr. William Kozicki assisted with the latent heat of vaporization measurements, and Henry E. Smith assisted with the boundary flow heat transfer measurements. H. Hollis Reamer was most generous with his cooperation and Dr. Emilio Venezian maintained an active interest in the project. Richard C. Seagrave and Elston C. Palmer took the time to review the thesis, Alrae Tingley typed it, June Gray traced the illustrations, and Virginia Moore reviewed the smoothed data. The faculty, staff, and fellow graduate students of the Chemical Engineering Department gave encouragement and helpful criticism throughout this research project.

The author wishes to thank the Standard Oil Company of California and the Union Carbide Corporation for the receipt of their fellowships. The financial support for the research projects and the apparatus made available by the Standard Oil Company of California, The Jet Propulsion Laboratory of the California Institute of Technology, and the Peter E. Fluor Foundation are gratefully acknowleged.

ABSTRACT

Part I

The enthalpy change upon vaporization of 1-pentene was experimentally determined by calorimetric measurements at temperatures between 100° and 280° F. The results are in good agreement with available data at the lower temperatures and are presented in graphical and tabular form.

Part II.

The heat transfer from a one-mil platinum wire was measured in isothermal and nonisothermal boundary flows about a one-inch copper cylinder. The flow of the 100° F air stream was normal to the 100° and 160° F cylinder at a Reynolds number of 3500. The measured wire Nusselt numbers and smoothed values at a wire temperature loading of 50° F are presented as a function of the position within the forward half of the flow about the cylinder for these two cases. For both cases, Nusselt numbers predicted from calculated velocity distributions gave reasonable agreement with the measured values at distances greater than ten wire-diameters from the surface of the cylinder.

Xerox copies of the photographic material on page 36 are adequate for reproduction.

TABLE OF CONTENTS

LIST OF FIGURES

LIST OF TABLES

Part I

LATENT HEAT OF VAPORIZATION OF 1-PENTENE[1]

---

[1] Cuffel, R. F., William Kozicki, and B. H. Sage, "Latent Heat of Vaporization of 1-Pentene," The Canadian Journal of Chemical Engineering, Vol. 41, pp. 19-21. (1963).

Permission has been granted by The Chemical Institute of Canada to present this published article as Part I of the author's Ph. D. thesis.

I. INTRODUCTION

The thermodynamic properties of 1-pentene have been the subject of limited experimental investigation. Scott and co-workers (1) measured the vapor pressure at temperatures between 32° and 143° F. Calorimetric measurements of the enthalpy change upon vaporization also were made (1) at 51.44°, 77° and 85.95° F with a reported accuracy of 0.1 per cent. In addition, the isobaric heat capacity of the ideal gas was established (1) between 100° and 288° F with an accuracy of approximately 0.3 per cent. Day (2) developed analytical expressions describing the effect of temperature upon vapor pressure between 32° and 392° F. Day (3) measured the volumetric behavior of the liquid phase at temperatures between 176° and 482° F with an accuracy of about 0.2 per cent except at temperatures above 350° F where the uncertainty is larger. Rossini (4) reported critically chosen values of the specific weight of the bubble-point liquid at 60°, 68° and 77° F, the isobaric heat capacity in the ideal gas state, and values of the latent heat of vaporization (1) at 77° and 85.94° F. It should be recognized that near the critical temperature of 1-pentene, rather rapid thermal rearrangement takes place which has made it difficult to carry out accurate measurements in this region.

Since the measurements of Scott (1), which were reported in part by Rossini (4), constitute the only directly measured values of latent heat of vaporization of 1-pentene, a series of such measurements were carried out at temperatures between 100° and 280° F.

The calorimetric measurements of the latent heat of vaporization were employed together with the vapor pressure and the specific volume of bubble-point liquid to establish the specific volume of the dew-point gas. Measurements were not obtained at temperatures higher than 280° F because of the thermal rearrangement of 1-pentane encountered at the higher temperatures.

II. EXPERIMENTAL METHODS

The experimental equipment used in this investigation was similar to that developed by Osborne and co-workers (5, 6) and has been described in detail (7, 8). In principle, the apparatus involved an isochoric vessel in which a heterogeneous mixture of 1-pentene was confined. The vessel was located in an adiabatic vacuum jacket and was provided with an agitator and an internal electric heater. The 1-pentene was withdrawn as a gas, and the quantity thus withdrawn was determined by gravimetric methods. Electrical energy was added at a rate to maintain the system under nearly isobaric, isothermal conditions. A detailed thermodynamic analysis of the actual process is available (9).

It does not seem necessary to consider in detail the applications of the numerous small corrections (9) associated with the evaluation of the latent heat of vaporization from the actual experimental measurements. These corrections are associated with the minor perturbations of pressure and temperature experienced during the withdrawal process. Under conditions of isobaric, isothermal evaporation and uniform temperature throughout both the liquid and gas phases, the enthalpy change upon vaporization is related to the measured thermal and certain other quantities by the following simple expression:

$$\ell = (H_g - H_\ell)_T = [Q]_{T,P}\left(\frac{V_g - V_\ell}{V_g}\right) \qquad (1)$$

The meaning of the symbols used is set forth in the nomenclature.

From the Clapeyron equation and the heat associated with an isobaric, isothermal evaporation process the specific volume of the dew-point gas may be determined from

$$V_g = \frac{[Q]_{T,P}}{T(dP''/dT)} \tag{2}$$

The residual specific volume of dew-point gas was established from the following equation:

$$V_g = \frac{bT}{P''} - V_g = \frac{bT}{P''} - \frac{[Q]_{T,P}}{T(dP''/dT)} \tag{3}$$

The latent heat of vaporization was calculated directly from the measured heat associated with the withdrawal process and other known properties (1, 2, 3) by application of the equation

$$\ell = (H_g - H_\ell)_T = [Q]_{T,P} - V_\ell T\left(\frac{dP''}{dT}\right) \tag{4}$$

Equation 4 was obtained by a combination of Equations 1 and 2 and was chosen for the evaluation of the latent heat of vaporization to avoid a need for knowledge of the specific volume of the dew-point gas. Extended forms of Equations 2 and 4 were actually employed in the evaluation of the experimental data since small deviations from isobaric, isothermal conditions were involved in the withdrawal.

Residual techniques were employed to establish the first derivatives of the relation of vapor pressure to temperature from the

data obtained by Scott (1) and Day (2) which were required for the solution of Equations 2 and 4. Directly measured values (3) of the specific volume of the liquid were extrapolated to the bubble-point pressure. Throughout all of the calculations the appropriate corrections for the mechanical energy added by the agitator located in the liquid phase of the 1-pentene, the superheat of the liquid evaporated, and the thermal transfers to or from the calorimeter were taken into account. The details of carrying out such corrections have been described (7). The values of $[Q]_{T,P}$ indicated in Equations 1, 2, 3, and 4 represent the thermal transfer per unit weight of material withdrawn from the calorimeter under isobaric, isothermal conditions after appropriate corrections for the mechanical agitator, superheat of the liquid and gas phases, and thermal transfer between the calorimeter and the jacket have been applied.

During the measurements upon 1-pentene, the total corrections for mechanical agitation, superheat, and thermal transfer between the calorimeter and the jacket were not more than 0.03 fraction of the total electrical energy added. The uncertainty of measurement estimated for each of the quantities involved in this investigation is set forth in Table I.

The internal energy change upon vaporization was evaluated from the latent heat of vaporization by application of the following:

$$(E_g - E_\ell)_T = \ell - P''(V_g - V_\ell) \qquad (5)$$

The change in internal energy was not affected by additional uncertainties of more than 0.06 per cent beyond those noted in Table I.

III. MATERIALS

The 1-pentene employed was obtained as research grade from the Phillips Petroleum Company and was reported to contain less than 0.00005 mole fraction of impurities. As a check on the reported purity, the index of refraction relative to the D-lines of sodium was measured and found to be 1.37145 at 68° F as compared to 1.37148 for air-saturated 1-pentene at the same temperature reported by Rossini (4). The specific weight of the sample at 68°F was 39.977 pounds per cubic foot as compared to 39.984 pounds per cubic foot reported for the same conditions for air-saturated material (4). The agreement is sufficiently good to lend credence to the vendor's reported purity. It should be recognized that small quantities of impurities do not influence the values determined for the enthalpy change upon vaporization as greatly as such impurities would affect measurements such as vapor pressure.

IV. EXPERIMENTAL RESULTS

Experimental data obtained for 1-pentene are recorded in Table II. The volumetric correction factors included are based upon the values calculated from the latent heat of vaporization with Equation 1. The data recorded in this tabulation take into account the perturbations from isobaric, isothermal conditions (7, 8) and were established from Equations 1 and 2. In order to permit a more accurate smoothing of the values of the latent heat of vaporization as a function of temperature, residual methods were employed. The residual latent heat of vaporization has been related to the temperature and the actual latent heat of vaporization by the following empirical expression:

$$\underset{\sim}{\ell} = \ell - 170.000\left(1 - \frac{t}{394.000}\right)^{1/2} \qquad (6)$$

which was chosen as a simple analytical equation approximating the experimental data. The experimental data expressed in terms of the residual latent heat of vaporization are shown in Figure 1. As a matter of interest the actual latent heat of vaporization of 1-pentene as measured in this investigation is presented in Figure 2. The latter figure was included in order that the reader may obtain a more realistic appraisal than is apparent from Figure 1 of the rate of change of the latent heat of vaporization with temperature and of the degree of agreement of the experimental data with a smooth curve. The standard error of estimate of the author's data shown in Figures 1 and 2, assuming all the uncertainty lies in the measured value of

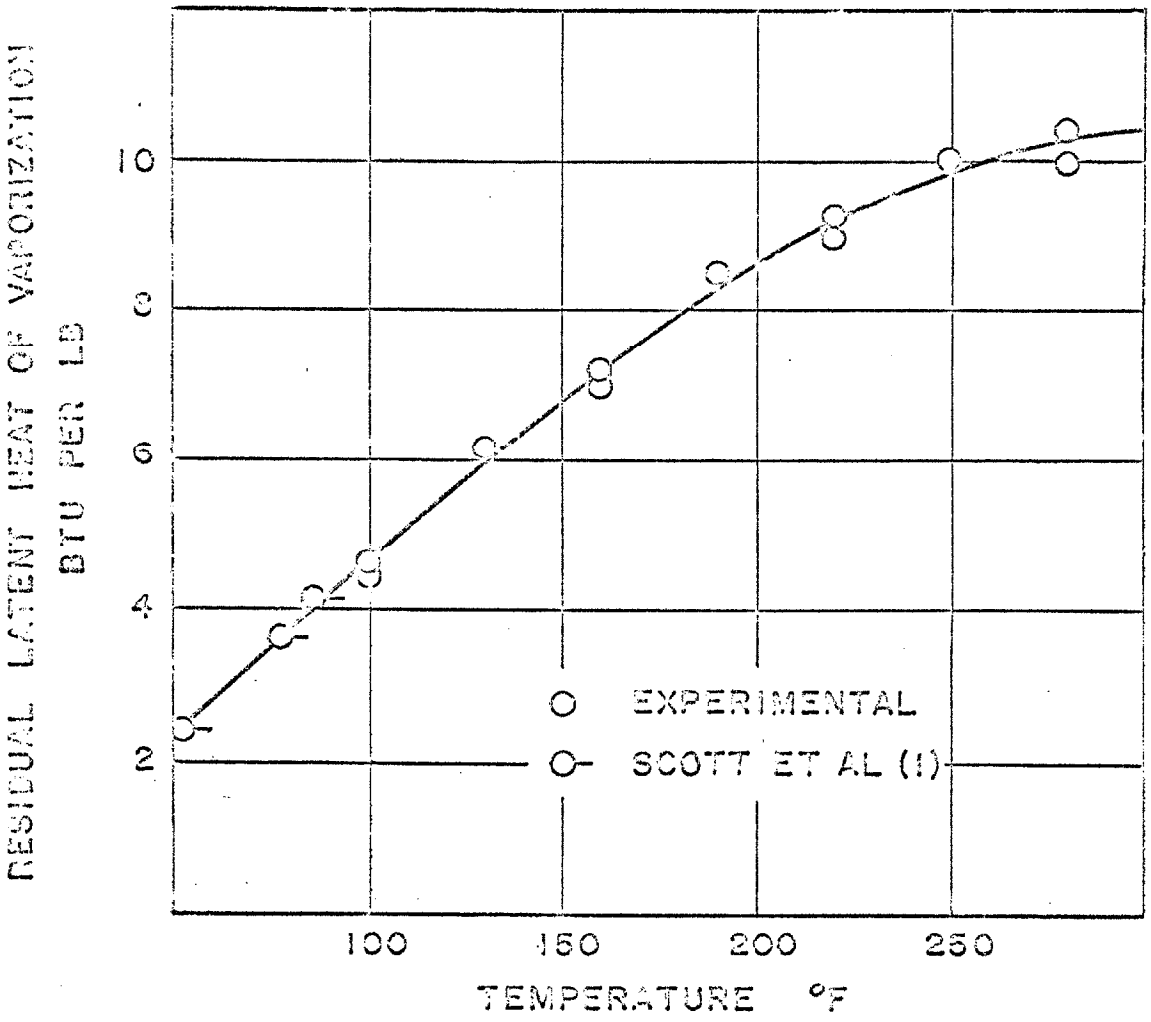

FIGURE 1. Experimental Values of Residual Latent Heat of Vaporization for 1-Pentene

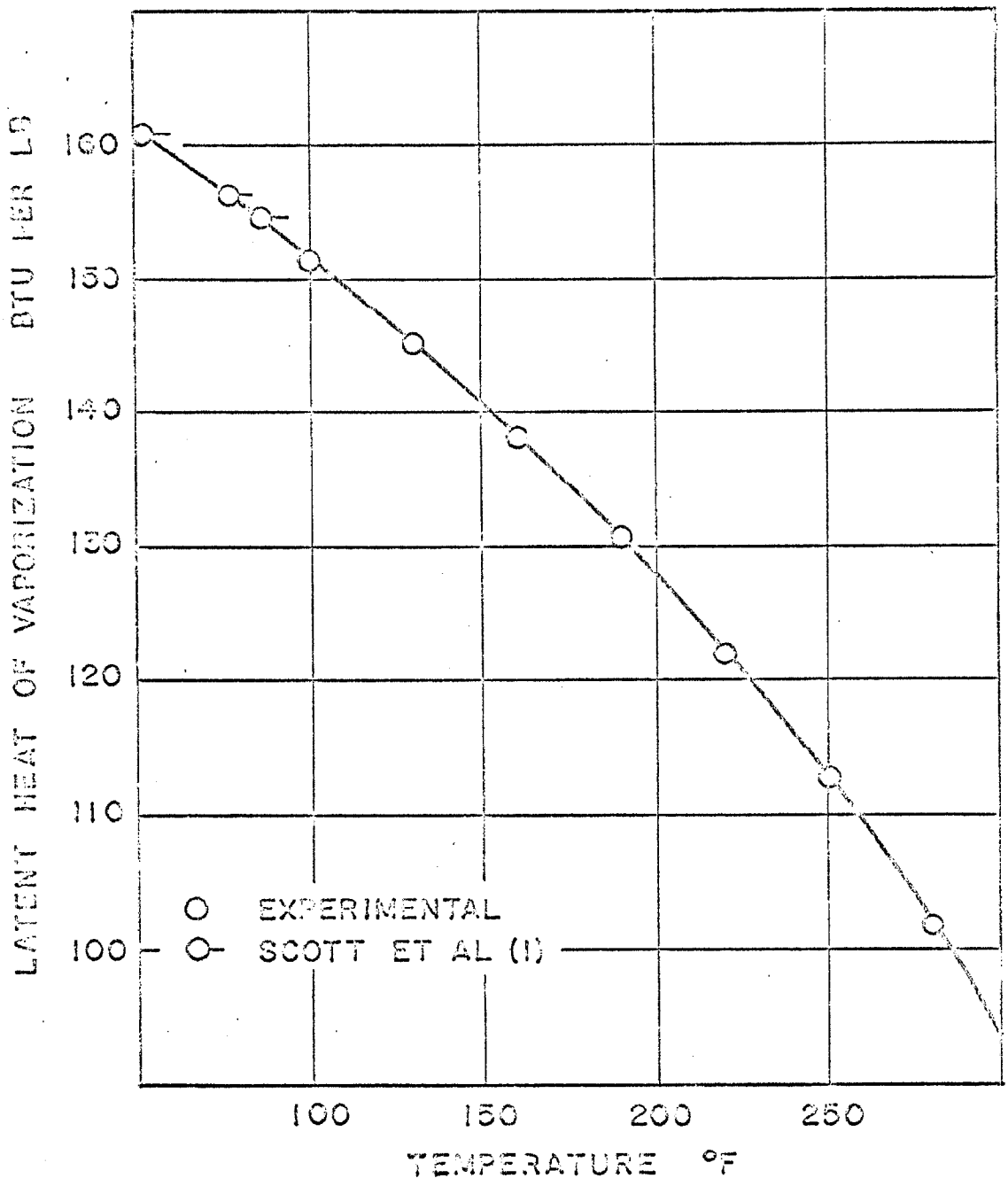

FIGURE 2. Latent Heat of Vaporization for 1-Pentene

the latent heat of vaporization and none in the temperature, was 0.18 Btu per pound. Values of the latent heat of vaporization calculated from the residual latent heat of vaporization portrayed by the smooth curve of Figure 1 are recorded in Table III.

The values reported by Scott (1) have been included in Figures 1 and 2. Good agreement was obtained between these values and the current experimental data. The standard error of estimate of the values of Scott (1) from the information submitted in Table III was 0.09 Btu per pound.

Table III records smooth values of the specific volume at dew point calculated by application of Equation 2 and appropriate graphical operations. The internal energy change upon vaporization has been included, along with the specific volume at bubble point (3) and the vapor pressure (1, 2).

V. REFERENCES

1. Scott, D. W., Guy Waddington, J. C. Smith, and H. M. Huffman, "Thermodynamic Properties of Three Isomeric Pentenes," The Journal of the Americal Chemical Society, Vol. LXXI, pp. 2767-2773. (1949).

2. Day, H. O. and D. E. Nicholson, with W. A. Felsing, "The Vapor Pressures and Some Related Quantities of Pentene-1 from 0 to 200°," The Journal of the American Chemical Society, Vol. LXX, pp. 1784-1785. (1948).

3. Day, H. O. with W. A. Felsing, "The Compressibility of Pentene-1," The Journal of the American Chemical Society, Vol. LXXIII, pp. 4839-4840. (1951).

4. Rossini, Frederick D., et. al., editors, Selected Values of Physical and Thermodynamic Properties of Hydrocarbons and Related Compounds. (American Petroleum Institute Research Project 44). Pittsburgh: Carnegie Press. (1953).

5. Osborne, N. S., H. F. Stimson, and E. F. Fiock, "A Calorimetric Determination of Thermal Properties of Saturated Water and Steam from 0° to 270° C," Bureau of Standards Journal of Research, Vol. 5, pp. 411-480. (1930).

6. Osborne, Nathan S., Harold F. Stimson, and Defoe C. Ginnings, "Measurements of Heat Capacities and Heat of Vaporization of Water in the Range 0° to 100° C," Journal of Research of the National Bureau of Standards, Vol. 23, pp. 197-260. (1939).

7. McKay, R. A. and B. H. Sage, "Latent Heat of Vaporization for n-Octane," Journal of Chemical and Engineering Data, Vol. 5, pp. 21-24. (1960).

8. Sage, B. H. and E. W. Hough, "Calorimeter for Some Corrosive Liquids," Analytical Chemistry, Vol. 22, pp. 1304-1309. (1950).

9. McKay, R. A. and B. H. Sage, Latent Heat of Vaporization for n-Octane, Document No. 6072. (American Documentation Institute). Washington D. C.: Library of Congress. (1959).

IV. NOMENCLATURE

A. Symbols

b	specific gas constant, (psi)(cu. ft. /lb. ^{o}R.).
d	differential operator.
E	internal energy, Btu/lb.
H	enthalpy, Btu/lb.
ℓ	latent heat of vaporization, Btu/lb.
$\mathfrak{l}$	residual latent heat of vaporization, Btu/lb.
P"	vapor pressure, psia.
[Q]	heat added per unit weight of material withdrawn under idealized conditions, Btu/lb.
T	thermodynamic temperature, ^{o}R.
t	temperature, ^{o}F.
V	specific volume, cu. ft. /lb.
$\mathcal{V}$	residual specific volume, cu. ft. /lb.

B. Subscripts

g	gas phase.
ℓ	liquid phase.
P	pressure.
T	temperature.

V. TABLES

TABLE I

ESTIMATED UNCERTAINTIES OF MEASUREMENT

Quantity	Probable Uncertainty per cent
Energy added electrically	0.03
Energy added by agitation	0.15
Energy exchange between calorimeter and jacket	0.008
Change in temperature of liquid and vapor	0.03
Weight of material withdrawn	0.02
Volumetric correction factor	0.06
Superheat of liquid	0.06

TABLE II

EXPERIMENTAL RESULTS FOR 1-PENTENE

Identification	Temperature °F.	Pressure[a] psia	Energy Added Electrically Btu	Energy Added by Agitation Btu	Energy Added by Conduction and Radiation Btu	Weight of Material Withdrawn lb.	Superheat of Liquid °F.	dP"/dT psi/°R.	Specific Volume Dew Point cu.ft./lb.	Specific Volume Bubble Point[b] cu.ft./lb.	Residual Specific Volume cu.ft./lb.	Volumetric Correction Factor[c]	Latent Heat of Vaporization Btu/lb.
322	100.012	19.11	4.4842	0.1115	-0.0032	0.030184	0.09	0.3472	4.2327	0.02577	0.2481	0.99391	151.26
324	100.009	19.11	3.6725	0.0915	-0.0003	0.024703	0.09	0.3472	4.2384	0.02577	0.2424	0.99392	151.47
326	129.990	31.95	3.4718	0.0822	0.0022	0.024135	0.10	0.5156	2.6092	0.02658	0.2147	0.98981	145.32
318	160.012	50.52	2.7670	0.0403	-0.0015	0.020007	0.13	0.7308	1.6742	0.02747	0.2029	0.98359	138.00
319	160.001	50.52	5.6248	0.0531	-0.0017	0.040423	0.15	0.7308	1.6764	0.02747	0.2007	0.98361	138.18
328	159.999	50.52	8.5408	0.0736	0.0006	0.061371	0.17	0.7308	1.6760	0.02747	0.2011	0.98361	138.15
330	190.000	76.34	5.0944	0.0498	-0.0012	0.038332	0.13	1.0001	1.1163	0.02847	0.1860	0.97449	130.81
331	220.013	111.07	8.9338	0.0655	-0.0017	0.070589	0.15	1.3245	0.7613	0.02961	0.17510	0.96110	121.89
332	219.994	111.07	4.4836	0.0851	0.0032	0.035978	0.08	1.3245	0.7631	0.02961	0.17332	0.96120	122.19
333	250.015	156.36	4.9248	0.0659	-0.0040	0.041675	0.08	1.7039	0.5349	0.03094	0.15961	0.94216	112.78
335	280.019	213.93	5.4226	0.0394	-0.0003	0.049038	0.10	2.1468	0.3792	0.03276	0.14996	0.91362	101.81
337	280.014	213.93	4.2504	0.0314	-0.0007	0.038539	0.08	2.1468	0.3778	0.03276	0.15134	0.91330	101.40

[a] Measurements of Scott (1) and Day (2).

[b] Measurements of Day (3).

[c] Not used in evaluation of latent heat of vaporization.

Table III

CRITICALLY CHOSEN VALUES OF SOME PROPERTIES OF 1-PENTENE

Temperature °F	Vapor Pressure P. S. I. A.	Specific Volume Dew Point cu. ft. /lb.	Specific Volume Bubble Point cu. ft. /lb.	Internal Energy Change upon Vaporization Btu/lb.	Latent Heat of Vaporization Btu/lb.
50	6.96	10.93	0.02460	147.12	161.16
60	8.67	8.899	0.02482	145.08	159.33
70	10.70	7.310	0.02505	143.01	157.44
80	13.09	6.053	0.02530	140.90	155.50
90	15.88	5.049	0.02553	138.76	153.52[a]
100	19.11	4.233	0.02577	136.60	151.48
110	22.84	3.583	0.02603	134.38	149.41
120	27.10	3.045	0.02630	132.14	147.28
130	31.95	2.6033	0.02658	129.86	145.10
140	37.44	2.2374	0.02686	127.54	142.86
150	43.60	1.9316	0.02716	125.18	140.55
160	50.52	1.6751	0.02747	122.76	138.17
170	58.24	1.4576	0.02779	120.30	135.71
180	66.83	1.2733	0.02812	117.76	133.16
190	76.34	1.1156	0.02847	115.18	130.54
200	86.85	0.9803	0.02884	112.52	127.81
210	98.40	0.8639	0.02922	109.29	124.99
220	111.07	0.7629	0.02961	107.01	122.08
230	124.91	0.6761	0.03003	104.11	119.04
240	139.99	0.6000	0.03046	101.13	115.88
250	156.36	0.5335	0.03094	98.04	112.58
260	174.09	0.4752	0.03148	94.83	109.13
270	193.25	0.4238	0.03209	91.49	105.50
280	213.93	0.3782	0.03276	88.02	101.69
290	236.22	0.3379	0.03355	84.37	97.67[b]
300	260.20	0.3021	0.03442	80.53	93.42[b]

[a]Values at 90° and lower temperatures based upon data of Scott (1).

[b]Extrapolated beyond range of current measurements.

Part II

THERMAL TRANSFER FROM A SMALL WIRE IN ISOTHERMAL AND NONISOTHERMAL BOUNDARY FLOWS ABOUT A CYLINDER

I. INTRODUCTION

The purpose of this work is to examine the effect of combined normal velocity and temperature gradients upon the heat transfer from a small wire. For these studies the two-dimensional flow about a heated cylinder in an air stream was selected. The heat transfer from a wire parallel to the axis of the cylinder in only the velocity gradient and then in the combined velocity and temperature gradients within the boundary layer was experimentally observed. This investigation was part of a research program being conducted into the effects on the heat transfer from small wires of the various phenomena encountered in boundary flows.

In hot-wire anemometry, it is frequently assumed that the heat transfer from small wires is dependent only upon the local stream velocity (1, 2). Previous experimental work by Short and Sage (3) has shown that this assumption is not valid in the three-dimensional boundary flow around spheres. This is probably due to the flow along the wire. A mathematical model (4) for two-dimensional flow indicates that the heat transfer from the wire will depend upon the relative distance from the surface as well as the velocity. Therefore, to investigate the effects of these and other phenomena upon the heat transfer from small wires, an experimental research program was commenced. Venezian (5, 6) started this program by measuring the heat transfer from a one-mil-diameter platinum wire in the forward half of the boundary flow about a one-inch-diameter

copper cylinder in 4-, 8-, and 16-foot-per-second air streams. Throughout his work the wire was aligned parallel to the cylinder and the cylinder was heated to the air stream temperature of 100^{o} F to maintain an isothermal boundary layer.

During the author's phase of the program, the same equipment was used to measure the heat transfer from the wire in the forward half of the boundary flow about the cylinder. The cylinder temperature was maintained at the air stream temperature of 100^{o} F and also at 60^{o} F above the stream temperature, for an air stream velocity of 7.81 feet-per-second. These two sets of measurements are compared with each other and with calculated values from an approximate solution of the boundary layer equations for compressible flow with heat transfer developed by Itō (7).

Future phases of this program will include studying the effects of mass transfer and non-parallel alignment of the cylinder and wire. From the knowledge obtained from these investigations it is hoped that a better analysis of the complicated three-dimensional case may be obtained.

II. THEORY

The theoretical considerations for the heat transfer from a wire in the boundary flow about a cylinder will be separated into three phases: 1) The material and energy transport in the air stream about the one-inch diameter cylinder, 2) The energy transport from the one-mil diameter wire, and 3) The combined effects of the energy transport from the wire in the presence of the boundary layer gradients introduced by the cylinder.

A. Flow About the Cylinder

The material and energy transport about the forward portion of the cylinder may be described by the following well-known continuity, energy, and momentum equations (8).

$$\frac{D\sigma}{D\theta} + \sigma \nabla \cdot \bar{u} = 0 \tag{1}$$

$$\sigma c_v \frac{DT}{D\theta} = \nabla \cdot (k \nabla T) - T \left(\frac{\partial p}{\partial T} \right)_v (\nabla \cdot \bar{u}) - g_c \bar{\bar{\tau}} \cdot \overline{\overline{\nabla u}} \tag{2}$$

$$\rho \frac{D\bar{u}}{D\theta} = \rho \bar{g} - \nabla p - [\nabla \cdot \bar{\bar{\tau}}] \tag{3}$$

For a Newtonian fluid, the components of the shear tensor, $\bar{\bar{\tau}}$, are given as follows:

$$\tau_{ii} = \eta \left(\frac{2}{3} \nabla \cdot \bar{u} - 2 \frac{\partial u_i}{\partial x_i} \right)$$

$$\tau_{ij} = \tau_{ji} = - \eta \left(\frac{\partial u_j}{\partial x_i} + \frac{\partial u_i}{\partial x_j} \right) \tag{4}$$

$$i = 1, 2, 3; \quad j = 1, 2, 3; \quad \text{and} \quad j \neq i$$

A simultaneous solution of Equations 1 through 3 for the two-dimensional flow of a real fluid around a cylinder is not available. Several methods for approximating the solution have been developed, however. These solve simplified forms of the above equations for a region near the cylinder, referred to as the boundary layer, where the flow is assumed to be laminar.

Itō (7) presents a generalization of Pohlhausen's method for a compressible fluid of arbitrary constant Prandtl number with heat transfer about a two-dimensional body with constant wall temperature. His method was adapted to the case investigated. Itō assumed the following behavior for the fluid properties, where a_∞ is the velocity of sound and the subscript ∞ indicates the evaluation of a quantity at the bulk stream conditions:

$$\frac{k}{k_\infty} = \frac{\eta}{\eta_\infty} = \left(\frac{T}{T_\infty}\right)^n \tag{5}$$

$$\frac{\sigma}{\sigma_\infty} = \frac{T_\infty p}{T p_\infty} \tag{6}$$

$$a_\infty = \left(\frac{\gamma p_\infty g_o}{\sigma_\infty g_c}\right)^{0.5} \tag{7}$$

A coordinate system was established in which X was the distance from stagnation along the surface of the cylinder, and Y was the normal distance from the surface of the cylinder. The compressibility effects were incorporated through the following variable change:

$$X_* = \int_0^X \frac{\sigma_w}{\sigma_\infty}\, dX \tag{8}$$

$$Y_* = \int_0^Y \frac{\sigma}{\sigma_\infty}\, dY \tag{9}$$

The ratio, χ, of the velocity boundary layer thickness, δ_*, to the thermal boundary layer thickness, δ'_*, expressed in terms of Y_*; and the quantities λ, Z, and λ_* were introduced as functions of the angular position from stagnation.

$$\chi = \frac{\delta_*}{\delta'_*} \tag{10}$$

$$\lambda = \frac{\delta_*^2}{\nu_\infty\left(1 - \dfrac{(\gamma - 1)u_1^2}{2a_\infty^2}\right)} \frac{du_1}{dX_*} = Z \frac{du_1}{dX_*} \tag{11}$$

$$\lambda_* = \frac{\Pr\left(2 + \dfrac{\lambda}{6}\right)^2 \dfrac{(\gamma - 1)u_1^2}{2a_\infty^2}}{3\chi^2\left[\dfrac{T_c}{T_\infty} - 1 + \dfrac{(\gamma - 1)u_1^2}{2a_\infty}\right]} \tag{12}$$

If $\chi \leq 1$, these quantities can be determined by the simultaneous solution of the following two equations:

$$\frac{dZ}{dX_*} = \frac{(8+\frac{5}{3}\lambda)Z^2}{(37 - 12\lambda - \frac{25}{12}\lambda^2)} \frac{d^2u_1}{dX_*^2} + \left\{1260(12+\lambda)\left(\frac{T_c}{T_\infty}\right)^n \right.$$

$$+ (4932\lambda - 87\lambda^2 - \frac{5}{2}\lambda^3) \frac{(\gamma-1)u_1^2}{2a_\infty^2} - 4044\lambda + 79\lambda^2$$

$$\left. + \frac{5}{3}\lambda^3 - \frac{756\lambda}{\chi}(3+\frac{\lambda_*}{2})\left(\frac{T_c}{T_\infty} - 1 + \frac{(\gamma-1)u_1^2}{2a_\infty^2}\right)\right\}$$

$$\div \left\{(37 - 12\lambda - \frac{25}{12}\lambda^2)\left(1 - \frac{(\gamma-1)u_1^2}{2a_\infty^2}\right)u_1\right\} \qquad (13)$$

$$\frac{0.3}{\chi} - 0.3 + \frac{\lambda}{120} + \left(\frac{2}{15} - \frac{\lambda}{180}\right)\chi + \left(-\frac{3}{140} + \frac{\lambda}{840}\right)\chi^3$$

$$+ \left(\frac{1}{180} - \frac{\lambda}{3024}\right)\chi^4 + \lambda_*\left\{\frac{0.05}{\chi} + \left(\frac{-1}{15} + \frac{\lambda}{360}\right)\chi\right.$$

$$\left. + \left(\frac{1}{14} - \frac{\lambda}{280}\right)\chi^2 + \left(\frac{-9}{280} + \frac{\lambda}{560}\right)\chi^3 + \left(\frac{1}{180} - \frac{\lambda}{3024}\right)\chi^4\right\}$$

$$= \frac{\left(1 - \frac{(\gamma-1)u_1^2}{2a_\infty^2}\right)^{\frac{1}{2}}}{Z^{\frac{1}{2}}u_1\left(\frac{T_c}{T_\infty} - 1 + \frac{(\gamma-1)u_1^2}{2a_\infty^2}\right)}$$

$$\cdot \int_0^{X_*} \left[\left\{\left(\frac{T_c}{T_\infty}\right)^n \frac{\chi(2-\lambda_*)}{Pr}\left(\frac{T_c}{T_\infty} - 1 + \frac{(\gamma-1)u_1^2}{2a_\infty^2}\right)\right.\right.$$

$$\left. + \frac{(\gamma-1)u_1^2}{2a_\infty^2}\frac{T_c}{T_\infty}\left(\frac{T_M}{T_\infty}\right)^{n-1}\left(\frac{104}{35} + \frac{8\lambda}{105} + \frac{\lambda^2}{210}\right)\right\}$$

$$\left. \div \left\{Z^{\frac{1}{2}}\left(1 - \frac{(\gamma-1)u_1^2}{2a_\infty^2}\right)^{3/2}\right\}\right] dX_* \qquad (14)$$

Itō also presents an alternate form of Equation 14 if $\chi \geq 1$. The form presented here, however, is adequate as long as χ is on the order of one.

The velocity at the edge of the boundary layer, u_1, is theoretically zero at the forward stagnation point. Therefore to ensure a finite slope for Z, the numerator in the brackets of the second term in Equation 13 was set equal to zero at stagnation. Also at stagnation the right side of Equation 14 reduces to $\frac{2\chi}{Pr\ \lambda}\left(\frac{T_c}{T_\infty}\right)^n$.

Equations 13 and 14 can easily be simplified for several special cases. The isothermal case is solved by removing the χ term in Equation 13 and solving only the resulting equation starting with $\lambda = 7.052$ at stagnation. For incompressible flow the term with u_1/a_∞ is removed from both equations. Finally, λ is zero for the flat plate case.

To solve Equations 13 and 14, Itō suggests that one first solve Equation 13 with an approximate χ obtained from a linear relationship with $\frac{X}{u_1}\frac{du_1}{dX}$. This linear relationship is established by the value of χ at stagnation where the function is one, and its value for the flat plate case where the function is zero. Based on the value of λ obtained, Equation 14 can be solved for χ. The approximation process can be continued until the values of χ and λ at each angular position are determined. Knowing these, the velocity and temperature distributions are given as follows.

$$\frac{u}{u_1} = (2 + \frac{\lambda}{6})\left(\frac{Y_*}{\delta_*}\right) - \frac{\lambda}{2}\left(\frac{Y_*}{\delta_*}\right)^2 + (-2 + \frac{\lambda}{2})\left(\frac{Y_*}{\delta_*}\right)^3 + (1 - \frac{\lambda}{6})\left(\frac{Y_*}{\delta_*}\right)^4 \qquad (15)$$

$$T = T_c + T_\infty \left\{1 - \frac{T_c}{T_\infty} - \frac{(\gamma - 1)u_1^2}{2a_\infty^2}\right\} \left\{(2 - \lambda_*)\frac{Y_*}{\delta_*'} + 3\lambda_*\left(\frac{Y_*}{\delta_*'}\right)^2 - (2 + 3\lambda_*)\left(\frac{Y_*}{\delta_*'}\right)^3 + (1 + \lambda_*)\left(\frac{Y_*}{\delta_*'}\right)^4\right\} \qquad (16)$$

It should be noted that knowledge of the velocity distribution, u_1, about the cylinder at the edge of the boundary layer and the corresponding pressure distribution are required for this approximate solution of the boundary layer equations. The solution is not applicable beyond separation where λ equals minus twelve.

Beyond separation the boundary layer equations are further complicated with the effects of turbulence. Theoretical considerations in this region are beyond the scope of this work.

Outside the boundary layer the potential flow solution is normally employed. This region is not of particular interest in this work. Therefore comparison with this approximation will not be included.

B. Energy Transfer from the Wire

The prediction of the heat transfer by convection from small wires has been reviewed and extended by Collis and Williams (9). In place of the usual dependence of the Nusselt number upon the square root of the Reynolds number, they present the following equation for the range $0.02 < Re_m < 44$:

$$Nu_{\ell, \lambda, m}\left(\frac{T_m}{T_a}\right)^{-0.17} = 0.24 + 0.56\ Re_m^{0.45} \tag{17}$$

Under steady state conditions with constant fluid properties and neglecting the dissipation term, Equation 2 becomes:

$$\bar{u} \cdot \nabla T = \frac{k}{\sigma c_p} \nabla^2 T \tag{18}$$

Equation 18 has been solved by Cole and Roshko (10) for the Oseen case where the velocity field is assumed uniform. This solution gives the limiting dependence as the Reynolds number approaches zero. The data of Collis and Williams clearly approach this limit. They therefore suggest the following correlation for $Re_m < 0.05$.

$$Nu_{\ell, \lambda, m}\left(\frac{T_m}{T_a}\right)^{-0.17} = \frac{1}{1.18 - 1.10 \log_{10} Re_m} \tag{19}$$

Collis and Williams also indicated, however, that buoyancy effects do occur in this region for a horizontal wire in a horizontal air stream. The onset of this effect depends upon the temperature loading for a given wire. The Nusselt number for a one-mil wire reaches a minimum at a Reynolds number on the order of 0.01 and then increases slightly to the value for free convection as the Reynolds number approaches zero.

C. The Wire in Boundary Flow

Piercy, Richardson, and Winny (4) have solved Equation 18 for the heat transfer from a wire in the boundary flow next to a flat plate, assuming potential flow in the air stream. The air flow was parallel to the flat plate and the plate was at the air stream temperature. Their solution was expected to apply for Peclet numbers, (Re Pr), below unity and at distances from the plate greater than one-wire diameter. Their experimental measurements in this range gave adequate agreement with the predicted behavior. Their predicted dependence of the Nusselt number on the Pectlet number and relative distance from the surface is presented as Figure 1.

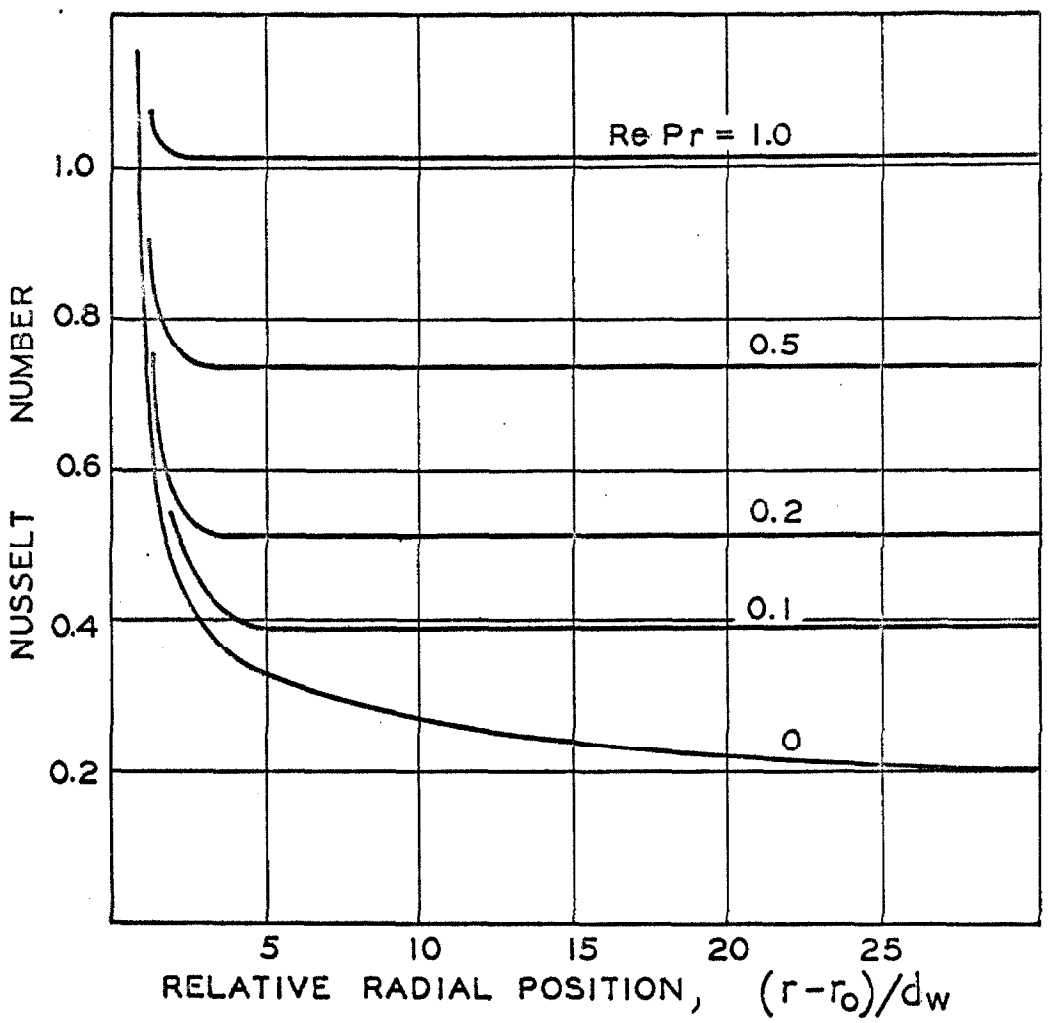

FIGURE 1. Predicted behavior for the Nusselt Number for a Small Wire in a Potential Flow Air Stream Near a Flat Plate (4)

III. EXPERIMENTAL APPARATUS

It was desired to experimentally study the heat transfer from a small wire in the boundary flow about a cylinder. To accomplish this, a horizontal cylinder was supported in a vertical air stream which emerged from a rectangular jet opening. The one-inch-diameter cylinder was a heating element covered with a sheet of polished copper. A one-and-one-quarter-inch section of one-mil-diameter platinum wire was supported by a platinum probe and maintained parallel to the axis of the cylinder. This wire was traversed to various positions in the air stream around the cylinder. At each point the wire was used as a platinum resistance thermometer to measure the air stream temperature and then heated electrically for the desired heat transfer measurements. The integral parts of this system are described in the subsequent sections. This apparatus was the same as that used by Venezian (5, 6) during his investigations.

A. Air Supply Equipment

A schematic drawing of the air supply equipment is presented as Figure 2. Filtered air from the room was withdrawn using a blower, A; forced over wire gird heaters, B; through a Venturi meter, C; and into a system of 12-inch square ducts. The various bends in this ductwork were equipped with vanes to reduce the disturbances to the air stream. This ductwork terminated with a smoothly coverging section to flatten the velocity profile at the 3- by 12-inch jet opening, D. The one-inch-diameter cylinder used in this investi-

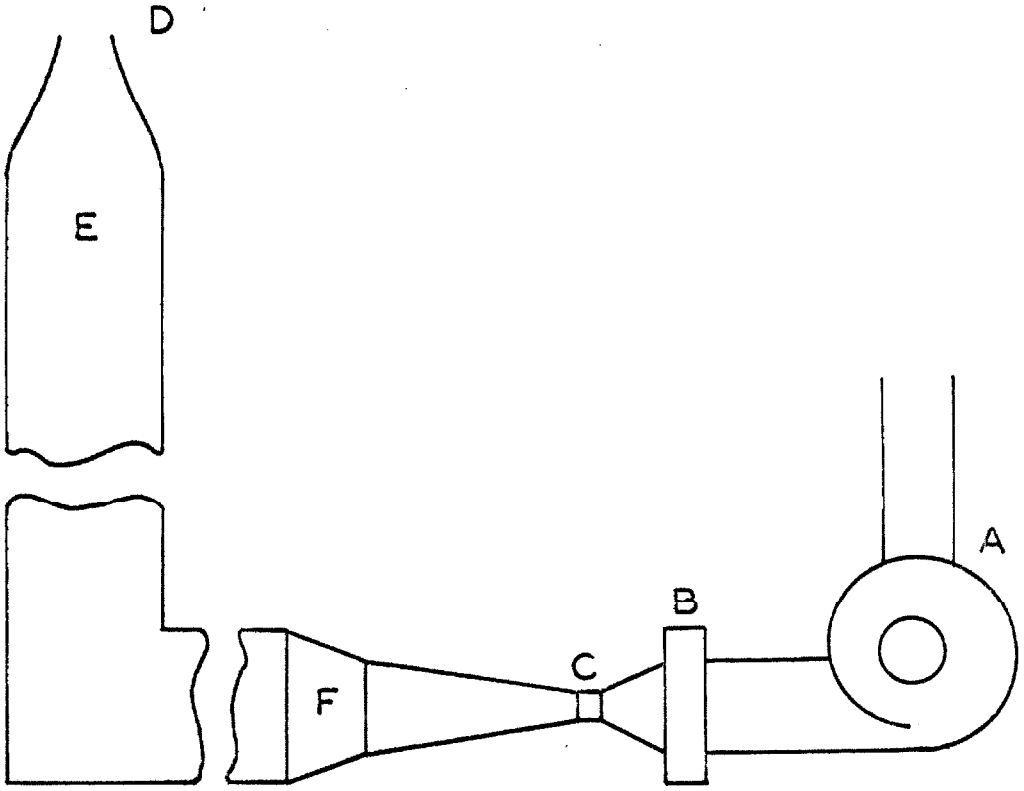

FIGURE 2. Schematic Diagram of the Air Supply Equipment

gation was centered about two inches above this jet opening.

The insulated ductwork and converging section downstream of the Venturi meter were provided with heaters. By monitoring the readings of eight thermocouples imbedded in the ductwork, these heaters were adjusted to maintain the ducts at the air stream temperature.

The wire grid heaters, B, were controlled by a Thyratron circuit and a platinum resistance thermometer located at E. The details of this temperature control system have been described by Corcoran and co-workers (11). The downstream temperature required for the Venturi meter measurements was determined by using another resistance thermometer in the air stream at F. Kerosene and mercury manometers along with a precision cathetometer were used in the Venturi meter measurement.

B. One-Inch Copper Cylinder

The copper cylinder was constructed with a copper shell over a core heater. The core heater consisted of a copper tube wound with electrically insulated heating elements in one-eighth-inch grooves separated by one-eighth-inch ridges. The 0.030-inch thick, one-inch external diameter, copper shell was soft-soldered to this copper core. The heating assembly with copper shell was 12-inches long and was supported at each end by 12-inch sections of bakelite tubing of the same external diameter.

Table I presents micrometer measurements of the external

diameter of the cylinder at 80° F for various angles from stagnation, ψ. The measurements were taken at the middle and at both ends of the one-and-one-quarter-inch section in the center of the 12-inch-long cylinder which was adjacent to the wire probe during the hot wire measurements. These data yield an average diameter of 0.9985 ± 0.0002 inches at 80° F. Correcting for the thermal expansion of copper, cylinder radii of 0.4994 ± 0.0001 inches and 0.4997 ± 0.0001 inches for 100° and 160° F cylinders are obtained. The radius at 160° F was confirmed with micrometer measurements.

The alignment of the cylinder was maintained at that described and used by Venezian (6). A level was employed to maintain the horizontal position of the cylinder. The surface was polished occasionally as required. The cylinder axis was approximately two inches above the jet opening.

Copper constantan thermocouples with electrically insulated leads were embedded in the inside of the copper shell at the middle, and at two inches on either side of the middle of the 12-inch-long cylinder. These thermocouples were monitored and the appropriate adjustments of the heater were made to maintain the cylinder at the desired temperature. The leads to the thermocouples and heater were brought through the hollow center of the assembly to a junction box at the end of one bakelite supporting section.

C. Wire Assembly

The wire was supported by a probe and maneuvered with a

traversing mechanism. These were described by Venezian (5, 6) and used in his work. The traversing mechanism was stabilized by mounting it on a one-half-inch steel plate attached to the angle-iron frame surrounding the apparatus.

Figure 3 is a diagram of the probe. The two platinum needles, A, were about 0.03 inches in diameter at their bases and tapered to about 0.005 inches in diameter at the ends where the wire was welded. The distance between the probes could be altered slightly to adjust the wire tension by using the set screws which held them in the bakelite supports, B. These supports were securely fastened to the steel head, C, which was bolted to the one-quarter-inch diameter steel shaft, D. This shaft was secured in the traversing mechanism. The insulated 30-gauge-platinum current and potential leads, E, were welded to the needles and extended about 6 inches along the shaft of the probe where they were connected to copper leads.

About a one-and-one-quarter-inch section of one-mill diameter platinum wire was welded to the ends of the probe needles. Replacement wires were obtained from the same spool. Figure 4 shows microphotographs of the wire and a scale, all taken at the same focal distance. Figure 4a is a section of unused wire from the spool. The diameter obtained from this microphotograph agrees within experimental accuracy with the value quoted by the manufacturer. Figure 4c is a section of a wire after a year's use during which the bulk of the measurements were taken. The buildup of foreign particles indicated in this figure may have a small effect on the experimental results.

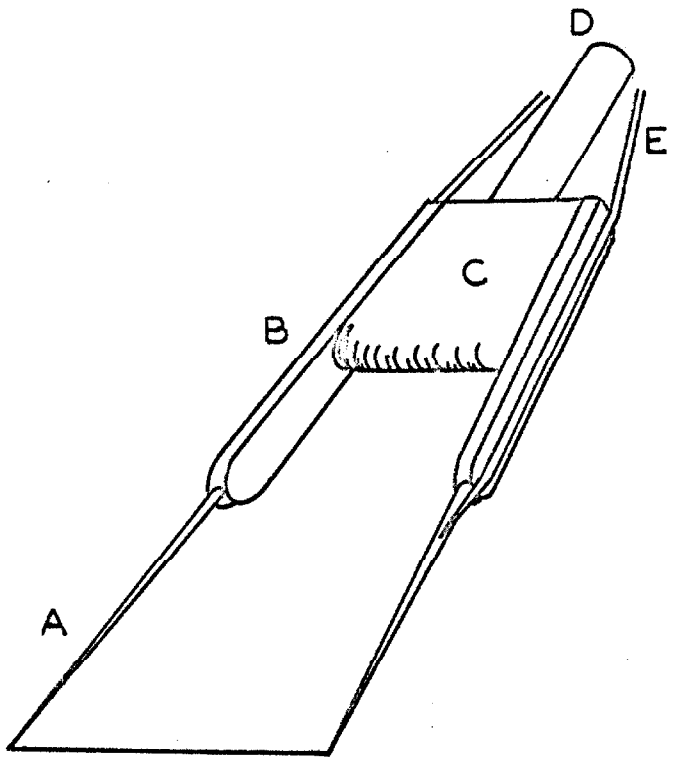

FIGURE 3. Diagram of the Supporting Probe for the Wire

a)

b)

c)

FIGURE 4. Microphotographs of:
a) A Section of Unused Wire
b) A Scale with One Unit Equal to 10 Microns
c) A Section of Wire After One Year's Use
All at the Same Focal Distance

This is discussed later.

The probe assembly was traversed horizontally and vertically by milling attachments like those used by jewelers. Relative distances in these two planes were measured with 0.1-inch-per-revolution dial gages with 0.001-inch divisions. A photograph of this probe and traversing mechanism was presented by Venezian (6) as Figure 7 of his thesis.

D. Wire Measuring Circuit

A circuit diagram for the wire is presented as Figure 5. Basically, it consisted of a Wheatstone bridge circuit to obtain a desired wire resistance when the current through the galvanometer, G, was adjusted to zero. Four-ohm and forty-ohm fixed resistors, and a variable resistor, R_V, formed three arms of the circuit. The wire itself and two manganin resistors of about 0.5 ohms and 0.05 ohms formed the fourth arm. Current was supplied by one or two 6-volt D. C. batteries and adjusted with another variable resistor, R_C. The voltage drops across the 0.05-ohm resistor and the wire were simultaneously observed on a White potentiometer and a K-2 type potentiometer, respectively. In the upward position of the six-leaf throw switch, a 7-ohm resistor replaces the wire in the Wheatstone bridge circuit so that current could be maintained while the wire was connected to the G-1 type Mueller bridge.

The current through the wire and the resistance of the wire were calculated from the simultaneous readings of the potential drop across the calibrated 0.05-ohm resistor and the wire. The Mueller

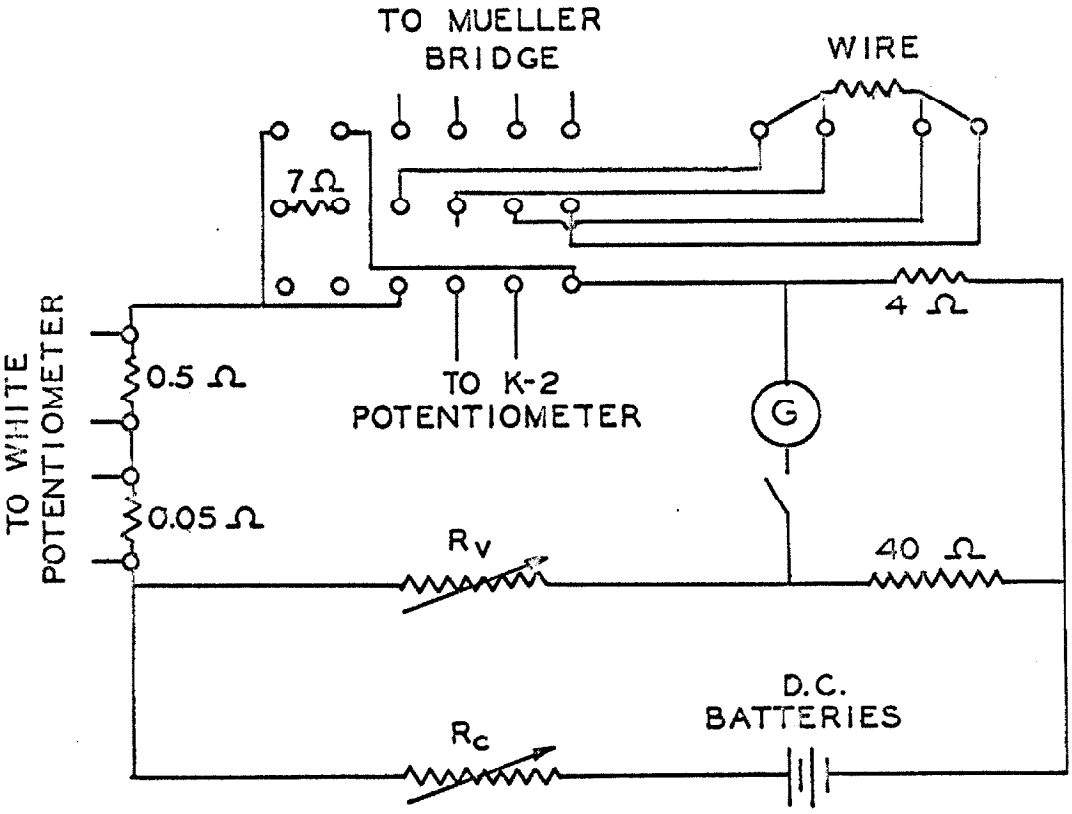

FIGURE 5. Circuit Diagram for Wire Measurements

bridge was used to measure the resistance of the wire in the air stream. From the calibration of the wire as a resistance thermometer, these resistances were converted into the corresponding temperatures. The current was used to determine the electrical energy input to the wire.

IV. EXPERIMENTAL MEASUREMENTS

Discussions about the calibrations, measurements, calculations, and the expected uncertainties are presented in this section.

A. Calibrations

To obtain temperatures from the resistance measurements of the wire, a calibration between these two properties for the wire was made. A section of the wire from the same spool as the wire used for the experimental measurements was mounted in a dry nitrogen atmosphere in a glass tube and annealed. This wire and the platinum resistance thermometer used in the air stream were calibrated together at 100°, 220°, and 340° F in an oil bath and at 32° F in an ice bath against a standard platinum resistance thermometer. This calibration produced the following temperature dependence for the resistance of the wire:

$$\frac{R}{R_o} = 0.9295746 + 2.20666 \times 10^{-3} t - 1.8321 \times 10^{-7} t^2 \qquad (20)$$

In Equation 20, R is the resistance of the wire in absolute ohms at the temperature t in degrees Farenheit, while R_o is the wire resistance at the ice point, 32° F. This calibration was assumed applicable to the work-hardened wires used in the measurements.

The resistance of the 0.05-ohm resistor, R_s, was calibrated as a function of its temperature using 10-ohm and 1-ohm standard resistors. A small temperature correction was added to the 0.0510969-absolute-ohm value measured at 30° C (86° F). Thus R_s

could be determined from its temperature with an uncertainty of 0.01 per cent.

At various places throughout the analysis the physical properties of air are required. The following linear equation for the temperature dependence of the thermal conductivity of air at atmospheric pressure was based on the values reported by Hsu (12) and in NBS Circular 564 (13).

$$k = 3.6760 \times 10^{-6} + 6.730 \times 10^{-9} t \qquad (21)$$

A comparison of these values with Equation 21 is presented as Figure 6. An absolute viscosity of 3.98×10^{-7} lb-seconds-per-square-foot for air at one atmosphere and 100° F was taken from Hsu (12). These properties were not corrected for the small variations in atmospheric pressure.

The thermal conductivity reported by Holm and Störmer (14) for pure platinum was evaluated at the average wire temperature, and used for the wire.

$$k_s = 0.011006 + 1.7639 \times 10^{-6} t_w \qquad (22)$$

The correlation obtained between the heat transfer from the wire and the velocity of the air stream past the wire will be presented later with the other results of this investigation.

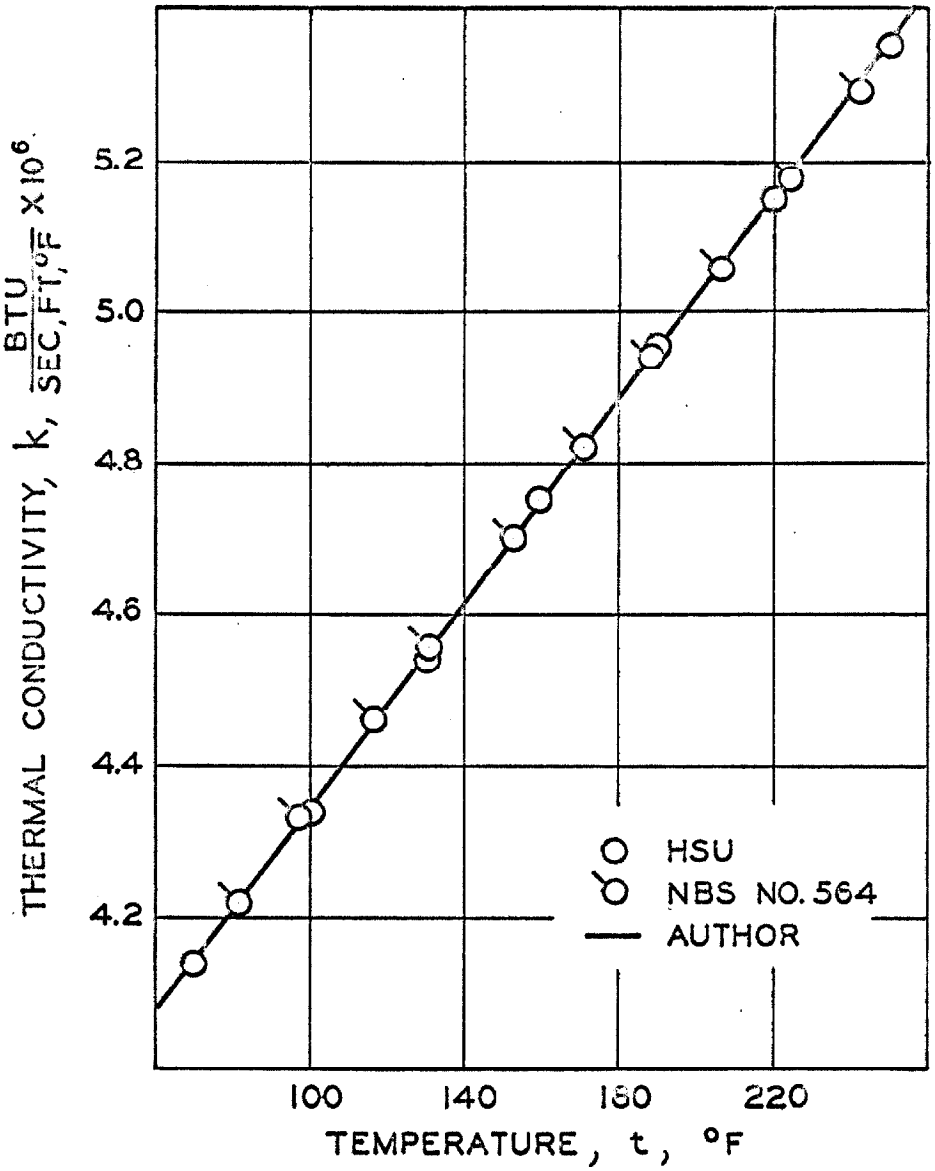

FIGURE 6. Thermal Conductivity of Air at Atmospheric Pressure

B. Measuring Procedure

The equipment was heated and stabilized at the desired operating conditions prior to each run. This stabilizing period was normally about five hours. During this time the air duct heaters were adjusted to maintain the corresponding thermocouples at $100.0^{\circ} \pm 0.3^{\circ}$ F. The cylinder core heaters were adjusted to maintain the center thermocouple at the desired temperature, either 100° or 160° F, within 0.2° F. The air temperature at the jet opening was similarly set at $100.0^{\circ} \pm 0.2^{\circ}$ F and the air grid heaters were controlled by the Thyratron circuit. The blower speed was adjusted to produce an air flow through the jet opening of 0.5384 ± 0.0012 lb-mass per second per square foot.

Once set, the temperatures were maintained within 0.1° F throughout the run by monitoring the corresponding thermocouples at about half-hour intervals. The height of the upstream Venturi manometer leg was checked continuously. Infrequent voltage surges did, however, throw the blower system out of control. When these were observed no data were taken until the equipment had again stabilized at the desired conditions.

During the conditioning period the wire was aligned and the location of the cylinder was determined on the arbitrarily positioned scale of the traversing mechanism. The wire was aligned parallel to the axis of the cylinder by observing it and its reflection on the cylinder with a telescope mounted outside the air stream. The positions of the surface of the cylinder at 0° and 90° from stagnation

were determined by plotting the difference on the telescope scale between the wire and its reflection in the cylinder along the appropriate traverse and extrapolating the curve to a zero difference. By alternating the traverses, the position of the centerline of the cylinder was determined within 0.001 inches. A section of the wire about half way between the probes was chosen for these positioning measurements. This process was repeated after the run to confirm the relative coordinate position of the cylinder.

The readings of the various thermocouples with the air duct and cylinder heaters, manometers with the Venturi meter, and air temperatures downstream of the Venturi meter and at the jet opening maintained throughout the run were recorded at the beginning and end of each run. The values of these control variables and the air humidity were used to calculate the average conditions for the test.

During a set of measurements, simultaneous readings of the voltages across the heated wire and the 0.05-ohm resistor preceded a measurement of the resistance of the unheated wire. These and the temperature of the 0.05-ohm resistor formed a complete set of wire measurements. Two or three such sets at different wire currents were taken at each point. Thus, the Nusselt number could be obtained as a function of the temperature difference between the heated wire and the local air stream. Since the galvanometers for the potentiometers and Mueller bridge employed for these readings were sensitive to the continuous fluttering of the voltages and wire resistance being observed, readings which averaged out these time

variations were recorded. This fluttering and averaging introduced uncertainties far beyond those indicated in the calibrations.

As the wire work-hardened, its ice point resistance increased from day to day. Therefore, this quantity was determined before and after each run. The wire and a platinum resistance thermometer were enclosed in a dewar of stagnant air. After allowing several hours to reach equilibrium, the resistances of both elements were measured. Knowing the resistance of the wire at the temperature determined with the normal resistance thermometer, Equation 20 was solved for the ice-point resistance of the wire. The ice-point resistances before and after a run generally agreed within 0.002 ohms, i.e. 0.1 ^{o} F.

As a further check the air stream temperature was measured with both the wire and the platinum resistance thermometer whenever the central variables were checked. These normally agreed within 0.05^{o} F. These measurements were used to adjust the ice-point resistance of the wire if any sizable change occurred in it during the run. These changes were normally caused by mistreating the wire, such as forcing the probes against the cylinder. The precautions taken were adequate to correct for the trend of the wire's ice-point resistance to increase at the rate of about seven per cent per year due to work-hardening.

C. Calculations

In the field of engineering, the flow of fluids is generally characterized by a Reynolds number, and heat transfer to fluids is generally characterized by a Nusselt number. Although each of these dimensionless groups has a prescribed combination of terms, several interpretations concerning the conditions under which these terms are measured are available. In this section the particular conditions chosen for this presentation are defined, the various terms are developed from the experimentally measured quantities, and the assumptions incorporated in this analysis are specified.

The bulk velocity, U_∞, for the bulk Reynolds number was based on the mass flow rate, $\dot{m}$, measured with the Venturi meter and the area, A, of the jet opening.

$$U_\infty = \frac{\dot{m}}{A\sigma_\infty} \tag{23}$$

The specific weight of air, σ_∞, used in Equation 23 was based on the conditions at the jet opening and the specific gas constant, b, deduced from the observed humidity of the air.

$$\sigma_\infty = \frac{p_\infty}{bT_\infty} \tag{24}$$

Using these properties, the bulk Reynolds number for the cylinder, $Re_{c,\infty}$, was defined as follows:

$$Re_{c,\infty} = \frac{2r_o U_\infty}{\nu_\infty} = \frac{2r_o \dot{m}}{Ag_c \eta_\infty} \tag{25}$$

Another Reynolds number, Re_m, based on the wire diameter and the average fluid properties between the local air temperature, t_a, and the average hot wire temperature, t_w, was also used.

$$Re_m = \frac{d_w u}{\nu_m} \tag{26}$$

By assuming a constant pressure, and using the fluid property correlations expressed in Equations 5 and 6, this mean wire Reynolds number was defined as follows:

$$Re_m = \frac{d_w u}{\nu_\infty \left(\frac{T_m}{T_\infty}\right)^{1+n}} \tag{27}$$

The temperature exponent, n, in Equations 5 and 27 was evaluated at 0.8719 from the air thermal conductivities at 100° and 160° F from Equation 21.

The Nusselt number was determined from the measurement of the following four quantities at a given position of the wire in the air stream: 1) the potential drop across the heated wire, E_w; 2) the potential drop across the fixed resistor, E_s; 3) the resistance of the fixed resistor, R_s; and 4) the resistance of the unheated wire, R_a.

A calibration of the wire as a resistance thermometer produced Equation 20. Using this and the measured ice-point resistance, R_o, for the particular test, the local air stream temperature, t_a, was calculated from the unheated wire resistance.

The current through the fixed resistor was calculated from its measured resistance and the voltage drop across it.

$$I = \frac{E_s}{R_s} \tag{28}$$

Since the wire was in series with the fixed resistor when the hot-wire measurements were taken, this was also the current through the wire. Therefore the total resistance of the wire was known.

$$R_w = \frac{E_w}{I} = \frac{E_w R_s}{E_s} \tag{29}$$

This total wire resistance, R_w, was assumed to be the average resistance of the wire and to produce the average temperature of the wire, t_w, through Equation 20.

The total electrical energy input to the wire, $\dot{q}_e$, was also calculated from the hot-wire measurements using a conversion factor of 3.41219 Btu per watt-hour.

$$\dot{q}_e = I^2 R_w = \frac{E_w E_s}{R_s} \tag{30}$$

Therefore, based directly on the experimental measurements with a wire of diameter d_w and length ℓ, an experimental heat transfer coefficient, h_e, was evaluated.

$$h_e = \frac{\dot{q}_e}{\pi d_w \ell (t_w - t_a)} = \frac{I^2 R_w}{\pi d_w \ell (t_w - t_a)} \tag{31}$$

To obtain this experimental heat transfer coefficient it was assumed that the electrical energy input was the only heat source and that the heat transfer from the surface characterized by the difference between the average hot-wire temperature and the local air temperature was the only heat loss. Corrections to a more realistic set of

assumptions are introduced below.

An experimental Nusselt number, $Nu_{e,a}$, was based on this experimental heat transfer coefficient and the fluid properties evaluated at the local air temperature.

$$Nu_{e,a} = \frac{h_e d_w}{k_a} = \frac{I^2 R_w}{k_a \pi \ell (t_w - t_a)} \tag{32}$$

Note that this Nusselt number was not dependent upon the evaluation of the diameter of the wire used. It was, however, dependent upon the particular experimental arrangement employed. For this reason it was only useful for comparing data obtained on this particular apparatus. To remove these limitations the following corrections were made to account for the finite length of the wire and the temperature discontinuity of its surface.

1. Correction for finite length. To correct the experimental measurements for the effect of the wire length, several assumptions were made to simplify the energy equation for the wire into a form which has been solved. For an electrically heated wire in which there are no radial or angular gradients, from which radiation is neglected, and which is at steady state in an air stream, the electrical heat input must equal the sum of the convective heat loss from the surface and the conductive heat loss along the wire. This is expressed in Equation 33 for a differential length dz.

$$I^2 \left(\frac{R}{\ell} \right) dz = \pi d_w h (t - t_a)\, dz + \frac{k_s \pi d_w^2}{4} \frac{d^2 t}{dz^2}\, dz \tag{33}$$

Equation 33 was solved by assuming that the heat transfer coefficient, h, and the wire thermal conductivity, k_s, were constant; and that the electrical resistance per unit length, R/ℓ, was linear with temperature.

$$\frac{R}{\ell} = \frac{R_a}{\ell}\left[1 + a(t - t_a)\right] \tag{34}$$

$$a = \frac{R_w - R_a}{t_w - t_a} \tag{35}$$

The constant wire thermal conductivity was evaluated using Equation 22 and was based on the average wire temperature. Noting that R_w has been assumed to be the average wire resistance, and the corresponding t_w to be the average wire temperature, the following expressions were valid:

$$R_w = \int_{-\ell/2}^{\ell/2} \frac{R}{\ell}\, dz \tag{36}$$

$$t_w = \int_{-\ell/2}^{\ell/2} \frac{t}{\ell}\, dz \tag{37}$$

The constant heat transfer coefficient necessary to solve Equation 33 was assumed to be that which would be observed for a wire of infinite length. Equation 38 expresses this quantity, h_ℓ, based on an infinite wire which was electrically heated by the current I to the temperature t_ℓ.

$$h_\ell = \frac{I^2\left(\frac{R_a}{\ell}\right)\left[1 + a(t_\ell - t_a)\right]}{\pi d_w (t_\ell - t_a)} \tag{38}$$

After Equation 34 was substituted into Equation 31, the comparison with Equation 38 produced the following relationship between the experimental and infinite length heat transfer coefficients when the quantities β_w and β_ℓ defined below were introduced:

$$h_\ell = h_e \frac{[1 + a(t_\ell - t_a)](t_w - t_a)}{[1 + a(t_w - t_a)](t_\ell - t_a)} = h_e \frac{(1 + \beta_\ell)\beta_w}{(1 + \beta_w)\beta_\ell} \tag{39}$$

$$\beta_w = a(t_w - t_a) \tag{40}$$

$$\beta_\ell = a(t_\ell - t_a) \tag{41}$$

The following equation was obtained by substituting Equations 34 and 38 into Equation 33, rearranging, and simplifying:

$$\frac{d^2(t - t_a)}{dz^2} - \frac{4I^2 R_a (t_\ell - t_a)}{\pi d_w^2 \ell k_s (t_\ell - t_a)} = - \frac{4I^2 R_a}{\pi d_w^2 \ell k_s} \tag{42}$$

If it is assumed that the larger platinum probes which support the wire maintain the ends of the wire at the air stream temperature, t_a, then the solution to Equation 42 has been presented by Carslaw and Jaeger (15) on page 152.

$$t = t_a + (t_\ell - t_a)\left\{1 - \frac{\cosh\left[\frac{2I}{d_w}\left(\frac{R_a}{\pi \ell k_s (t_\ell - t_a)}\right)^{\frac{1}{2}} z\right]}{\cosh\left[\frac{2I}{d_w}\left(\frac{R_a}{\pi \ell k_s (t_\ell - t_a)}\right)^{\frac{1}{2}} \frac{\ell}{2}\right]}\right\} \tag{43}$$

If the following substitution of the known quantity s is made, Equation 45 is obtained from Equations 43 and 44.

$$s = \frac{d_w}{\ell I}\left(\frac{\pi \ell k_s (t_w - t_a)}{R_a}\right)^{\frac{1}{2}} \tag{44}$$

$$t = t_a + (t_\ell - t_a)\left\{1 - \frac{\cosh\left[\frac{2z}{\ell s}\left(\frac{\beta_w}{\beta_\ell}\right)^{\frac{1}{2}}\right]}{\cosh\left[\frac{1}{s}\left(\frac{\beta_w}{\beta_\ell}\right)^{\frac{1}{2}}\right]}\right\} \tag{45}$$

By integrating Equation 45 as prescribed by Equation 37 and rearranging, the following defining equation for β_ℓ is obtained:

$$\frac{\beta_w}{\beta_\ell} = 1 - s\left(\frac{\beta_\ell}{\beta_w}\right)^{\frac{1}{2}} \tanh\left[\frac{1}{s}\left(\frac{\beta_w}{\beta_\ell}\right)^{\frac{1}{2}}\right] \tag{46}$$

Since s was on the order of 0.02, Equation 47 was used as an adequate series solution of Equation 46.

$$\frac{\beta_w}{\beta_\ell} = 1 - s - \frac{s^2}{2} - 0.645\, s^3 \tag{47}$$

A Nusselt number, $Nu_{\ell,a}$, based on the infinite length wire heat transfer coefficient is expressed in Equation 48.

$$Nu_{\ell,a} = \frac{hd_w}{k_a} = Nu_{e,a}\left[\frac{\frac{\beta_w}{\beta_\ell} + \beta_w}{1 + \beta_w}\right] \tag{48}$$

2. Correction for the temperature discontinuity at the wire surface. This correction was necessary because the size of the wire was approaching the order of magnitude of the mean free path of the air molecules. The basis for this correction was established by Kennard (16). The correction procedure used was presented by Collis and Williams (9).

As indicated in Equation 49, the difference between the wall temperature and the temperature, t_{ai}, at which the gas would be if the radial temperature gradient in the air were constant up to the wall was assumed proportional to the radial temperature gradient in the air at the surface.

$$t_\ell - t_{ai} = -\xi\left(\frac{\partial t}{\partial r}\right)_{ai} \tag{49}$$

The constant ξ is called the temperature jump distance. Based on the properties of air at the surface, Kennard derived the following expression for ξ.

$$\xi = \frac{2 - a}{a}\ \frac{4C}{\gamma + 1}\ \frac{\lambda}{Pr} \tag{50}$$

In Equation 50, a is the accommodation coefficient of the surface for the particular gas, $\gamma = c_p/c_v$ is the ratio of the specific heats of the gas at constant pressure and constant volume, C is a constant such that $0.491 \leq C \leq 0.499$, Pr is the Prandtl number

for the gas, and λ is the mean free path of the gas molecules which was calculated with the following equation for an ideal gas:

$$\lambda = \frac{\mu}{p}\left(\frac{\pi b T}{2 g_c}\right)^{\frac{1}{2}} \tag{51}$$

By noting that α is about 0.9 for platinum in air[9] and setting C at 0.498, ξ was evaluated for the wire in air as follows:

$$\xi = 3.5204 \times 10^{-7} + 1.1286 \times 10^{-9} t + 6.667 \times 10^{-14} t^2 \tag{52}$$

The average wire temperature was assumed to give the best approximation of ξ using Equation 52.

It was assumed that the measured conductive heat loss per unit area was that which would occur in a continuum with a surface temperature of t_{ai} and that this correction appeared in the heat transfer coefficient as follows:

$$h_\ell (t_\ell - t_a) = h_{ai}(t_{ai} - t_a) = - k_{ai}\left(\frac{\partial T}{\partial r}\right)_{ai} \tag{53}$$

Therefore the corrected surface temperature, heat transfer coefficient and Nusselt number can be expressed as follows:

$$t_{ai} = t_\ell - (t_\ell - t_a)\frac{h_\ell \xi}{k_{ai}} \tag{54}$$

$$h_{ai} = \frac{h_\ell}{1 - \frac{h_\ell \xi}{k_{ai}}} \tag{55}$$

$$Nu_{\ell, \lambda, a} = \frac{Nu_{\ell, a}}{1 - \frac{Nu_{\ell, a} k_a \xi}{d_w k_{ai}}} \tag{56}$$

3. Corrected Nusselt number. Combining Equations 32, 48, and 56, the corrected Nusselt number is expressed as follows:

$$N_{\ell, \lambda, a} = \frac{\frac{E_w E_s}{R_s k_a \pi \ell (t_w - t_a)} \left[\frac{\frac{\beta_w'}{\beta_\ell} + \beta_w}{1 + \beta_w} \right]}{1 - \frac{E_w E_s \xi}{R_s k_{ai} \pi d_w \ell (t_w - t_a)} \left[\frac{\frac{\beta_w}{\beta_\ell} + \beta_w}{1 + \beta_w} \right]} \tag{57}$$

The correction for the finite wire length reduced the Nusselt number by about three per cent. A one per cent increase resulted from the correction due to the temperature discontinuity at the wire surface. Thus the corrected Nusselt number was on the order of two per cent lower than the experimental Nusselt number.

D. Experimental Uncertainties

The possible errors and uncertainties in the measurements fell into three categories: 1) uncertainties in the calibration of the measuring equipment, 2) uncertainties in the measurements due to the continuous fluttering of the values of the variables being measured, and 3) errors introduced by the overall variations in the stream conditions during the measurement sequence. In addition

to these, there was also the uncertainty in the relative coordinate position of the wire during the measurements.

The 0.01 per cent uncertainty in the calibration of the 0.05-ohm resistor represents the discrepancy between the potentiometric and Mueller bridge methods of measuring the resistance. This results in a 0.05° F uncertainty in the temperature difference between the hot wire temperature and air stream temperature. Although the ice-point measurement introduces another 0.05° F uncertainty in the temperature, the effect on the temperature difference is not noticeable.

The standard cells in the two potentiometers disagreed by about 0.06 per cent. Therefore the K-type potentiometer was standardized with the standard cell in the White potentiometer. In this way the ratio of the two readings used for the wire resistance was accurate and any error which resulted when the product of the readings was used for the calculation of the electrical input was tolerable.

The length of the wire was determined within about 0.2 per cent.

As previously indicated, the time fluctuations in the quantities being measured were a major source of errors. Although these fluctuations appeared to be quite large on the sensitive galvanometers connected to the fine instruments, the variations were only a few hundreths of a per cent of the values being measured. Unfortunately, the resistance of platinum is not too sensitive to temperature change.

Therefore two tenths of a per cent error in the resistance was equivalent to one Farenheit degree. On this basis these fluctuations amount to tenths of degrees which rapidly add up to one per cent of a 50 degree temperature difference.

There was also some variation in the apparent air temperature during the few minute's interval between the hot- and unheated-wire measurements. These oscillations about the mean temperature were of about the same order of magnitude as the above mentioned fluttering. The longer term trends during the day were controlled through manual adjustments of the apparatus.

The fluctuations were smaller in the free stream region beyond the boundary layer. In this region the readings were fairly stable and the major error was in the stream stability between the potentiometer and Mueller bridge readings at a point. Within the boundary layer the fluctuations became quite noticeable and increased as the cylinder was approached. Furthermore, the time average stream characteristics seemed to be more unstable in this region.

Table II presents the estimated maximum uncertainties for the Nusselt number for the data within the boundary layer. The total of 1.5 per cent noted in this region would increase to about two per cent for data obtained within 0.01 inches of the cylinder, and be reduced to about one per cent for data obtained in the free stream. In addition to this uncertainty in the value of the Nusselt number, there was about a 0.001 inch uncertainty in each of the coordinates relative to the position of the cylinder. Further errors in the

relative position will be discussed later.

A buildup of foreign particles on the wire was noted with Figure 4. It will be noted in Section V-B that the observed correlation between the Nusselt and Reynolds numbers could be adjusted to agree with the Collis and Williams (9) correlation, Equation 17, by using an effective wire diameter of 1.08 mils rather than 1 mil. Such an increase in the average wire diameter appears to be reasonable when viewing Figure 4-c. Fortunately, the wire diameter cancels out the experimental Nusselt number. Only about a 0.1 per cent change would be introduced by such a diameter change into the Nusselt number through the corrections for finite length and temperature discontinuity at the wire surface. However, by adjusting the Nusselt number and Reynolds number correlation rather than the diameter of the wire, the conversion of the measured heat transfer can be correlated with the air velocity without introducing further uncertainties.

Such a change in the effective wire diameter would greatly affect the reported heat transfer coefficients. In addition the heat transfer characteristics of the foreign particles would further complicate the heat transfer coefficient expressions. The reported heat transfer coefficients are based on the one-mil diameter reported by the manufacturer for the clean wire. This diameter was confirmed by the microphotograph presented as Figure 4 and by comparison of the wire resistance with that for pure platinum (14).

V. RESULTS

A. Smoothed Experimental Data

These measurements were taken on a cartesian coordinate system. Relative to the axis of the cylinder, x increased vertically in the direction of the air flow, and y was horizontal and positive in the quadrants investigated. This coordinate system is illustrated in Figure 7. Within this coordinate system, measurements were taken on vertical and horizontal traverses at 0.1-inch intervals around the cylinder. For these traverses, data were taken at a high density of points at the approach of and within the boundary layer, and a few points were taken in the free stream. At each point, measurements at several wire currents were taken. From these measurements the corrected Nusselt number, $Nu_{\ell, \lambda, a}$, was calculated. The latter were plotted for each point against $\Delta t = t_w - t_a$, and a linear interpolation to a Δt of 50° F obtained. The adjusted Nusselt numbers, $(Nu_{\ell, \lambda, a})_{\Delta t = 50^\circ F}$, were plotted for each traverse. The traverse curves were then smoothed using angular, radial, and Nusselt number contour plots within the boundary layer; and using horizontal, vertical, and Nusselt number contour plots for the free stream regions. This method was used for both the isothermal and the nonisothermal Nusselt number data. These smoothed, adjusted, wire Nusselt numbers will be denoted by Nu^*.

The air stream temperatures obtained during the nonisothermal measurements were corrected as follows for relative variations in the temperatures if necessary.

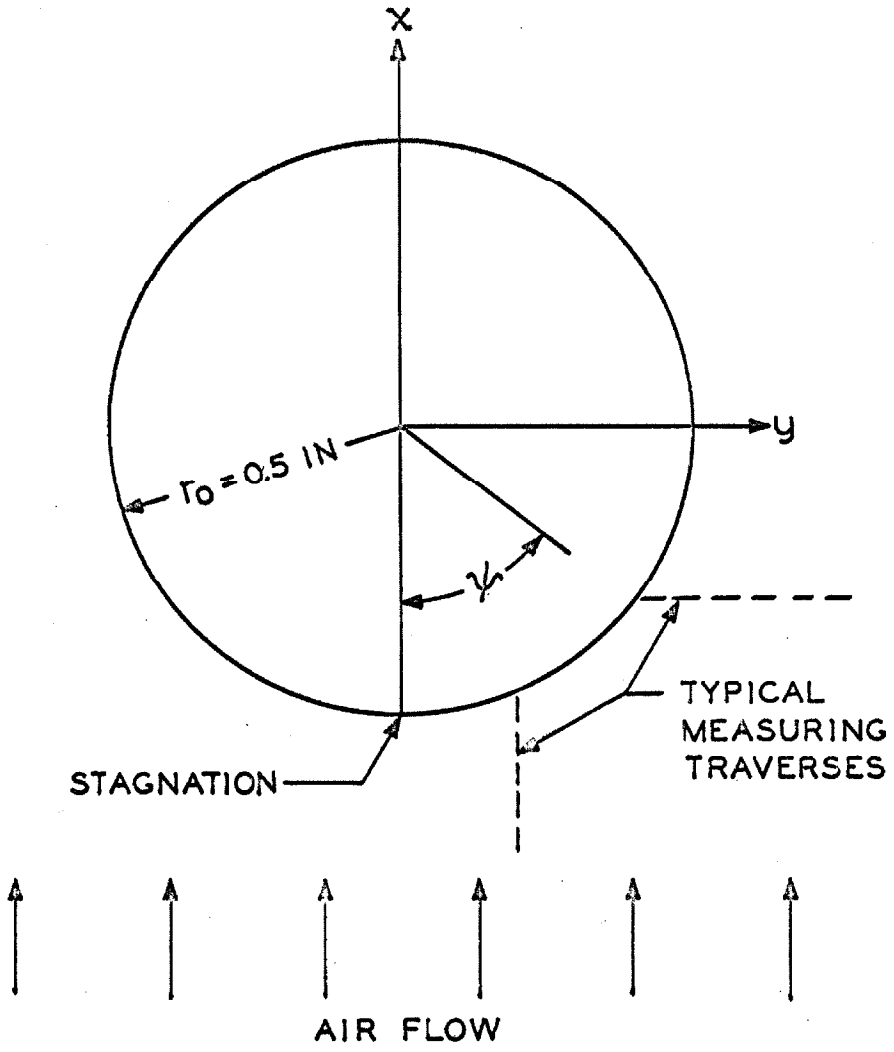

FIGURE 7. Coordinate Systems for the Air Flow about the Cylinder

$$t_a^* = 100^\circ \text{ F} + \frac{t_a - t_\infty}{t_c - t_\infty} 60^\circ \text{ F} \qquad (58)$$

These values were plotted for their respective traverses and similar smoothing procedures were begun. It was then noted that these temperatures could not be extrapolated to 160° F at the coordinate position for the surface of a "round" cylinder.

Figure 8 will be helpful in visualizing the subsequent discussion of the position of the surface of the 160° F cylinder on the coordinate system used for the measurements. As previously noted, the micrometer measurements of the cylinder diameter presented as Table I indicated that the diameter was constant. The cylinder was round, but it did not appear to be so on the coordinate system employed. The position of the cylinder on the coordinate system was established by extrapolating the difference on the telescope scale between the wire and its image in the cylinder to zero at $\psi = 0$ degrees and $\psi = 90$ degrees. This method was used to observe the position of the surface at three other angular positions. The position of the surface was also obtained by extrapolating the air stream temperatures to 160° F. These extrapolated coordinate positions for 160° F are represented by the solid curve whose position was confirmed by the more direct telescope measurements. This 160° F isotherm position was referred to as r_o' and was subsequently used to correct the radial location of the data.

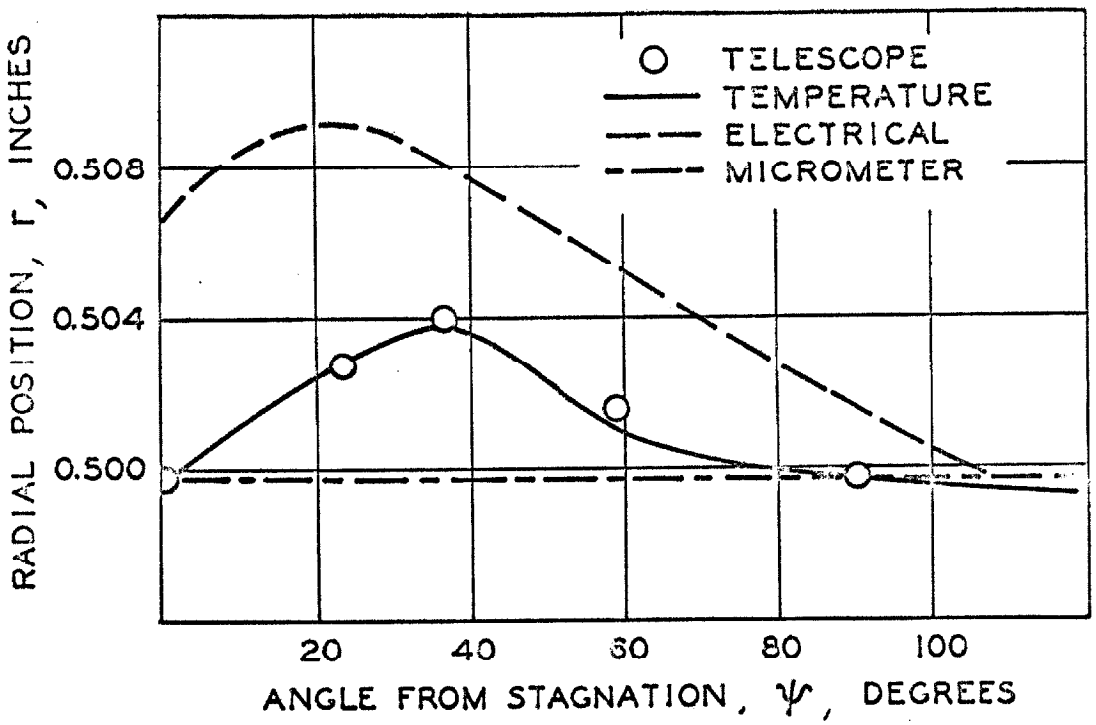

FIGURE 8. Radial Position of the Wire at the Surface of the 160° F Cylinder

The other curve in Figure 8 indicates the radial position of the wire on the measured coordinate system when the probe assembly came into electrical contact with the cylinder surface. Since the probe was horizontal, the point of contact progressed back along the probe at stagnation. This curve is merely an indication of the closest that the wire could be placed to the cylinder.

Throughout the investigation of the coordinate discrepancy no faults could be located in the traversing mechanism. The traversing guide tracks were within one minute of a right angle. The dial indicator scales were accurate. Thus it appears that perhaps the wire may have sagged slightly and have been supported at different positions by the air stream as it was traversed around the cylinder. This could cause the discrepancies noted since the coordinates were determined relative to the middle of the wire and the traversing probes obviously changed the position of the ends of the wire. However, the stability of the wire in the air stream and its alignment with the cylinder surface as observed through the telescope leave some doubts about even this explanation.

Table III presents a summary of the conditions observed for the various tests. The experimentally observed positions, temperatures, and the corrected and the adjusted Nusselt numbers are presented in Tables IV and V for the isothermal and nonisothermal cases, respectively. All of the precautions and checks previously mentioned were not taken for the early, 400-series, tests. Therefore only the portion of this data in the free stream which was used

in the analysis is reported. Throughout all the reported data, an X is placed beside the Nusselt numbers which were eliminated during the analysis. Lines of data were disregarded if the corrected Nusselt number was greater than one per cent from the linear correlation with Δt since such a large deviation was not normal. The complete point was eliminated if the adjusted Nusselt number was greater than three times the relative standard deviation from the smoothed values. Complete runs were not reported for which the various checks did not meet the desired standards.

The relative standard deviation used as a criterion to discard data was evaluated as the square root of the sum of the squared differences between the adjusted and smoothed Nusselt numbers, each divided by the smoothed value at the point, and this sum divided by the number of points in the sum minus one. The relative standard deviation was 0.6 per cent for the isothermal Nusselt number data and 1.0 per cent for the nonisothermal Nusselt number data.

Of the lines of data reported, three per cent were disregarded due to large disagreement with the linear correlation with Δt, and an additional ten per cent were eliminated as being greater than three times the relative standard deviation from the smoothed data. Half of the data eliminated in the latter manner were in four tests: 499, 500, 504, 515, and 520. The others are randomly scattered throughout the remaining tests.

The smoothed Nusselt number fields for the isothermal and nonisothermal cases are presented as Figures 9 and 10 respectively.

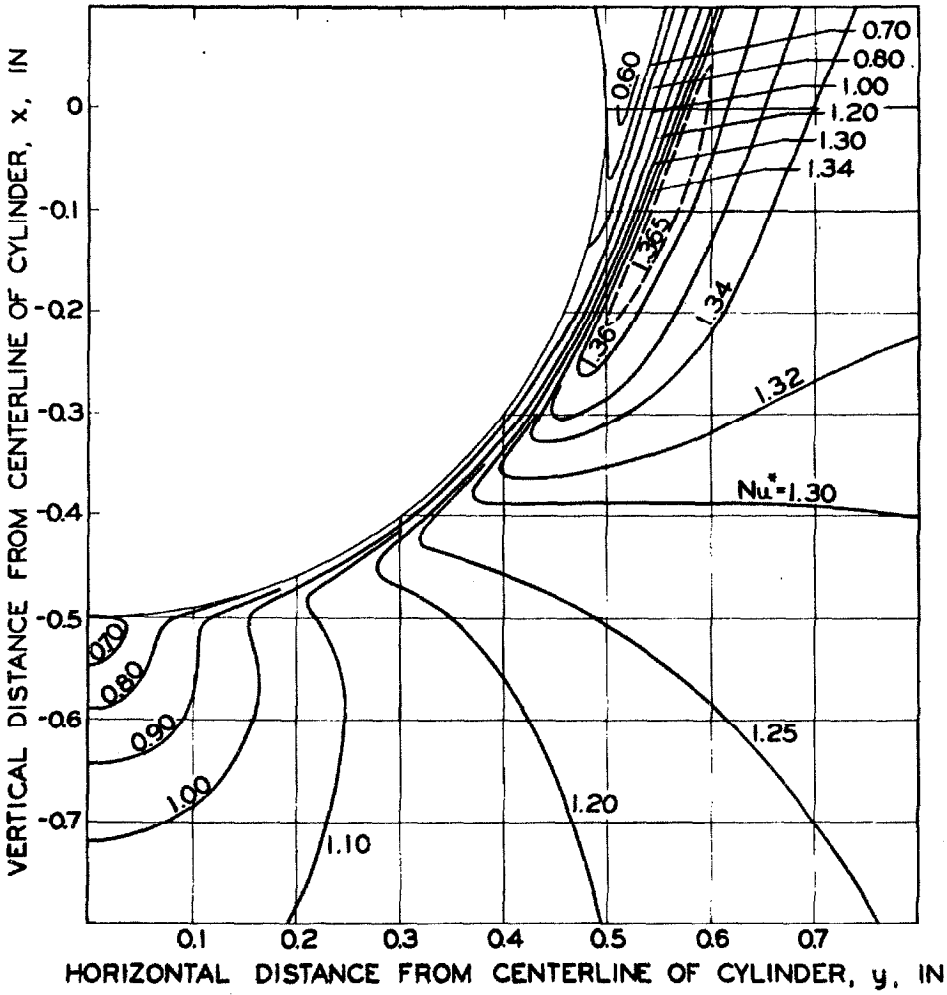

Air Stream:	Flow in Positive Vertical Direction	
	U_∞	= 7.81 ft/sec
	t_∞	= 100° F
Cylinder:	r_o	= 0.4994 in.
	t_c	= 100° F
	$Re_{c,\infty}$	= 3500
Wire:	d_w	= 0.001 in.
	$t_w - t_a$	= 50° F

FIGURE 9. Wire Nusselt Number Contours in the Isothermal Flow about a Cylinder

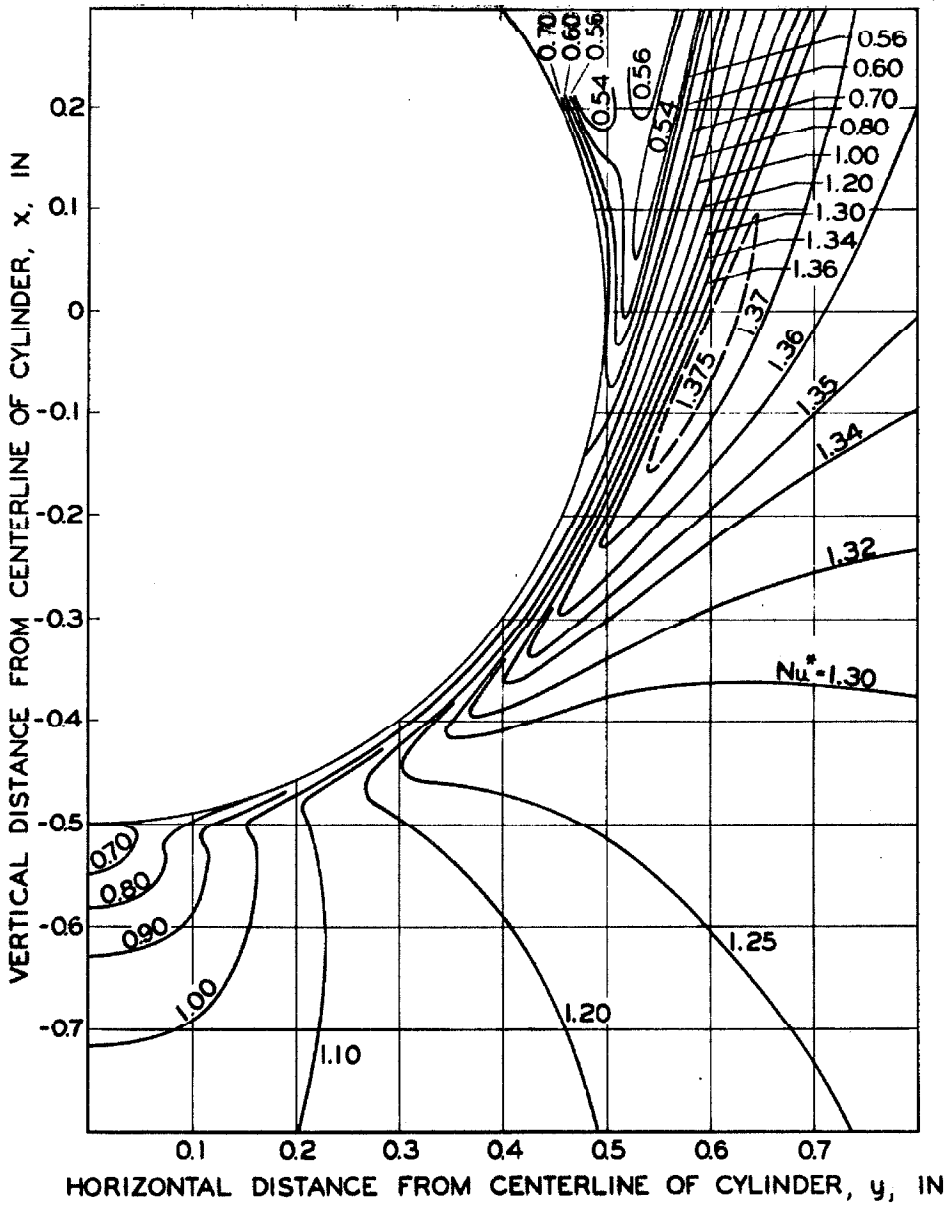

Air Stream: Flow in Positive Vertical Direction
U_∞ = 7.81 ft/sec
t_∞ = 100° F

Cylinder: r_o = 0.4997 in.
t_c = 160° F
$Re_{c,\infty}$ = 3500

Wire: d_w = 0.001 in.
$t_w - t_a$ = 50° F

FIGURE 10. Wire Nusselt Number Contours in the Nonisothermal Flow about a Cylinder

The smoothed temperature field for the nonisothermal case is presented as Figure 11. The measured coordinates were used in the preparation of these figures. The smoothed values near the cylinder are listed in Table VI at 15-degree intervals from stagnation for the experimentally investigated region. Similarly the smoothed values in the air stream around the cylinder are presented in Table VII relative to the cartesian coordinate system.

Both the smoothed and adjusted Nusselt numbers are based on a temperature difference of 50° F. This temperature loading was interpolated with small uncertainties from data at loadings between 40 and 120° F. The data were not extrapolated to a zero temperature loading due to experimental considerations. At a zero temperature loading it can be seen from Equation 31 that the heat transfer ceofficient becomes experimentally indeterminate as both the electrical energy input in the numerator and the temperature difference in the denominator become zero. Therefore, experimental data produces unrealistic Nusselt numbers as a zero temperature loading is approached due to the experimental errors.

Venezian (6) suggested that the Nusselt number based on a thermal conductivity evaluated at one-fourth the temperature loading above the air temperature was almost independent of the temperature loading. Using such an approximation to convert the reported data to a zero temperature loading, the conversion factor would be constant for the isothermal case and vary slightly with the local air temperature for the nonisothermal case.

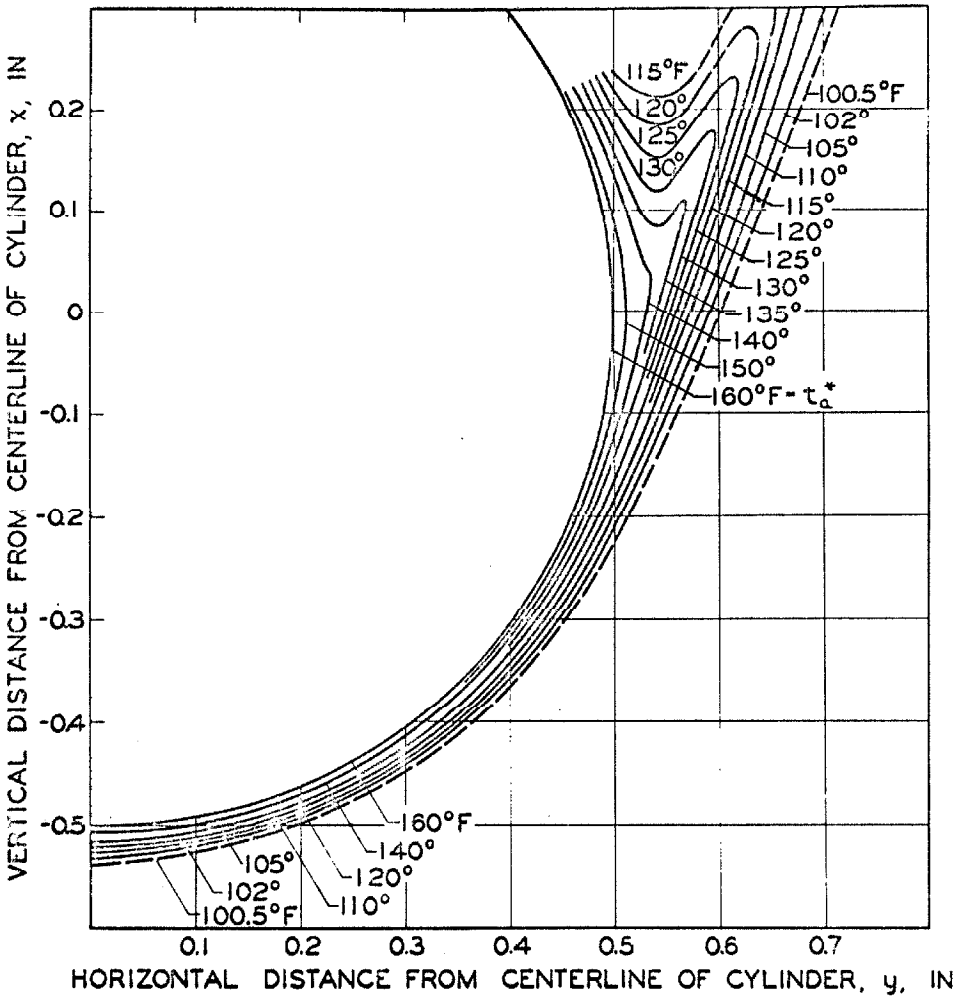

Air Stream: Flow in Positive Vertical Direction

U_∞ = 7.81 ft/sec

t_∞ = 100° F

Cylinder:

r_o = 0.4997 in.

t_c = 160° F

$Re_{c,\infty}$ = 3500

FIGURE 11: Temperature Contours in the Nonisothermal Boundary Flow about a Cylinder

B. Nusselt Number Calibration for the Wire

To obtain the velocity distribution in the jet opening and a calibration of the heat transfer from the wires employed, data were taken at several positions within the air stream at three bulk velocities. The cylinder was removed from the jet opening for these measurements after the relative coordinate system had been established. These data at 6.76, 7.87, and 9.13 feet per second are presented in Table VIII.

Collis and Williams (9) developed the following correlation between the Nusselt numbers from small cylinders for $0.02 < Re_m < 44$ which was presented as Equation 17:

$$Nu_{\ell, \lambda, m} \left(\frac{T_m}{T_z} \right)^{-0.17} = 0.24 + 0.56 \, Re_m^{0.45}$$

A similar calibration was obtained from the author's data.

$$Nu_{\ell, \lambda, m} \left(\frac{T_m}{T_a} \right)^{-0.17} = 0.2768 + 0.5646 \, Re_m^{0.45} \quad (59)$$

In these expressions the dimensionless groups are based on the fluid properties evaluated at the average of the wire and air temperatures. The correlation of the left side of Equation 59 for the experimental data with the 0.45 power of the Reynolds number is presented as Figure 12. The calculated velocity profiles obtained by applying Equations 17 and 59 to the data at 7.87 feet per second is presented as Figure 13.

The slightly higher constant on the right side of Equation 59

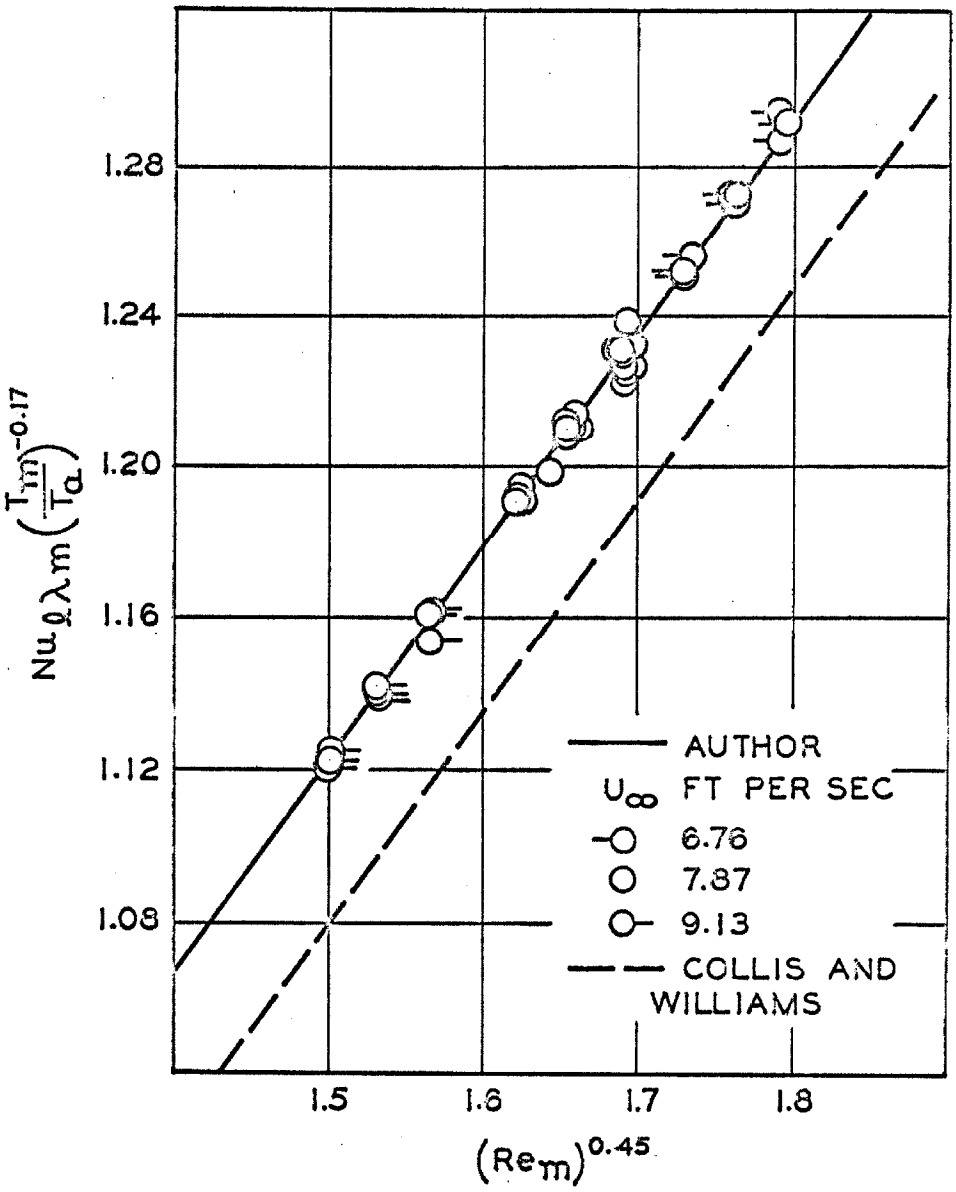

FIGURE 12. Correlations of the Nusselt Number with the Reynolds Number for Small Wires

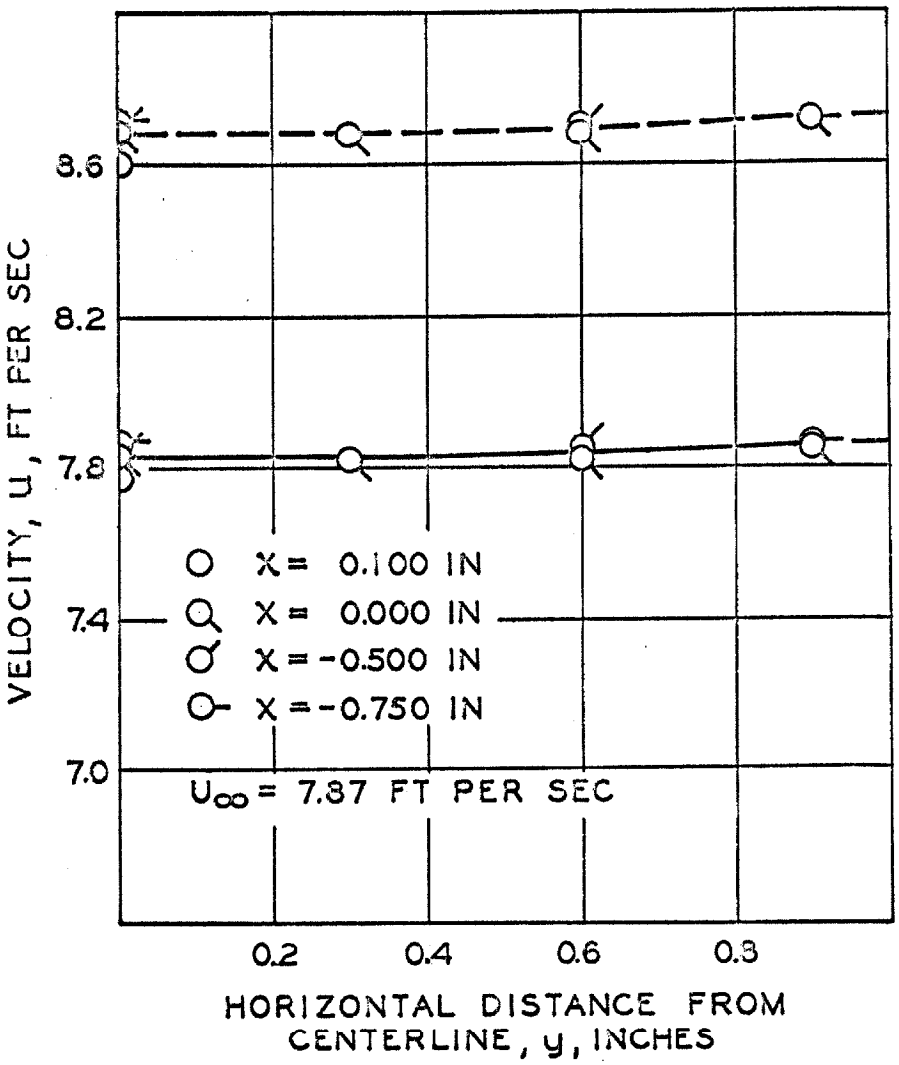

_____ Author's Calibration

-------- Collis and Williams' Calibration

FIGURE 13. Velocity Distribution in the Unobstructed Air Stream Relative to the Coordinates Established Before Removing the Cylinder

compared with Equation 17 could be caused by the small degree of turbulence in the air stream. Measurements in the unobstructed jet opening indicated a 0.7 per cent turbulence level using the Schubaurer (17) method. Variations in the evaluation of the various fluid properties could also account for some of the difference.

The most likely cause of the disagreement between the correlation of the authors and that of Collis and Williams is the buildup of foreign particles noted on the author's wire. These observed data can be adjusted to coincide with the Collis and Williams correlation by using a wire diameter of 1.08 mils in the Reynolds number.

C. Comparison with Theory

Theory predicts that the heat transfer, and therefore the Nusselt number, from a small wire in an air stream will be dependent only upon the fluid velocity except within a few wire diameters of a solid surface. Under the latter circumstances, the relative distance from the surface must also be considered.

In this section a comparison is made between the experimental results and the predicted behavior based on a calculated flow distribution in the boundary layer about the cylinder. Data were not taken sufficiently close to the cylinder to justify more than a superficial discussion concerning the behavior within a few wire diameters of the cylinder.

The velocity and temperature fields predicted for the air flow about the cylinder for the cases investigated were calculated using

the method described by Itō (7) and outlined with Equations 5 through 16. The power for the temperature dependence for the fluid properties, n in Equation 5, was evaluated at 0.8719 from the air thermal conductivity expressed in Equation 21. The following properties were assumed for the 100° F air stream: an air velocity of 7.81 feet-per-second, a total pressure of 14.33 pounds-per-square-foot, and a kinematic viscosity for air of 0.00018592 square-feet-per-second. The ratio of the heat capacities and Prandtl numbers were obtained from NBS Circular 564 (13) for the average boundary layer temperatures.

It was also necessary to assume a velocity distribution around the cylinder at the edge of the boundary layer. Yuge (18) suggested the following equation for $0 \leq \phi \leq \pi/2$ based on agreement with experimental pressure distributions reported by several investigators at Reynolds numbers near 40,000.

$$\frac{u_1}{U_\infty} = 1.81382\,\phi - 0.3511\,\phi^3 - 0.0196\,\phi^5 \qquad (60)$$

Appropriately positioned Nusselt numbers were also selected from the radial plots used for smoothing the experimental data and converted into velocities using the wire calibration presented as Equation 59. A least squares fit of these data produced the following equations for the isothermal, Equation 61, and nonisothermal, Equation 62, cases:

$$\frac{u_1}{U_\infty} = 1.6437\,\phi - 0.5946\,\phi^3 + 0.0938\,\phi^5 \qquad (61)$$

$$\frac{u_1}{U_\infty} = 1.7078\,\phi - 0.6323\,\phi^3 + 0.0988\,\phi^5 \qquad (62)$$

The thickness of the boundary layer was not clearly defined after about 60 degrees from stagnation. Therefore Equations 61 and 62 should only be used up to about 70 degrees. These velocity distributions are compared in Figure 14.

Using Equation 59, the velocity distributions within the boundary layer obtained from these calculations were converted into the corresponding Nusselt numbers, $(Nu_{\ell,\,\lambda,\,a})_{\Delta t=50^\circ F}$, for comparison with the experimental data. The comparison of these results with the experimental data is presented at 15-degree intervals from 15 degrees to 75 degrees from stagnation as Figures 15 through 19. No comparison was made at stagnation since at a velocity of zero in the boundary layer the Nusselt number correlation is not valid due to buoyancy effects.

From Figures 15 through 18 it is apparent that the results of Itō's approximation method with Yuge's velocity distribution predicts the shape of the Nusselt number profile near the edge of the boundary layer. By using Equations 61 and 62 to adjust the velocity at the edge of the boundary layer to fit the experimentally measured Nusselt numbers, the agreement with the calculated distribution within the boundary layer was good from about 0.01 inch from the cylinder to the edge of the boundary layer. It is noticeable even in the latter case, however, that the theory predicted a greater variation between the isothermal and nonisothermal Nusselt numbers at a point than

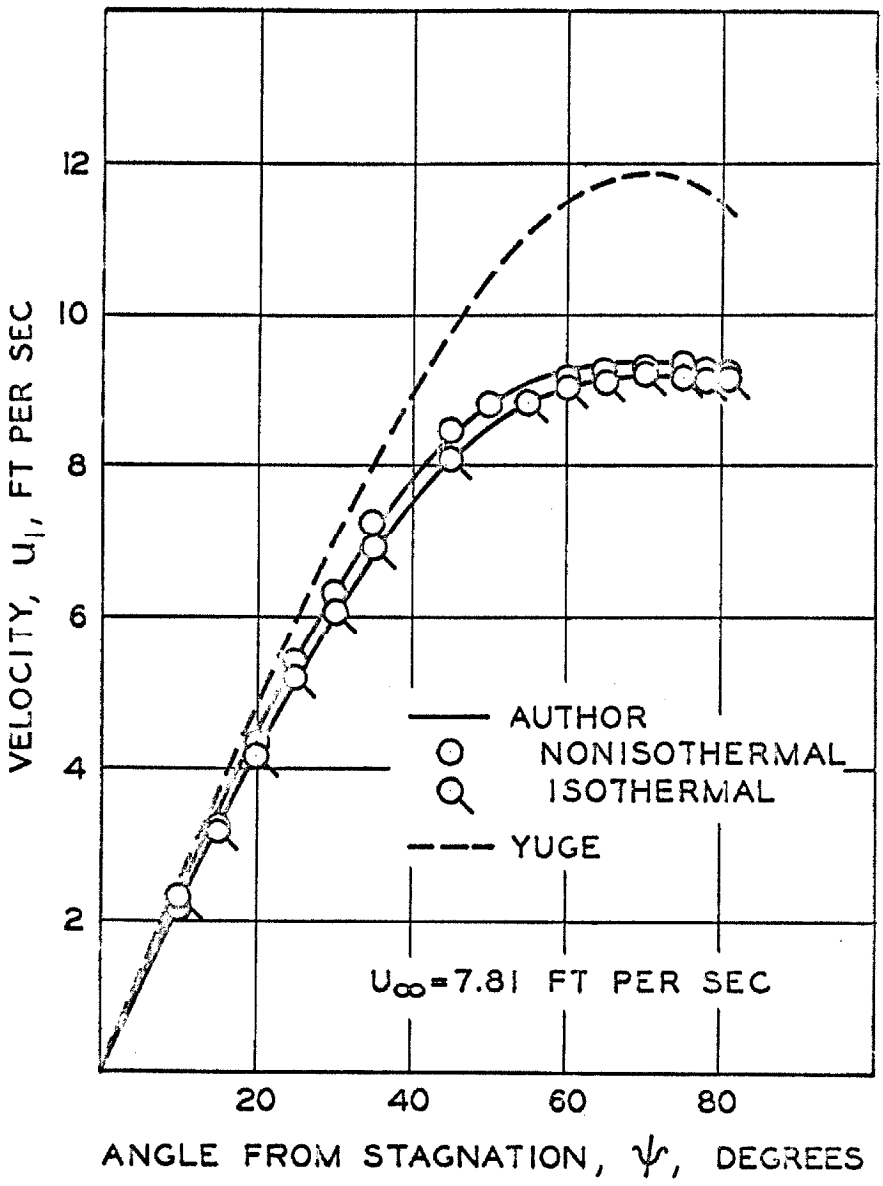

FIGURE 14. Velocity Distributions Around the Cylinder at the Edge of the Boundary Layer

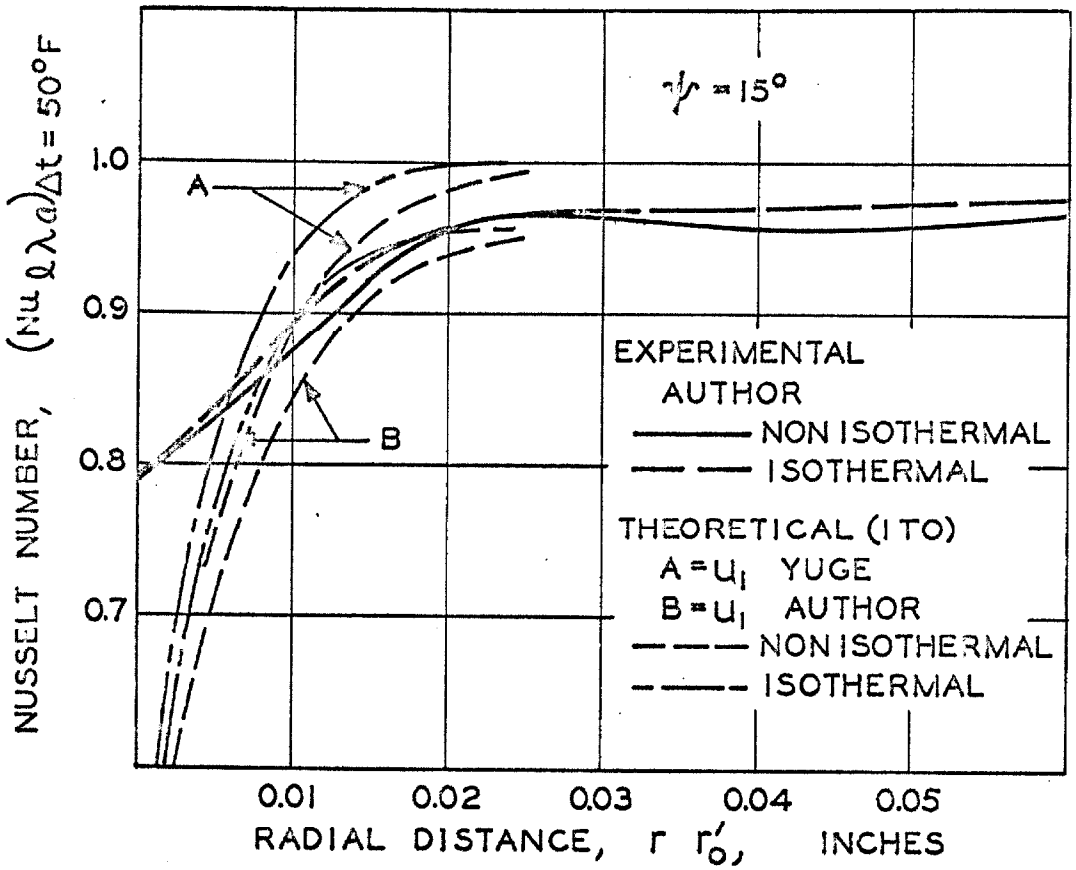

FIGURE 15. Radial Variation of the Nusselt Number for the Wire in the Boundary Flow near the Cylinder at 15 Degrees from Stagnation

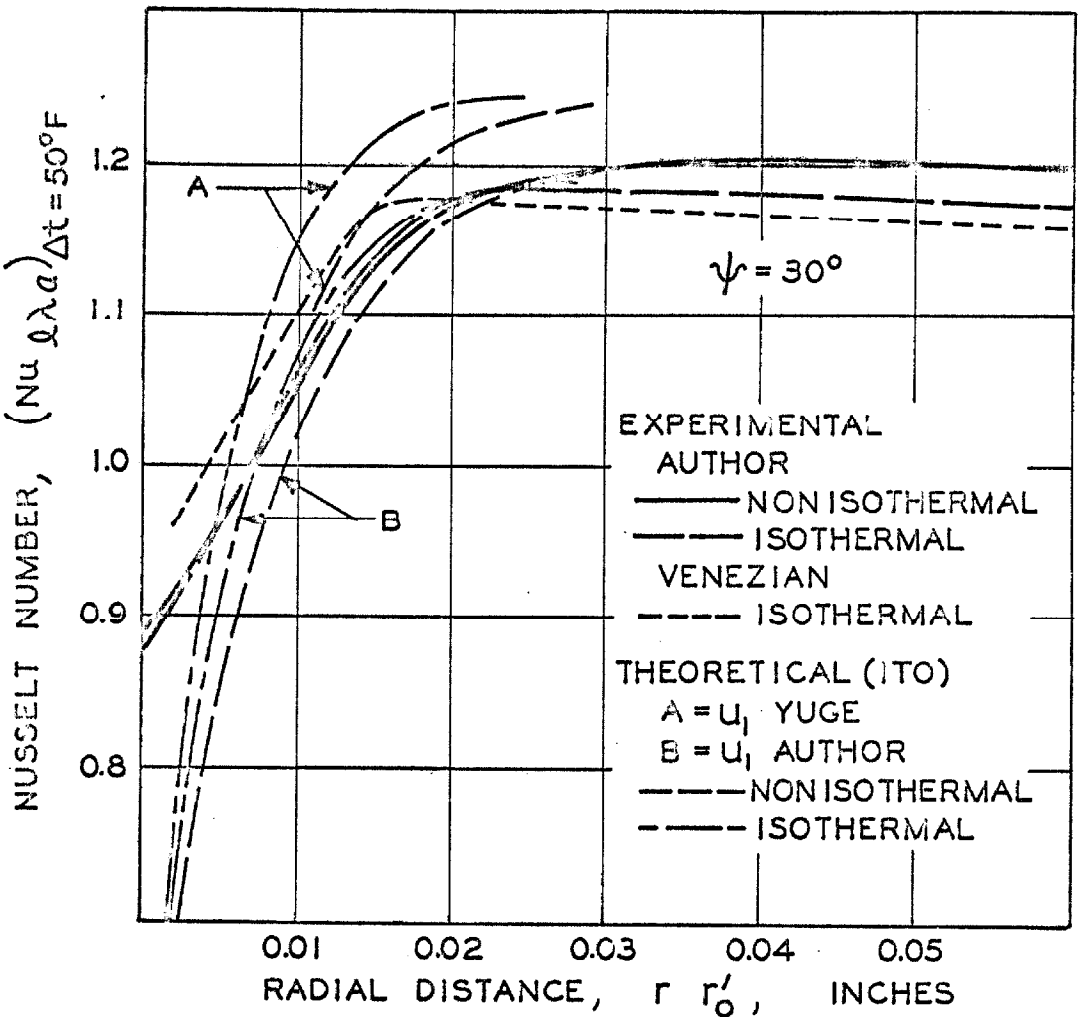

FIGURE 16. Radial Variation of the Nusselt Number for the Wire in the Boundary Flow near the Cylinder at 30 Degrees from Stagnation

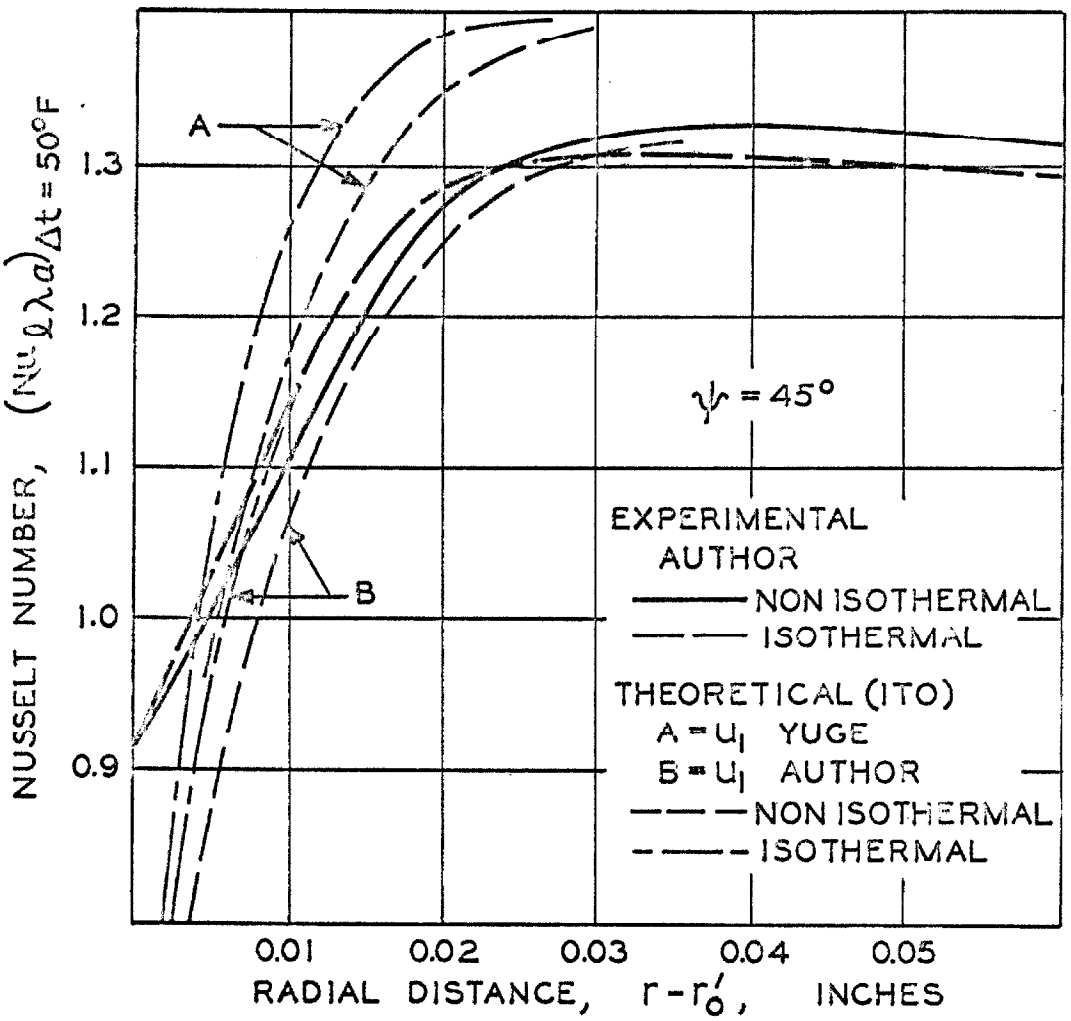

FIGURE 17. Radial Variation of the Nusselt Number for the Wire in the Boundary Flow near the Cylinder at 45 Degrees from Stagnation (The Theoretical Isothermal Curve B Coincides with the Experimental Isothermal Curve Beyond 0.01 Inches from the Surface)

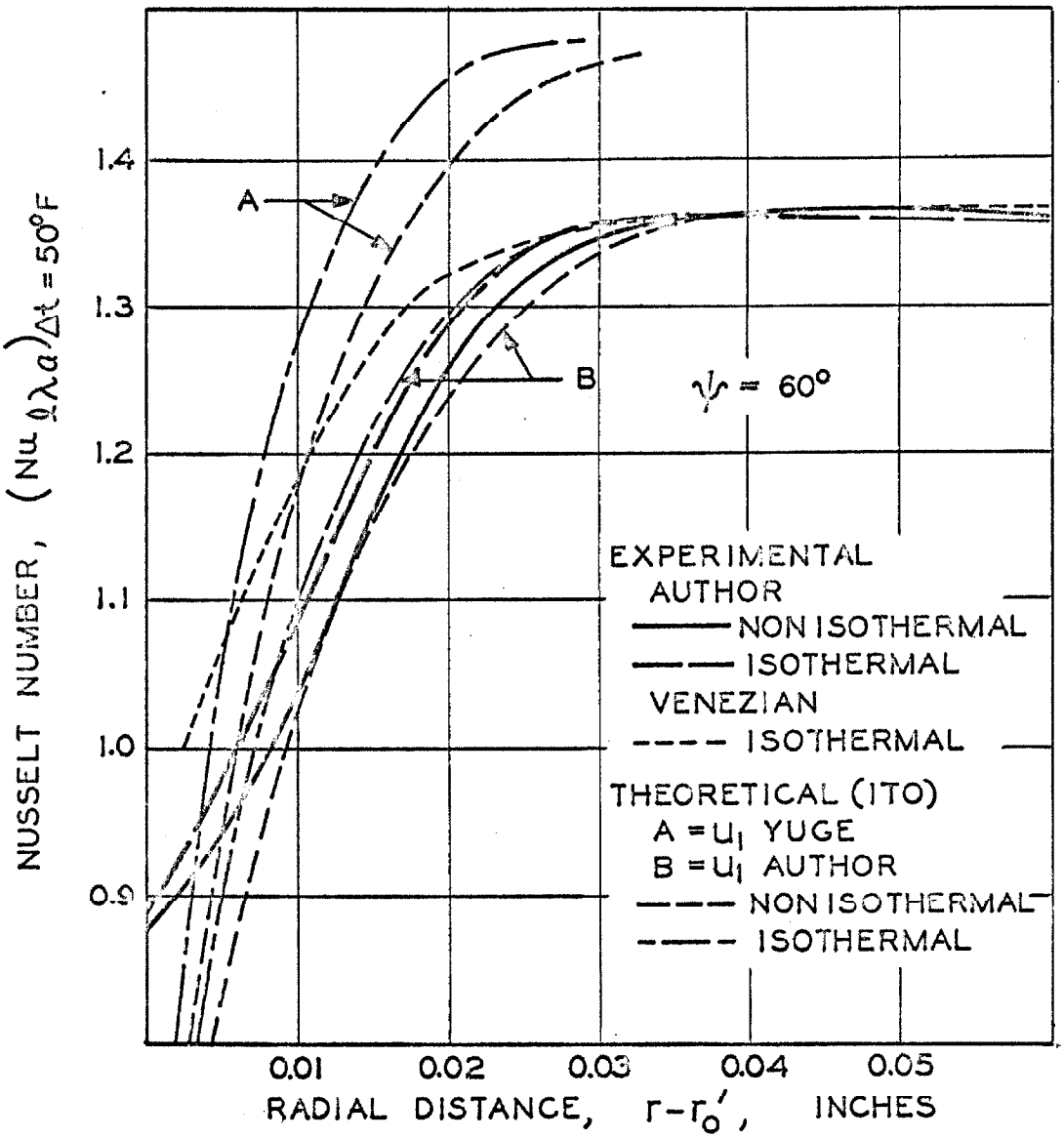

FIGURE 18. Radial Variation of the Nusselt Number for the Wire in the Boundary Flow near the Cylinder at 60 Degrees from Stagnation

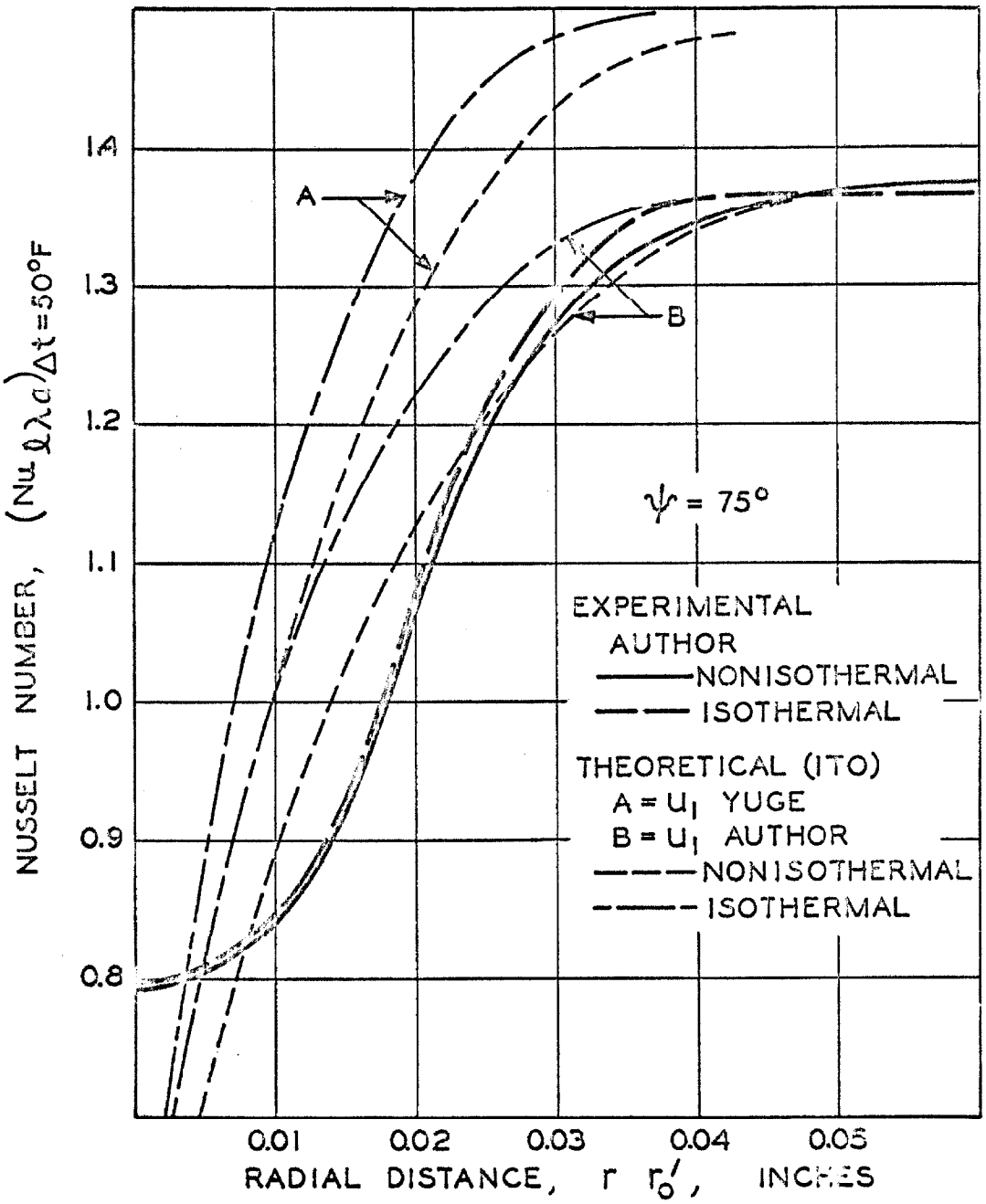

FIGURE 19: Radial Variation of the Nusselt Number for the Wire in the Boundary Flow near the Cylinder at 75 Degrees from Stagnation

was observed experimentally. Viewing this difference as a position phenomenon, the theoretical calculations predicted the nonisothermal curves to be out four or five mils further than the isothermal curves. The experimental curves are between the ones predicted using the author's velocity distribution and have from zero to about two mils separation. For the experimental case, the significance of this separation is questionable due to the experimental uncertainties. Similarly the differences between the experimental and calculated curves for each case also approach the magnitude of the experimental uncertainties. Thus neither the confirmation nor the rejection of these predicted differences by the experimental data is shown. Nevertheless, the magnitude and the observed shape difference were predicted as the edge of the boundary layer was approached. In addition, it should be noted how well the calculated and experimental boundary layer thicknesses agree.

In Figure 19 at 75 degrees from stagnation, the agreement between the calculated and observed curves is poor. Not only does the author's velocity distribution become questionable at this point, but also Itō's approximation solution is known to fail at separation, which is predicted to be between 80 and 82 degrees from stagnation. Furthermore, the smoothing of the experimental data by the graphical techniques used forced sharp but continuous curves through the data in this region. This required a more gradual development of the separation phenomenon than if discontinuities had been incorporated in either the curves or their partial derivatives. Therefore, the

departure between the predicted and calculated curves in this region is not alarming.

The measured Nusselt numbers were extrapolated to the cylinder during the smoothing process. The dashed electrical contact curve in Figure 8 indicates the limit at which data could be obtained relative to the surface of the cylinder. The closest points on nearly all traverses indicated an inflection point in the traverse Nusselt number curves. For the extrapolation to the surface in the smoothing process, the reverse bend of the curve was started and then straightened as the cylinder was approached. Based on the mathematical model by Piercy, Richardson, and Winny (4) which is expressed through Figure 1 for the Nusselt number from a wire in the boundary flow next to a flat plate, the experimental curves should have been sharpened more and made asymptotic to the surface of the cylinder. Such an extrapolation would probably have been a better fit for the points closest to the cylinder than the one indicated in Figures 15 through 19. It should be noted, however, that the expected uncertainties for these close points are much greater than the other points due not only to the multiplication of the fluctuations and oscillations observed, but also to their lower numerical values. Therefore, only the reverse trend indicated by these points was incorporated, not the full significance of the extremely sharp change.

Contrary to the curves indicated in Figure 1, however, the minimum adjusted Nusselt number observed before separation was 0.6 on the curve at stagnation.

The smoothed experimental Nusselt number distributions presented by Venezian (5, 6) were also included on Figures 16 and 18. He used the same equipment for his measurements as the author. Since his investigations several small improvements have been made in taking the hot-wire measurements, and the determination of the relative positions between the cylinder and the wire have been greatly improved. Venezian established the position of the cylinder on the wire traversing scales by observing through the telescope the points of contact of the wire with the surface of the cylinder at several positions between 75 and 105 degrees from stagnation. Graphical techniques were employed to deduce the position of the cylinder axis from these data. Once determined, this position was assumed applicable for several weeks' runs. During the author's investigation, daily measurements and checks were made of the position of the cylinder. It was found that the position shifted due to vibrations throughout the laboratory. This most likely explains the large disagreements, up to ten per cent of the Nusselt number or 0.005 inches in position, between the author's and Venezian's smoothed data within the boundary layer, and reasonable agreement of these data outside the boundary layer where position errors have very little effect.

The variations between the observed and calculated temperature distributions are indicated in Figures 20 and 21. The reasonable prediction of the thermal boundary layer thickness regardless of which velocity distribution was assumed is reassuring. At stagnation

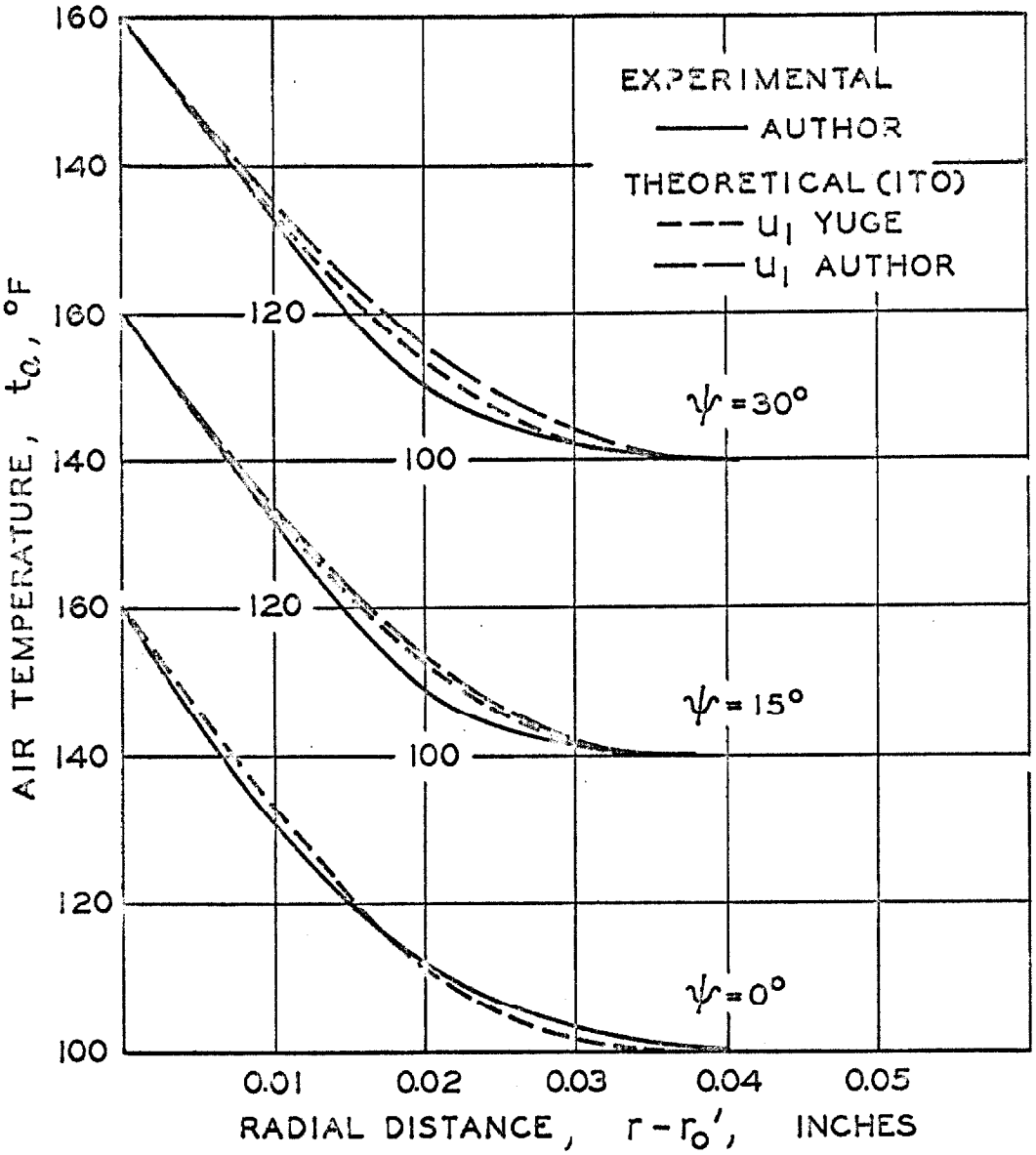

FIGURE 20. Radial Temperature Distribution in the Boundary Layer about the 160° F Cylinder at 0, 15, and 30 Degrees from Stagnation

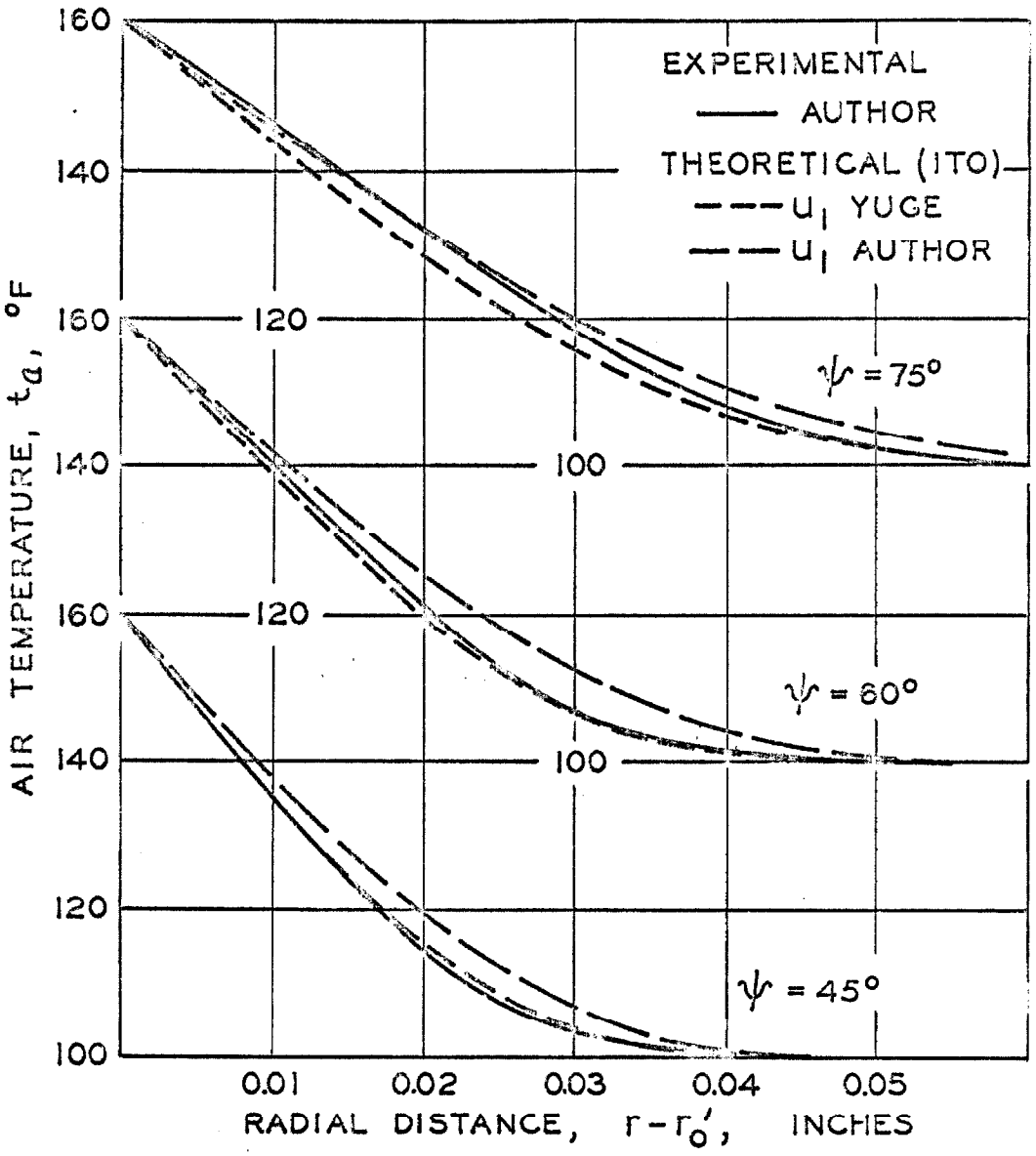

FIGURE 21. Radial Temperature Distributions in the Boundary Layer about the 160° F Cylinder at 45, 60, and 75 Degrees from Stagnation

the predicted velocity distributions are identical. The temperature distributions using Yuge's velocities expressed in Equation 60 apparently gave better agreement with the experimental curves than those using the velocities of Equation 62. However the disagreement with the latter is consistent. There appears to be a fundamental difference in the shape of the temperature distribution between the experiment and the calculations. When compared with the calculated curves, the experimental data indicated that the temperature profile remained straighter in the velocity boundary layer, bent more sharply near the edge of the velocity boundary layer, and then tapered more gradually to the air stream temperature at the edge of the thermal boundary layer. This indicates that the predicted temperature curve through the thermal boundary layer, Equation 16, could be improved for the case where the velocity boundary layer is smaller than the thermal boundary layer. This shape discrepancy probably explains why Yuge's velocity profile with its larger values produced a better fitting temperature distribution than the author's velocity profile.

D. Heat Transfer from the Cylinder

Although the heat input to the cylinder or any portion thereof was not measured directly, the local heat transfer from the cylinder can be obtained from the observed and calculated temperature gradients in the air stream. This relationship is expressed in Equation 63, and converted into a Nusselt number in Equation 64.

$$h_c = \frac{-k_c}{(t_c - t_\infty)} \left(\frac{\partial t_a}{\partial r}\right)_{r'_o} \tag{63}$$

$$Nu_{c,\infty} = \frac{2h_c r_o}{k_\infty} = \frac{-2k_c r_o}{k_\infty (t_c - t_\infty)} \left(\frac{\partial t_a}{\partial r}\right)_{r'_o} \tag{64}$$

Knudsen and Katz (19) presented the following empirical equation for evaluating the local Nusselt number from the cylinder in the region from stagnation to 80 degrees:

$$Nu_{c,\infty} = 1.14(Pr)^{0.4}(Re)^{0.5}\left[1 - \left(\frac{\psi}{90}\right)^3\right] \tag{65}$$

Figure 22 presents the local Nusselt numbers from the cylinder obtained from the measured and calculated temperature distributions compared with those which were correlated empirically. The various curves show reasonable agreement with the author's measurements.

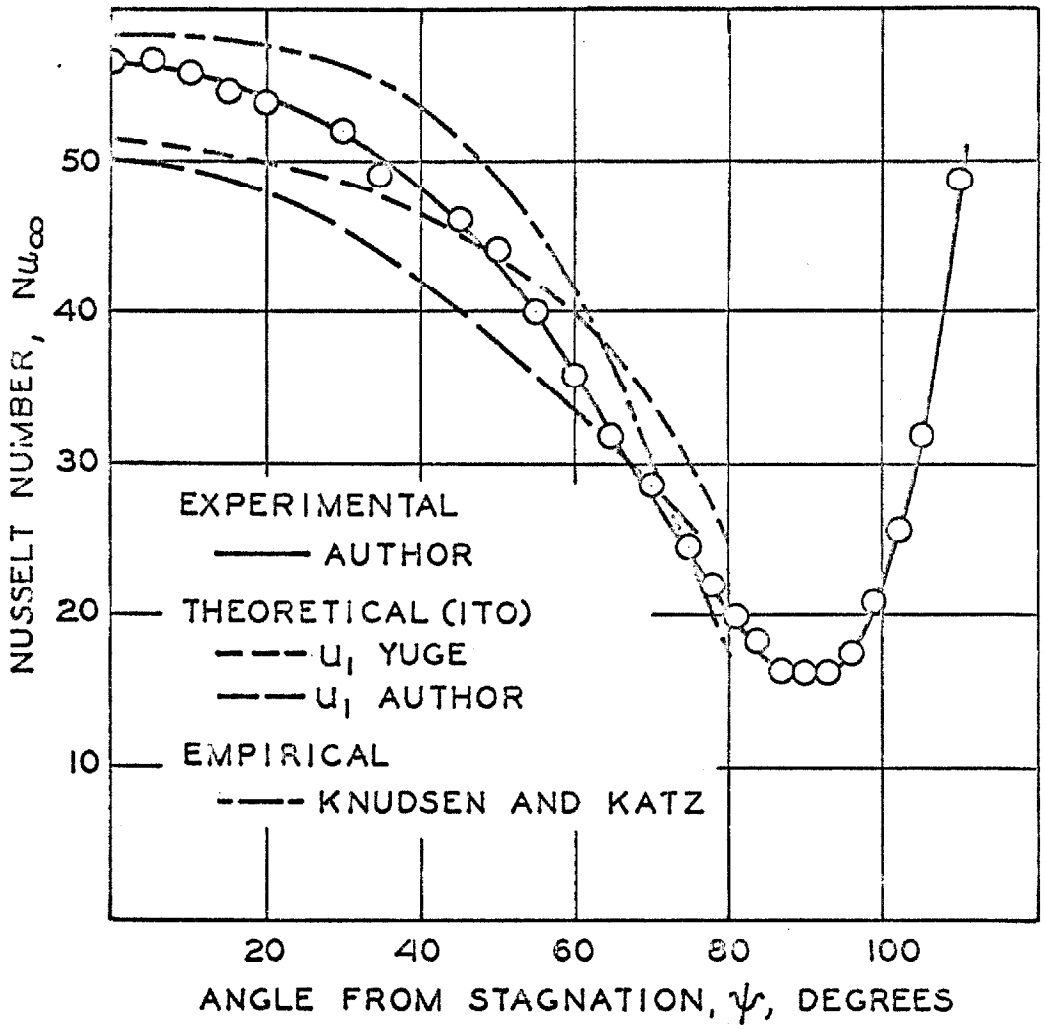

FIGURE 22. Local Nusselt Numbers for a 160° F Cylinder Normal to a 100° F, 7.81-foot-per-second Air Stream

VI. SUMMARY

A. Experiment

Experimental heat transfer measurements have been presented for a 0.001-inch diameter wire in isothermal and nonisothermal air flows about a 1-inch cylinder. The 100° F, 7.81-foot-per-second air stream was normal to the cylinder to give a Reynolds number of about 3500. The cylinder was maintained at 100° F for the isothermal case and heated to 160° F for the non-isothermal case. The wire was aligned parallel to the cylinder. Measurements were taken for several temperature loadings at a number of points within the forward portion of the air flow about the cylinder. The measured heat transfer from the wire was expressed as a Nusselt number and corrected for the effects of the length of the wire and the temperature discontinuity in the air stream at its surface (9). These corrected Nusselt numbers were interpolated to a local wire temperature loading of 50° F. The adjusted Nusselt numbers were smoothed throughout the boundary flow using graphical techniques. A similar process was used to smooth the temperature field in the nonisothermal boundary layer.

These experimental results of the heat transfer from small wires in the isothermal and nonisothermal boundary flows about a cylinder are of interest due to their correlation with the local fluid velocities. As such they are of considerable value as a reference for evaluating the quantitative accuracy of the various approximate theoretical solutions to this particular flow situation.

B. Comparison With Theory

The radial Nusselt number distributions based on the velocity and temperature distributions calculated from an approximate solution presented by Itō (17) of the boundary layer continuity, energy, and momentum equations were compared with the smoothed experimental values. For these calculations the heat transfer from the wire was assumed to depend only upon the local air flow. This assumption gave reasonable agreement with the observed values beyond ten wire-diameters from the cylinder if the velocity distribution around the cylinder at the edge of the boundary layer corresponded with the experimental data. The general behavior of the Nusselt numbers, but not their magnitudes, was obtained using a velocity distribution based on pressure measurements at a Reynolds number of 40,000 (18). A comparison of the observed and calculated temperature gradients in the boundary layer indicated that the radial temperature distribution equation should be changed slightly for the cases where the velocity thickness is less than the thermal thickness.

As the cylinder is approached, Piercy, Richardson, and Winny (4) predicted that the Nusselt number from the wire should tend toward infinity due to the conduction between them. This is a predicted deviation from an extrapolation to the Nusselt number for a zero Reynolds number at the surface. The onset of this deviation was noted, but data could not be obtained sufficiently close to the surface to confirm the predicted trend toward infinity.

C. Conclusions

1. Experimental data and smoothed values for the Nusselt number for a small wire in the isothermal and the nonisothermal boundary flows about a cylinder at a Reynolds number of 3,500 are presented with a maximum uncertainty of 1.5 per cent and an uncertainty of one mil in relative position. The experimental data are presented in Tables III through V, the smoothed values in Tables VI and VII, and the Nusselt number and temperature fields through Figures 9 through 11.
2. The isothermal Nusselt number field presented is displaced by up to five mils in the boundary layer relative to the data presented by Venezian (5, 6) due to a significant improvement in the determination of the relative positions of the wire and the cylinder. These two sets of data agree in the free stream where such positions errors are not important.
3. The nonisothermal boundary layer is slightly thicker than the isothermal boundary layer as indicated by the small outward radial displacement of the nonisothermal Nusselt number data.
4. With reasonable accuracy, the heat transfer from a small wire at distances greater than 10 wire-diameters from the cylinder surface may be assumed to be a function of only the two-dimensional flow normal to it.
5. The velocity distribution at the edge of the boundary layer about the cylinder suggested by Yuge (18) based on pressure measurements at a Reynolds number of 40,000 is not appli-

cable for the vertical flow about a cylinder at a Reynolds number of 3,500.

6. The indicated radial heat transfer from the surface of the cylinder is in reasonable agreement with the empirical correlation of other experimental data presented by Knudsen and Katz (19) for angles from stagnation up to 80 degrees.

Based on the comparison of the behavior indicated using Itō's (7) method of calculation with the observed Nusselt number behavior, the following conclusions were drawn:

7. The velocity distributions predicted by Itō's (7) approximate method of solution for the boundary layer equations for both the isothermal and nonisothermal cases were confirmed by the experimental measurements up to 70 degrees from stagnation.

8. The radial temperature distribution function used in Itō's solution could be revised to better predict the situation where the velocity thickness of the boundary layer is smaller than the temperature thickness. The experimental measurements indicated that in the region of large radial variation of the velocity, the radial temperature gradient across the boundary layer was greater than predicted by Itō's solution.

From the comparison of the experimental results with the predicted Nusselt-number behavior within several wire-diameters of the cylinder as reported by Piercy, Richardson, and Winny (4),

the following conclusions were drawn:

9. Data were not taken sufficiently close to the surface of the cylinder to confirm the predicted asymptotic increase in the Nusselt number toward infinity as the surface was approached radially.

10. The proximity of the solid surface affected the wire's Nusselt number starting at about 10 wire-diameters distance from the surface rather than the predicted 5 wire-diameters distance.

11. The limiting wire Nusselt number at stagnation (zero Reynolds number for the wire) is on the order of 0.6 rather than 0.2.

VII. REFERENCES

1. Hinze, J. O.,
   Turbulence. New York: McGraw-Hill Book Co., Inc. (1959).

2. Kovasznay, L. S. G.,
   "Turbulence Measurements," Physical Measurements in Gas Dynamics and Combustion. Edited by R. W. Ladenburg. Princeton: Princeton University Press. (1954).

3. Short, W. W. and B. H. Sage,
   "Temperature Measurements in a Spherical Field: Transfer Coefficients and Corrections for Thermocouples in Boundary Flows," A. I. Ch. E. Journal, Vol. 6, pp. 163-167. (1960).

4. Piercy, N. A., E. G. Richardson, and H. F. Winny,
   "On the Convection of Heat from a Wire Moving through Air Close to a Cooling Surface," Proceedings of the Physical Society (London), Vol. 69B, pp. 731-742. (1956).

5. Venezian, Emilio and B. H. Sage,
   "Thermal Transfer from a Small Wire in the Boundary Flow about a Cylinder," International Journal of Heat and Mass Transfer, Vol. 5, pp. 225-237. (1962).

6. Venezian, E. C.,
   "Part II. Thermal Transfer from Small Wires in the Boundary Flow about a Cylinder," Unpublished Ph. D. dissertation, California Institute of Technology. (1962).

7. Itō, Hidesato,
   "An Approximate Method of Solution of the Compressible Laminar Boundary Layer with Heat Transfer," Reports of the Institute of High Speed Mechanics, Tohoku University (Sendai, Japan), Vol. 4, No. 32, pp. 11-36. (1954).

8. Bird, R. G., W. E. Stewart, and E. N. Lightfoot,
   Transport Phenomena. New York: John Wiley and Sons. (1960).

9. Collis, D. C. and M. J. Williams,
   "Two-Dimensional Convection from Heated Wires at Low Reynolds Numbers," Journal of Fluid Mechanics, Vol. 6, pp. 357-384. (1959).

10. Cole, J., and A. Roshko,
    "Heat Transfer from Wires at Reynolds Numbers in the Oseen Range," Proceedings of the Heat Transfer and Fluid Mechanics Institute. (University of California at Berkeley, June 30 - July 2, 1954), pp. 13 - 23.

11. Corcoran, W. H., F. Page Jr., W. G. Schlinger, and B. H. Sage, "Temperature Gradients in Turbulent Gas Streams, Methods and Apparatus for Flow Between Parallel Plates," Industrial and Engineering Chemistry, Vol. 44, pp. 410-419. (1952).

12. Hsu, N. T., and B. H. Sage, Thermal and Material Transfer in Turbulent Gas Streams. Local Transport from Spheres. Document No. 5311. American Documentation Institute, Library of Congress, Washington D. C. (1957).

13. National Bureau of Standards, Tables of Thermal Properties of Gases. Circular No. 564. National Bureau of Standards, Washington D. C. (1955).

14. Holm, R. and R. Störmer, "Measurement of the Heat Conductivity of a Platinum Test Piece in the Temperature Region 19 - 1020°," Wissenschafliche Veroeffentlichichungen aus dem Siemes-Konzern, Vol. 9, pp. 312-322. (1930). [Chemical Abstracts, Vol. 25, p. 23^2, (1931)].

15. Carslaw, H. S. and J. C. Jaeger, Conduction of Heat in Solids. 2nd ed. London: Oxford University Press. (1959).

16. Kennard, E. H., Kinetic Theory of Gases. New York: McGraw-Hill Book Co., Inc. (1938).

17. Schubauer, G. B., A Turbulence Indicator Utilizing the Diffusion of Heat. Report No. 524. National Advisory Committee for Aeronautics, Washington D. C. (1935).

18. Yuge, T., "Theory of Distributions of the Coefficients of Heat Transfer of Two Dimensional Bodies of Various Shapes," Reports of the Institute of High Speed Mechanics, Tohoku University (Sendai, Japan), Vol. 6, No. 58, pp. 153-173. (1956)

19. Knudsen, James G. and Donald L. Katz, Fluid Dynamics and Heat Transfer. New York: McGraw-Hill Book Co., Inc. (1958).

VIII. NOMENCLATURE

A. Roman Type Symbols

A	Area of jet opening, sq ft.
a	Coefficient for the linear temperature dependence of the resistance of the wire per unit length, $(^{o}F)^{-1}$. (See equations 34 and 35).
a_{∞}	The velocity of sound in air evaluated at the bulk air stream conditions, ft/sec.
b	Specific gas constant for air, (ft, lb-force)/(lb-mass, ^{o}R).
C	A constant in Equation 50, dimensionless.
c_p	Heat capacity of air at constant pressure, Btu/lb-mass.
c_v	Heat capacity of air at constant volume, Btu/lb-mass.
cosh	Hyperbolic cosine function, dimensionless.
d_w	Diameter of the wire, ft.
E_s	Potential drop across the fixed resistor, volts.
E_w	Potential drop across the wire, volts.
$\bar{g}$	Gravitational force vector, ft/sec^2.
g_c	Conversion factor = 32.174 (ft, lb-mass)/(lb-force, sec^2).
g_o	Local acceleration due to gravity, ft/sec^2.
h	Heat transfer coefficient, Btu/(ft^2, sec, ^{o}F).
I	Current through the wire and fixed resistor, amps.
k	Thermal conductivity of air, Btu/(sec, ft, ^{o}F).
k_s	Thermal conductivity of the platinum wire, Btu/(sec, ft, ^{o}F).
ℓ	Length of wire, ft.
$\log_{10}$	Logarithm function to the base 10, dimensionless.
$\dot{m}$	Mass flow rate of air through the Venturi, lb-mass/sec.

n	Exponential power for the fluid property dependence upon temperature, dimensionless. (See Equation 5).
Nu	Nusselt number from the wire = hd_w/k, dimensionless.
Nu^*	Smoothed $(Nu_{\ell, \lambda, a})_{\Delta t=50^\circ F}$, dimensionless.
Nu_c	Local Nusselt number from the cylinder at a particular radial position, dimensionless. (See Equation 63).
p	Air pressure, lb-force/sq ft.
Pr	Prandtl number for air = $c_p\mu/k$, dimensionless.
$\dot{q}_e$	Electrical energy input rate to the wire, Btu/sec.
R	Total electrical resistance of the wire, absolute ohms.
R_o	Total electrical resistance of the wire at the ice point (32° F), absolute ohms.
R_s	Electrical resistance of the fixed resistor, absolute ohms.
r	Radial distance from the axis of the cylinder, ft.
r_o	Radius of the cylinder at a aprticular temperature from micrometer measurements, ft.
r_o'	Radial position of the surface of the cylinder relative to the axis of the cylinder as observed on the measuring coordinate system at a particular angular position, ft.
Re	Reynolds number for the flow about the wire = $d_w u/\nu$, dimensionless.
Re_c	Reynolds number for the flow about the cylinder = $2r_o U_\infty/\nu$, dimensionless.
s	A variable defined by Equation 44, dimensionless.
T	Absolute temperature, $^\circ R$.
t	Temperature, $^\circ F$.
t_a^*	Smoothed or adjusted (see Equation 58) air temperature, $^\circ F$.
$\tanh$	Hyperbolic tangent function, dimensionless.
U_∞	Bulk velocity of air stream, ft/sec.

u — Local air velocity parallel to surface of cylinder, ft/sec.

$\bar{u}$ — Local air velocity vector, ft/sec.

X — Distance from stagnation along the surface of the cylinder, ft/sec.

X_* — A function of the angle from stagnation defined by Equation 8, ft.

x — Measured vertical coordinate distance of the wire above the axis of the cylinder, in.

Y — Normal distance from the surface of the cylinder, ft.

Y_* — A function of the normal distance from the surface of the cylinder at a particular angular position defined by Equation 9, ft.

y — Measured horizontal coordinate distance of the wire from the axis of the cylinder, in.

Z — A function of the angular position defined in Equation 11, sec.

z — Distance along the length of the wire from its middle, ft.

B. Greek Type Symbols

α — Accommodation coefficient of the surface for the particular gas, dimensionless.

β — The fractional change of the hot-wire resistance relative to that at the local air stream temperature, dimensionless.

γ — Ratio of the specific heat of air at constant pressure to that at constant volume = c_p/c_v, dimensionless.

δ_* — Velocity boundary layer thickness in terms of Y_*, ft.

δ'_* — Thermal boundary layer thickness in terms of Y_*, ft.

Δt — Temperature difference between the average hot wire and local air stream temperatures = $t_w - t_a$, $^{\circ}F$.

η — Viscosity of air in force units, (lb-force, sec)/sq ft.

θ — Time, sec.

λ — Mean free path of air molecules, defined by Equation 51, ft.

λ — A function of the angular location from stagnation defined by Equation 11, used in Equations 11 through 16, dimensionless.

λ_* — A function of the angular position from stagnation as defined by Equation 12, dimensionless.

u — Viscosity of air in mass units, lb-mass/sq ft.

ν — Kinematic viscosity of air = η/ρ, sq ft/sec.

ξ — Temperature jump distance defined by Equations 49 and 50, ft.

π — 3.141596... .

ρ — Density of air = σ/g_o, (lb-mass, sec^2)/ft^4.

σ — Specific weight of air, lb-mass/cu ft.

$\bar{\bar{\tau}}$ — Shear tensor, lb-force/sq ft.

τ_{ii} — Diagonal components of the shear tensor, lb-force/sq ft.

τ_{ij}, τ_{ji} — Off diagonal components of the shear tensor, lb-force/sq ft.

ϕ — Angle from stagnation, radians.

χ — The ratio of the velocity boundary layer thickness to the thermal boundary layer thickness = δ_*/δ_{t_*}, dimensionless.

ψ — Angle from stagnation, degrees.

C. Subscripts

a — Evaluated at, or based on the properties evaluated at, the local air stream temperature.

ai — Evaluated at, or based on the properties evaluated at, the extrapolated air side interface temperature at the surface of the wire.

c — From the surface of the cylinder, or based on the properties evaluated at the surface of the cylinder (g_c specifically defined in Section A).

e — Due to the electrical energy source.

i, j, k	The three orthogonal coordinates of particular interest. Used in vector, tensor, and dyadic notation.
ℓ	Corrected to that of a wire of infinite length.
M	Based on the properties evaluated at the mean temperature between those of the cylinder and the bulk air stream.
m	Based on the properties evaluated at the mean temperature between the average hot-wire temperature and the local air stream temperature.
o	See g_o, R_o, r_o, and r_o' definitions.
p	At constant pressure.
s	See E_s, k_s, and R_s definitions.
v	At constant volume.
w	Based on the properties evaluated at the average hot-wire temperature.
1	Evaluated at the "edge of the boundary layer."
∞	Based on the bulk air stream properties or conditions.
λ	Corrected for the temperature discontinuity at the surface of the wire.

D. Operators

$\frac{D}{D\theta}$	Substantial derivative operator.
d	Total derivative operator.
∂	Partial derivative operator.
$\int$	Integral operator.
∇F	Gradient of a scalar F.
$\nabla^2 F$	Laplacian of a scalar, $F = \nabla \cdot (\nabla F)$
$\nabla \cdot \overline{F}$	Divergence of a vector, $\overline{F}$.
$[\nabla \cdot \overline{\overline{F}}]$	Divergence of a dyadic, $\overline{\overline{F}}$.
$\overline{\overline{S}} : \overline{\overline{F}}$	Scalar product of two dyadics, $\overline{\overline{S}}$ and $\overline{\overline{F}}$.

IX. TABLES

TABLE I

Micrometer Measurements of the Diameter of the One-Inch Diameter Cylinder at 80° F

Angle from Stagnation, degrees	Cylinder Diameter, inches		
	North[a]	Middle[a]	South[a]
0	0.9982	0.9985	0.9987
30	0.9982	0.9984	0.9986
60	0.9983	0.9984	0.9985
90	0.9986	0.9985	0.9986
120	0.9986	0.9987	0.9987
150	0.9984	0.9986	0.9987

[a]Longitudinal position relative to the one-and-one-quarter inch section on the cylinder adjacent to the probe.

TABLE II

Estimated Maximum Uncertainties for the Nusselt Number Measurements Within the Boundary Layer

1.	Electrical energy input:		0.1% of Nu
	a. E_w fluctuations	0.02% of $\dot{q}$	
	b. E_s fluctuations	0.01%	
	c. R_s calibration	0.01%	
	d. Standard cell difference	0.06%	
		0.10% of $\dot{q}$	
2.	Temperature difference term: ($\Delta t = 50\ F^o$)		1.0% of Nu
	a. E_w fluctuations	0.02% of R_w	
	b. E_s fluctuations	0.01%	
	c. R_s calibration	0.01%	
		0.04% of R_w, or 0.2 F^o in t_w	
	d. R_a fluctuations	0.03% of R_a, or 0.15 F^o in t_a	
	e. Stream stability	0.15 F^o in Δt / 0.5 F^o in Δt	
3.	Length of wire:	0.2% of ℓ	0.2% of Nu
4.	Corrections for finite length and temperature discontinuity at the surface of the wire:		0.1% of Nu
			1.5% of Nu
5.	Position at the centerline of the cylinder:		±0.001 in. for x
			±0.001 in. for y

TABLE III

Summary of the Experimental Operating Conditions

Test	Date	Wire No.	Pressure psia	Weight Fraction Water	Air Stream Temperature °F	Cylinder Temperature °F	Gross Air Velocity ft/sec	Gross Reynolds Number
406	9/15/61	5	14.29	0.0123	100.99	160.13	7.96	3541
407	9/18/61	5	14.28	0.0102	101.01	160.48	7.89	3512
411	10/12/61	5	14.32	0.0077	100.65	159.90	7.84	3502
499	8/9/62	7	14.31	0.0151	100.08	100.26	7.80	3468
500	8/16/62	7	14.29	0.0130	100.02	160.38	7.81	3473
502	9/5/62	7	14.28	0.0091	100.04	160.70	7.82	3484
504	9/7/62	7	14.27	0.0116	100.02	160.50	7.86	3497
505	9/18/62	7	14.27	0.0119	100.00	99.89	7.85	3487
508	10/18/62	7	14.28	0.0095	100.02	160.64	7.88	3507
510	11/8/62	7	14.31	0.0085	99.94	160.15	7.99	3504
511	11/14/62	7	14.33	0.0084	99.99	160.37	7.86	3515
513	11/20/62	7	14.37	0.0058	100.02	160.14	7.78	3494
514	11/21/62	7	14.29	0.0070	100.05	100.01	7.82	3489
515	11/28/62	7	14.31	0.0105	100.02	100.05	7.81	3487
516	12/11/62	7	14.35	0.0085	100.01	160.19	7.82	3502
517	12/12/62	7	14.39	0.0091	100.02	160.18	7.79	3497
518	12/13/62	7	14.40	0.0083	100.03	160.17	7.78	3497
519	12/14/62	7	14.39	0.0076	100.01	160.02	7.77	3494

TABLE III. (Continued)

Test	Date	Wire No.	Pressure psia	Weight Fraction Water	Air Stream Temperature °F	Cylinder Temperature °F	Gross Air Velocity ft/sec	Gross Reynolds Number
520	12/17/62	7	14.24	0.0076	100.01	160.15	7.87	3497
521[a]	12/18/62	7	14.27	0.0084	100.01		7.87	(3505)
522A[a]	12/19/62	7	14.37	0.0089	100.04		9.13	(4092)
522B[a]	12/19/62	7	14.35	0.0094	99.94		6.76	(3027)
523	1/4/63	7	14.34	0.0062	99.97	159.81	7.81	3502
524	2/19/63	7	14.39	0.0094	99.93	160.33	7.77	3491
525	2/20/63	7	14.36	0.0080	100.07	160.29	7.80	3497
530	3/22/63	7	14.31	0.0067	100.00	160.20	7.84	3504
532	3/26/63	7	14.38	0.0075	100.00	160.21	7.79	3499
533	3/27/63	7	14.32	0.0060	100.02	160.19	7.83	3502
534	3/28/63	7	14.34	0.0075	100.04	160.16	7.82	3502
536	4/2/63	7	14.41	0.0053	100.02	160.22	7.77	3502
537	4/3/63	7	14.41	0.0049	100.00	160.46	7.77	3502
538	4/4/63	7	14.31	0.0054	99.99	100.12	7.81	3494
539	5/21/63	7	14.32	0.0102	100.03	100.22	7.85	3502
540	5/22/63	7	14.34	0.0100	100.01	100.20	7.83	3994
541	5/23/63	7	14.32	0.0097	99.93	100.12	7.83	3494
542	5/27/63	7	14.32	0.0088	100.09	100.16	7.84	3502

[a]No cylinder in air jet opening.

TABLE IV

Isothermal Experimental Data

Position		Temperatures		Coefficient	Nusselt Numbers	
x	y	t_a	Δt	$h_{ai} \times 10^2$	$Nu_{\ell, \lambda, a}$	$(Nu_{\ell, \lambda, a})$
in.	in.	$^\circ F$	$^\circ F$	$\frac{Btu}{sec, ft^2, ^\circ F}$		$\Delta t = 50\ ^\circ F$
			Test 505			
-0.800	0.000	100.00	51.67	5.562	1.0658	1.0650
		99.91	82.14	5.610	1.0751	
		99.95	118.30	5.679	1.0883	
-0.700	0.000	99.92	51.49	5.109	0.9792	0.9796
		99.92	81.81	5.174	0.9915	
		99.95	118.04	5.227	1.0017	
-0.600	0.000	100.10	51.73	4.371	0.8374	0.8368
		99.99	82.46	4.417	0.8464	
-0.540	0.000	99.94	53.35	3.570	0.6841	0.6835
		99.93	83.68	3.597	0.6892	
		99.99	120.03	3.655	0.7004	
-0.520	0.000	99.93	53.13	3.212	0.6155	0.6154
		99.96	91.20	3.019	0.5786	
		99.94	120.07	3.316	0.6355	
-0.512	0.000	99.93	54.32	3.168	0.6070	0.6054
		99.90	84.96	3.228	0.6185	
		99.98	115.52	3.287	0.6293	
-0.508	0.000	100.33	51.89	3.245	0.6215	0.6204
		100.36	81.98	3.297	0.6314	
		100.13	118.51	3.376	0.6467	
-0.530	0.000	99.96	51.89	3.240	0.6209	0.635
		99.91	50.65	3.348	0.6417	
		99.53	82.49	3.344	0.6413	
		99.82	117.32	3.472	0.6655	
-1.000	0.000	99.85	50.64	6.036	1.1568	1.156
		99.93	80.98	6.109	1.1707	
		99.90	117.88	6.156	1.1798	

TABLE IV (Continued)

x in.	y in.	t_a ^{o}F	Δt ^{o}F	$h_{ai} \times 10^2$ $\frac{Btu}{sec, ft^2, {}^{o}F}$	$Nu_{\ell, \lambda, a}$	$(Nu_{\ell, \lambda, a})$ $\Delta t = 50\ ^{o}F$
			Test 540A			
-0.499	0.101	100.17	55.59	4.366	0.8364	0.8344
		100.15	81.68	4.415	0.8458	
		100.17	105.77	4.460	0.8544	
-0.504	0.101	99.99	56.31	4.508	0.8637	0.8614
		99.99	81.08	4.568	0.8754	
		99.97	104.50	4.612	0.8838	
-0.507	0.101	99.90	54.05	4.583	0.8783	0.8746
		99.94	80.10	4.632	0.8877	
		99.93	103.13	4.683	0.8974	
-0.515	0.101	99.79	53.16	4.629	0.8872	0.8862
		99.95	80.16	4.702	0.9011	
		99.83	105.18	4.730	0.9065	
-0.520	0.101	99.96	53.89	4.648	0.8907	0.8891
		99.79	79.91	4.700	0.9008	
		99.91	103.46	4.748	0.9099	
-0.530	0.101	99.89	57.47	4.652	0.8916	0.891
		99.91	83.06	4.719	0.9044	
		99.86	106.45	4.741	0.9086	
-0.550	0.101	99.84	56.16	4.682	0.8974	0.8956
		99.89	81.67	4.730	0.9065	
		99.88	104.78	4.767	0.9135	

TABLE IV (Continued)

x in.	y in.	t_a ^{o}F	Δt ^{o}F	$h_{ai} \times 10^2$ $\frac{Btu}{sec, ft^2, {}^{o}F}$	$Nu_{\ell, \lambda, a}$	$(Nu_{\ell, \lambda, a})$ $\Delta t = 50\ ^{o}F$
			Test 541A			
-0.467	0.200	100.28	53.83	5.034	0.9641	0.9624 X
		100.18	80.07	5.084	0.9740	
		100.13	102.27	5.135	0.9838	
-0.470	0.200	100.05	52.37	5.020	0.9619	0.9609
		100.09	78.27	5.074	0.9721	
		100.13	102.03	5.126	0.9820	
-0.474	0.200	100.13	55.96	5.410	1.0363 X	1.024
		100.10	82.83	5.407	1.0359	
		100.05	105.35	5.449	1.0440	
-0.477	0.200	100.11	55.13	5.508	1.0552	1.0520
		99.90	81.67	5.551	1.0638	
		100.03	106.20	5.619	1.0766	
-0.482	0.200	100.01	57.09	5.626	1.0781	1.0762
		99.87	83.22	5.689	1.0903	
		99.84	106.80	5.729	1.0981	
-0.489	0.200	99.97	56.24	5.666	1.0858	1.0826
		99.80	82.84	5.702	1.0930	
		99.93	105.21	5.782	1.1081	
-0.499	0.200	99.93	55.88	5.643	1.0813	1.0792
		99.91	81.97	5.697	1.0918	
		99.78	105.63	5.739	1.1000	
-0.600	0.200	99.81	58.66	5.498	1.0538	1.0506
		99.81	84.89	5.550	1.0637	
		99.86	108.40	5.597	1.0727	
-0.800	0.200	99.72	58.45	5.772	1.1064	1.1023
		99.68	85.08	5.815	1.1149	
		99.66	107.80	5.881	1.1275	
			Test 542A			
-0.600	0.400	100.01	59.12	6.235	1.1947	1.1904
		99.80	84.44	6.275	1.2028	
		99.73	109.13	6.338	1.2151	
-0.800	0.400	99.72	59.23	6.128	1.1747	1.1700
		100.06	84.08	6.198	1.1875	
		100.02	108.34	6.254	1.1983	

Table IV (Continued)

x	y	t_a	Δt	$h_{ai} \times 10^2$	$Nu_{\ell, \lambda, a}$	$(Nu_{\ell, \lambda, a})$
in.	in.	^oF	^oF	$\frac{Btu}{sec, ft^2, ^oF}$		$\Delta t = 50\ ^oF$
			Test 542B			
-0.800	0.600	99.84	59.02	6.409	1.2284	1.2262
		99.79	84.41	6.456	1.2375	
		99.76	109.17	6.485	1.2432	
-0.600	0.600	99.94	58.74	6.531	1.2515	1.2474
		99.87	85.20	6.580	1.2612	
		99.92	108.54	6.638	1.2722	
-0.200	0.600	99.85	58.75	7.023	1.3460	1.3422
		99.85	84.11	7.082	1.3573	
		99.92	108.68	7.142	1.3686	
0.000	0.600	99.90	58.91	7.058	1.3527	1.3485
		99.89	84.04	7.122	1.3649	
		99.93	108.63	7.189	1.3776	
			Test 542C			
0.000	0.800	99.91	54.81	6.962	1.3342	1.3318
		99.93	101.20	7.074	1.3556	
-0.200	0.800	99.94	51.99	6.930	1.3280	1.323
		99.96	76.53	6.941	1.3300	
		99.92	101.53	7.007	1.3428	
-0.600	0.800	99.87	51.04	6.620	1.2687	1.2680
		99.85	76.31	6.683	1.2808	
		99.90	101.12	6.740	1.2916	
-0.800	0.800	99.82	51.70	6.549	1.2552	1.2530
		99.79	76.08	6.604	1.2659	
		99.92	100.68	6.665	1.2773	

TABLE IV (Continued)

x	y	t_a	Δt	$h_{ai} \times 10^2$	$Nu_{\ell, \lambda, a}$	$(Nu_{\ell, \lambda, a})$
in.	in.	^oF	^oF	$\frac{Btu}{sec, ft^2, ^oF}$		$\Delta t = 50\ ^oF$
			Test 538A			
-0.400	0.317	100.31	94.66	5.676	1.0872	1.0676
		100.24	114.48	5.722	1.0961	
		100.29	132.51	5.763	1.1038	
-0.400	0.326	100.01	91.58	6.311	1.2092	1.1922
		100.04	111.72	6.355	1.2177	
		100.06	130.16	6.393	1.2249	
-0.400	0.342	99.91	90.90	6.730	1.2898	1.273
		99.96	110.75	6.761	1.2957	
		99.97	129.01	6.813	1.3056	
-0.400	0.357	99.93	83.46	6.786	1.3005	1.286
		99.97	110.17	6.854	1.3134	
		100.01	128.66	6.893	1.3208	
			Test 541B			
-0.400	0.320	99.90	58.51	5.743	1.1006	1.0978
		99.93	84.58	5.817	1.1147	
		99.94	108.08	5.853	1.1216	
-0.400	0.330	99.83	58.25	6.379	1.2226	1.2184
		99.80	84.75	6.425	1.2315	
		99.82	107.78	6.494	1.2448	
-0.400	0.600	99.66	58.74	6.765	1.2969	1.295
		99.66	84.55	6.872	1.3175	
		99.61	107.62	6.904	1.3238	
-0.400	0.800	99.55	57.95	6.804	1.3047	1.301
		99.58	83.36	6.923	1.3274	
		99.55	107.59	6.914	1.3258	
-0.400	0.400	99.62	57.81	6.758	1.2958	1.2918
		99.69	84.06	6.829	1.3092	
		99.73	107.70	6.885	1.3199	

TABLE IV (Continued)

x	y	t_a	Δt	$h_{ai} \times 10^2$	$Nu_{\ell, \lambda, a}$	$(Nu_{\ell, \lambda, a})$
in.	in.	^{o}F	^{o}F	$\frac{Btu}{sec, ft^2, {}^{o}F}$		$\Delta t = 50\ ^{o}F$
			Test 515			
-0.300	0.414	100.43	46.71	6.000	1.1489	1.1501
		100.38	76.21	6.040	1.1568	
		100.46	105.05	6.087	1.1656	
-0.300	0.409	100.18	46.69	5.430	1.0403	1.0418
		100.18	76.10	5.509	1.0552	
		100.26	105.18	5.594	1.0715	
-0.300	0.406	100.35	45.41	6.008	1.1505	1.1508 X
		100.20	74.35	6.044	1.1577	
		100.25	105.44	6.154	1.1788	
-0.300	0.424	100.10	46.68	6.574	1.2594	1.2607
		100.19	75.59	6.633	1.2706	
		100.03	105.47	6.697	1.2832	
-0.300	0.444	99.85	45.63	7.250	1.3895	1.3910 X
		100.01	75.30	7.336	1.4056	
		99.75	103.49	7.364	1.4115	
-0.300	0.474	99.85	42.50	7.227	1.3851	1.3860 X
		99.97	77.19	7.280	1.3951	
		99.85	104.15	7.357	1.4100	
-0.300	0.494	100.01	43.91	7.223	1.3840	1.3849 X
		99.85	71.73	7.253	1.3901	
		100.07	99.63	7.317	1.4020	
			Test 538B			
-0.300	0.414	100.13	82.28	5.943	1.1386	1.1236
		100.17	104.48	5.989	1.1474	
		100.19	127.19	6.053	1.1594	
-0.300	0.420	100.19	81.27	6.495	1.2442	1.233
		100.04	103.10	6.539	1.2529	
		100.08	126.81	6.584	1.2614	
-0.300	0.432	100.04	81.11	7.007	1.3425	1.3276
		100.04	102.67	7.051	1.3511	
		99.97	116.43	7.092	1.3590	

TABLE IV (Continued)

x	y	t_a	Δt	$h_{ai} \times 10^2$	$Nu_{\ell, \lambda, a}$	$(Nu_{\ell, \lambda, a})$
in.	in.	^oF	^oF	$\frac{Btu}{sec, ft^2, ^oF}$		$\Delta t = 50\ ^oF$
			Test 539B			
-0.203	0.465	100.25	56.30	5.060	0.9691	0.9666 X
		100.27	82.19	5.140	0.9845	
		100.28	105.55	5.190	0.9940	
-0.203	0.471	100.13	56.35	5.457	1.0455	1.0416
		100.20	83.01	5.505	1.0545	
		100.18	105.79	5.578	1.0685	
-0.203	0.476	100.14	56.33	6.042	1.1575	1.1544
		100.13	82.47	6.087	1.1661	
		100.14	105.44	6.151	1.1783	
-0.203	0.501	99.88	56.60	7.140	1.3683	1.3656
		99.97	82.80	7.224	1.3843	
		99.94	105.86	7.278	1.3947	
			Test 540B			
-0.203	0.483	99.81	55.60	6.790	1.3015	1.2982
		99.94	81.47	6.863	1.3151	
		99.96	103.58	6.930	1.3279	
-0.203	0.490	99.95	55.86	7.087	1.3581	1.3546
		99.83	82.95	7.121	1.3649	
		99.96	105.75	7.194	1.3785	
-0.203	0.520	99.84	56.59	7.120	1.3647	1.3622
		99.85	82.43	7.206	1.3811	
		99.76	104.86	7.258	1.3913	

TABLE IV (Continued)

x	y	t_a	Δt	$h_{ai} \times 10^2$	$Nu_{\ell, \lambda, a}$	$(Nu_{\ell, \lambda, a})$
in.	in.	^{o}F	^{o}F	$\frac{Btu}{sec, ft^2, {}^{o}F}$		$\Delta t = 50\ ^{o}F$
			Test 539A			
-0.100	0.499	100.20	56.64	4.084	0.7824	0.7766
		100.23	82.57	4.152	0.7954	
		100.27	104.66	4.256	0.8152	
-0.100	0.506	100.22	56.54	4.541	0.8699	0.8666
		100.22	82.60	4.578	0.8770	
		100.20	105.50	4.639	0.8886	
-0.100	0.514	100.22	56.16	5.630	1.0784	1.0764
		100.16	83.24	5.653	1.0829	
		100.15	106.50	5.691	1.0903	
-0.100	0.520	100.13	56.86	6.342	1.2149	1.2098
		100.12	83.35	6.402	1.2265	
		100.06	105.74	6.484	1.2423	
-0.100	0.526	100.09	56.49	6.757	1.2946	1.2898
		100.07	83.06	6.800	1.3028	
		100.07	105.77	6.881	1.3184	
-0.100	0.539	100.04	55.74	7.201	1.3798 X	1.360
		100.03	82.86	7.134	1.3669	
		99.99	106.09	7.186	1.3770	
-0.100	0.551	99.91	56.66	7.184	1.3767	1.369
		99.94	82.84	7.184	1.3766	
		99.87	104.96	7.310	1.4010	
-0.100	0.571	100.04	56.35	7.132	1.3665	1.3634
		99.91	82.83	7.181	1.3762	
		99.92	106.12	7.238	1.3871	

TABLE IV (Continued)

x in.	y in.	t_a ^{o}F	Δt ^{o}F	$h_{ai} \times 10^2$ $\frac{Btu}{sec, ft^2, {}^{o}F}$	$Nu_{\ell, \lambda, a}$	$(Nu_{\ell, \lambda, a})$ $\Delta t = 50\ ^{o}F$
			Test 499			
0.000	1.000	99.94	50.04	7.130	1.3664	1.3664 X
		100.08	80.37	7.193	1.3781	
		99.75	108.61	7.244	1.3887	
0.000	0.800	99.97	49.86	7.200	1.3798	1.3796 X
		99.97	80.62	7.244	1.3880	
		99.97	108.44	7.306	1.4001	
0.000	0.640	99.92	50.23	7.265	1.3923	1.3922 X
		99.97	81.04	7.312	1.4012	
		99.89	109.02	7.374	1.4132	
0.000	0.570	99.92	50.54	7.078	1.3564	1.3561
		99.97	81.13	7.119	1.3642	
		100.00	108.92	7.193	1.3783	
0.000	0.520	100.25	50.25	3.130	0.5995	0.5994
		100.23	80.55	3.202	0.6134	
		100.20	108.08	3.249	0.6224	
0.000	0.540	100.22	108.19	4.364	0.8360	0.8170 X
		100.20	80.52	4.325	0.8285	
		100.18	50.14	4.268	0.8175	
			Test 514			
+0.001	0.561	99.60	51.87	6.658	1.2765	1.2756
		99.65	82.64	6.710	1.2864	
		99.82	111.65	6.754	1.2946	
+0.001	0.541	99.90	52.92	4.870	0.9333	0.9294
		99.92	82.53	5.042	0.9662	
		99.99	111.20	5.138	0.9845	
+0.001	0.531	100.04	51.88	4.066	0.7791	0.7798
		100.04	83.04	4.063	0.7785	
		100.03	111.72	4.154	0.7959	
+0.001	0.507	100.16	71.86	3.319	0.6358	0.6242
		100.18	91.66	3.365	0.6445	
		100.22	111.16	3.397	0.6506	
+0.001	0.511	100.20	71.52	3.140	0.6016	0.5925
		100.18	91.34	3.180	0.6092	
		100.18	111.52	3.205	0.6140	

TABLE V

Nonisothermal Experimental Data

Position		Temperatures		Coefficient	Nusselt Numbers	
x	y	t_a	Δt	$h_{ai} \times 10^2$	$Nu_{\ell, \lambda, a}$	$(Nu_{\ell, \lambda, a})$
in.	in.	°F	°F	$\frac{Btu}{sec, ft^2, °F}$		$\Delta t = 50$ °F
			Test 504			
-0.800	0.000	99.78	51.62	5.550	1.0639	1.0635
		99.96	118.09	5.671	1.0866	
		100.00	82.00	5.603	1.0737	
-0.700	0.000	100.00	51.41	5.136	0.9841	0.9838
		99.94	82.68	5.169	0.9906	
		99.93	119.21	5.236	1.0033	
-0.600	0.000	100.16	52.02	4.401	0.8431	0.8428
		99.85	82.91	4.436	0.8503	
		99.92	117.90	4.554	0.8726	
-0.540	0.000	100.06	52.01	3.736	0.7158	0.7154 X
		99.98	83.04	3.777	0.7237	
		100.01	118.28	3.862	0.7399	
-0.520	0.000	108.13	110.77	3.612	0.6836	0.6578 X
		108.08	75.08	3.531	0.6682	
		108.14	44.34	3.464	0.6555	
-0.508	0.000	133.28	39.71	3.654	0.6658	0.6307
			Test 508			
-0.521	-0.006	108.01	39.51	3.182	0.6022	0.6048
		108.23	78.67	3.246	0.6142	
		107.88	93.04	3.234	0.6122	
-0.507	-0.006	132.17	35.97	3.491	0.6372	0.6402
		132.19	66.69	3.513	0.6413	

TABLE V (Continued)

x in.	y in.	t_a ^oF	Δt ^oF	$h_{ai} \times 10^2$ $\frac{Btu}{sec, ft^2, ^oF}$	$Nu_{\ell, \lambda, a}$	$(Nu_{\ell, \lambda, a})$ $\Delta t = 50\ ^oF$
			Test 510			
-0.521	0.000	110.07	37.98	3.136	0.5916	0.6000
		110.10	75.14	3.342	0.6305	
		110.07	96.41	3.312	0.6250	
-0.515	0.000	119.85	58.50	3.316	0.6164	0.6124
		119.85	36.76	3.252	0.6046	
		119.76	87.12	3.362	0.6251	
-0.509	0.000	129.38	36.46	3.449	0.6322	0.6360
		129.51	65.94	3.491	0.6398	
		129.24	77.61	3.523	0.6458	
-0.531	0.000	102.25	44.93	3.331	0.6361	0.6380
		102.22	84.19	3.401	0.6495	
		102.28	104.33	3.430	0.6550	
-0.561	0.000	99.56	47.15	3.830	0.7343	0.7348
		99.61	67.28	3.850	0.7381	
			Test 511			
-0.520	0.101	102.31	44.61	4.670	0.8917	0.879
		101.74	74.67	4.639	0.8864	
		101.75	104.85	4.708	0.8996	
-0.510	0.101	111.62	34.14	4.579	0.8620	0.8661
		111.79	64.58	4.623	0.8700	
		111.73	94.40	4.666	0.8782	
-0.504	0.101	125.02	41.60	4.477	0.8259	0.8283
		125.09	61.25	4.505	0.8309	
		125.15	81.14	4.517	0.8331	
-0.498	0.101	140.69	25.43	4.415	0.7959	0.8016
		140.37	46.10	4.417	0.7966	
		140.60	65.01	4.487	0.8089	
-0.497	0.101	143.24				

TABLE V (Continued)

x in.	y in.	t_a ^oF	Δt ^oF	$h_{ai} \times 10^2$ $\frac{Btu}{sec, ft^2, ^oF}$	$Nu_{\ell, \lambda, a}$	$(Nu_{\ell, \lambda, a})_{\Delta t = 50\ ^oF}$
			Test 513B			
-0.530	0.100	100.18	50.73	4.499	0.8619	0.8614
		100.28	80.97	4.557	0.8728	
		100.30	109.59	4.617	0.8843	
-0.550	0.100	99.87	50.09	4.524	0.8671	0.8671
		99.82	80.66	4.585	0.8788	
		99.88	109.76	4.647	0.8905	
			Test 530B			
-0.468	0.200	142.35	42.72	5.142	0.9247	0.9274
		142.39	52.74	5.165	0.9287	
		142.51	63.63	5.177	0.9308	
-0.471	0.200	134.10	42.60	5.317	0.9677	0.9682
		134.01	55.04	5.335	0.9712	
		134.93	68.64	5.340	0.9707	
-0.474	0.200	126.47	44.39	5.653	1.0406 X	1.0160
		126.47	61.10	5.533	1.0185	
		126.48	76.27	5.552	1.0219	
-0.477	0.200	119.01	48.14	5.660	1.0535	1.049
		119.01	62.70	5.652	1.0521	
		118.95	85.29	5.704	1.0619	
-0.482	0.200	110.41	47.13	5.737	1.0819	1.0814
		110.38	65.64	5.744	1.0833	
		110.30	85.86	5.781	1.0903	
			Test 532C			
-0.499	0.202	100.43	53.98	5.671	1.0859	1.0849
		100.27	82.61	5.740	1.0993	
		100.32	112.96	5.800	1.1107	
-0.489	0.202	103.27	52.77	5.725	1.0916	1.0904
		103.14	80.36	5.776	1.1014	
		103.19	110.51	5.843	1.1140	
-0.474	0.202	125.74	48.21	5.706	1.0515 X	1.020
		125.67	64.28	5.567	1.0259	
		125.56	87.72	5.618	1.0354	

TABLE V (Continued)

x, in.	y, in.	t_a, °F	Δt, °F	$h_{ai} \times 10^2$, $\frac{Btu}{sec, ft^2, °F}$	$Nu_{\ell, \lambda, a}$	$(Nu_{\ell, \lambda, a})_{\Delta t = 50\ °F}$
			Test 536B			
-0.800	0.804	100.05	56.58	6.584	1.2615	1.2592
		100.07	75.62	6.642	1.2726	
		99.86	103.65	6.679	1.2801	
-0.800	0.604	99.97	56.41	6.416	1.2295	1.2278
		100.04	79.84	6.480	1.2416	
		100.10	103.16	6.523	1.2496	
-0.800	0.404	100.04	56.24	6.136	1.1757	1.1726
		99.99	79.82	6.194	1.1869	
		99.94	102.97	6.262	1.1999	
-0.800	0.204	99.95	56.09	5.762	1.1042	1.1006
		99.95	79.87	5.793	1.1101	
		99.95	113.84	5.873	1.1254	
			Test 536C			
-0.600	0.804	99.96	55.99	6.659	1.2760	1.2738
		100.01	79.32	6.721	1.2878	
		100.03	102.65	6.768	1.2967	
-0.600	0.604	100.00	56.18	6.546	1.2543	1.2516
		99.96	79.63	6.589	1.2626	
		100.00	103.03	6.648	1.2738	
-0.600	0.404	99.88	56.00	6.264	1.2006	1.1984
		100.01	79.50	6.307	1.2086	
		99.98	103.03	6.355	1.2178	
			Test 411			
-0.400	0.941	100.71	76.98	6.856	1.3123	1.3013
		100.71	105.27	6.916	1.3238	
-0.400	0.641	100.63	76.82	6.868	1.3147	1.3032
		100.63	105.02	6.931	1.3268	
-0.400	0.441	100.63	76.81	6.875	1.3160	1.3041
		100.63	105.22	6.940	1.3284	
-0.400	0.431	100.60	77.07	6.873	1.3157	1.2996
		100.60	105.22	6.960	1.3324	
-0.400	0.417	100.66	76.86	6.867	1.3145	1.3015
		100.66	105.21	6.925	1.3255	

TABLE V (Continued)

x	y	t_a	Δt	$h_{ai} \times 10^2$	$Nu_{\ell, \lambda, a}$	$(Nu_{\ell, \lambda, a})$
in.	in.	^{o}F	^{o}F	$\frac{Btu}{sec, ft^2, {}^{o}F}$		$\Delta t = 50\ ^{o}F$
			Test 523A			
-0.400	0.335	113.93	67.34	6.555	1.2295	1.2204
		113.90	100.87	6.661	1.2495	
		114.02	130.81	6.749	1.2658	
-0.400	0.345	107.65	73.53	6.677	1.2645	1.2524
		107.66	106.92	6.771	1.2821	
			Test 524			
-0.400	0.317	141.25	21.91	5.485	0.9879	1.0156
		141.52	39.39	5.630	1.0137	
		141.38	58.49	5.647	1.0169	
-0.400	0.322	135.68	17.61	6.008	1.0910 X	1.072
		135.80	35.48	5.851	1.0624	
		135.63	55.17	5.923	1.0757	
-0.400	0.332	120.54	33.19	6.539	1.2143 X	1.206
		120.64	49.21	6.469	1.2012	
		120.63	70.13	6.499	1.2067	
-0.400	0.342	112.26	32.41	6.581	1.2376	1.2440
		112.25	50.34	6.612	1.2434	
		112.28	68.52	6.671	1.2544	
-0.400	0.352	105.01	29.08	6.609	1.2567	1.2716
		105.02	58.14	6.720	1.2777	
		104.99	75.34	6.767	1.2867	
-0.400	0.367	100.55	22.63	6.777	1.2974	1.297
		100.55	53.20	6.786	1.2992	
		100.56	80.24	6.894	1.3199	

TABLE V (Continued)

x in.	y in.	t_a ^oF	Δt ^oF	$h_{ai} \times 10^2$ $\frac{Btu}{sec, ft^2, ^oF}$	$Nu_{\ell, \lambda, a}$	$(Nu_{\ell, \lambda, a})$ $\Delta t = 50\ ^oF$
			Test 525A			
-0.400	0.317	141.36	22.95	5.685	1.0238	1.0335
		141.24	36.29	5.934	1.0688 X	
		141.31	59.58	5.758	1.0370	
-0.400	0.322	136.37	30.20	5.918	1.0736	1.0820
		136.31	47.28	5.954	1.0801	
		136.36	65.09	6.005	1.0893	
-0.400	0.327	128.06	40.81	6.286	1.1543	1.1582
		127.98	61.44	6.334	1.1633	
		127.97	78.51	6.373	1.1705	
-0.400	0.337	111.77	40.38	6.730	1.2664	1.2675
		111.75	58.50	6.735	1.2676	
		111.77	78.22	6.778	1.2754	
-0.400	0.347	106.28	36.67	6.758	1.2825	1.2874
		106.24	53.36	6.782	1.2871	
		106.32	71.35	6.846	1.2991	
-0.400	0.357	102.34	28.38	6.754	1.2894	1.302
		102.23	59.64	6.875	1.3128	
		102.18	86.83	6.894	1.3165	
-0.400	0.372	100.14	31.41	6.913	1.3243	1.327
		100.09	65.56	6.931	1.3279	
		100.08	87.85	6.978	1.3369	
			Test 530A			
-0.399	0.322	131.63	45.38	6.126	1.1190	1.1204
		131.50	60.14	6.151	1.1239	
		131.46	74.81	6.176	1.1284	
			Test 532A			
-0.399	0.324	130.54	48.02	6.162	1.1274	1.1276
		130.54	63.02	6.173	1.1294	

TABLE V (Continued)

x in.	y in.	t_a ^oF	Δt ^oF	$h_{ai} \times 10^2$ $\frac{Btu}{sec, ft^2, ^oF}$	$Nu_{\ell, \lambda, a}$	$(Nu_{\ell, \lambda, a})$ $\Delta t = 50\ ^oF$
			Test 533A			
-0.400	0.324	130.91	70.08	6.175	1.1292	1.1186
		130.95	85.28	6.219	1.1373	
			Test 534A			
-0.399	0.323	130.16	68.21	6.200	1.1350	1.1256
		130.17	88.53	6.260	1.1459	
			Test 535A			
-0.400	0.324	126.69	75.43	6.324	1.1637	1.148
		126.61	90.78	6.372	1.1727	
			Test 536A			
-0.400	0.328	125.41	58.97	6.320	1.1651	1.1584
		125.46	73.64	6.390	1.1779	
			Test 537A			
-0.400	0.323	133.31	51.85	6.026	1.0981	1.0974
		133.32	66.73	6.074	1.1068	

TABLE V (Continued)

x	y	t_a	Δt	$h_{ai} \times 10^2$	$Nu_{\ell, \lambda, a}$	$(Nu_{\ell, \lambda, a})$
in.	in.	$^{\circ}F$	$^{\circ}F$	$\frac{Btu}{sec, ft^2, {}^{\circ}F}$		$\Delta t = 50\ ^{\circ}F$
			Test 533B			
-0.300	0.410	146.01	63.87	5.639	1.0087	1.0028
		145.97	73.71	5.661	1.0127	
		145.87	84.89	5.686	1.0174	
-0.300	0.415	136.62	63.21	6.088	1.1039	1.0988
		136.67	78.26	6.148	1.1147	
		136.65	94.22	6.171	1.1191	
-0.300	0.425	120.60	70.37	6.821	1.2666	1.2556
		120.77	88.83	6.844	1.2706	
		120.69	110.06	6.887	1.2787	
-0.300	0.435	108.40	72.75	7.113	1.3454	1.3354
		108.43	90.32	7.152	1.3529	
		108.43	121.69	7.228	1.3672	
-0.300	0.450	101.22	69.40	7.156	1.3686	1.3588
		101.30	89.40	7.204	1.3776	
		101.30	118.81	7.281	1.3923	
			Test 525B			
-0.260	0.436	144.13	23.11	5.559	0.9971	1.02 X
		144.14	44.92	5.564	0.9980	
		144.14	60.05	5.801	1.0406	
-0.260	0.446	132.60	27.05	6.322	1.1532	1.142
		132.54	41.64	6.252	1.1405	
		132.58	60.12	6.275	1.1447	
-0.260	0.456	117.54	29.86	6.919	1.2908	1.3204
		117.47	49.30	6.981	1.3025	
		117.48	68.12	7.026	1.3108	

TABLE V (Continued)

x in.	y in.	t_a °F	Δt °F	$h_{ai} \times 10^2$ $\frac{Btu}{sec, ft^2, °F}$	$Nu_{\ell, \lambda, a}$	$(Nu_{\ell, \lambda, a})$ $\Delta t = 50$ °F
			Test 520			
-0.260	0.433	149.82	38.20	5.662	1.0072	1.010 X
		149.88	48.87	5.676	1.0096	
		149.78	67.66	5.646	1.0045	
-0.260	0.440	142.80	56.06	5.576	1.0021	0.9976 X
		142.90	64.61	5.616	1.0091	
		143.01	72.85	5.648	1.0147	
-0.260	0.450	122.66	65.29	6.707	1.2417	1.227
		122.56	76.32	6.688	1.2382	
		122.35	94.30	6.732	1.2469	
-0.260	0.460	109.47	78.75	7.099	1.3405	? X
		109.27	97.02	7.255	1.3706	
		109.57	56.66	7.223	1.3639	
-0.260	0.470	104.01	52.50	7.109	1.3538	1.3522
		104.11	84.10	7.204	1.3717	
-0.260	0.480	101.02	55.62	7.107	1.3597	1.3570
		101.05	87.13	7.178	1.3731	
		100.99	116.09	7.241	1.3853	
-0.260	0.500	99.88	54.27	7.077	1.3562	1.353
		100.09	88.86	7.127	1.3655	
		99.86	116.76	7.223	1.3843	
-0.260	0.520	99.92	53.68	7.048	1.3506	1.3490
		99.84	88.52	7.117	1.3641	
-0.260	0.600	99.71	56.26	6.947	1.3318	1.3295
		99.89	87.97	7.021	1.3455	
			Test 523B			
-0.260	0.446	129.98	46.11	6.276	1.1493	1.1494
		129.92	72.27	6.282	1.1505	
-0.260	0.436	146.89	37.14	5.366	0.9587	0.9637
		146.90	63.91	5.429	0.9699	
-0.260	0.456	118.94	37.98	6.728	1.2524	1.2576 X
		118.89	66.06	6.791	1.2642	
		118.94	93.04	6.840	1.2734	

TABLE V (Continued)

x in.	y in.	t_a °F	Δt °F	$h_{ai} \times 10^2$ $\frac{Btu}{sec, ft^2, °F}$	$Nu_{\ell, \lambda, a}$	$(Nu_{\ell, \lambda, a})$ $\Delta t = 50$ °F
			Test 407			
-0.204	0.940	101.18	79.15	7.037	1.3459	1.3212
		101.18	106.63	7.159	1.3692	
-0.204	0.740	100.97	79.21	7.081	1.3548	1.3334
		100.97	107.03	7.183	1.3743	
-0.204	0.540	100.94	79.37	7.248	1.3868	1.3671
		100.94	107.19	7.346	1.4055	
			Test 534B			
-0.203	0.475	132.05	66.66	6.048	1.1041	1.100
		132.17	79.79	6.102	1.1138	
		132.26	102.00	6.118	1.1166	
-0.203	0.470	139.75	62.88	5.540	1.0001	0.995
		139.70	78.70	5.541	1.0003	
		139.70	94.98	5.580	1.0074	
-0.203	0.483	119.44	74.79	6.836	1.2716	1.2596
		119.51	92.96	6.879	1.2794	
		119.47	114.10	6.938	1.2905	
-0.203	0.490	111.26	72.89	7.144	1.3454	1.3400
		111.17	91.89	7.167	1.3499	
-0.203	0.500	103.90	71.04	7.220	1.3752	1.3660
		103.96	93.45	7.288	1.3881	
		103.89	118.92	7.342	1.3983	
-0.203	0.464	148.62	63.86	5.240	0.9337	0.925
		148.68	74.38	5.277	0.9402	

TABLE V (Continued)

x in.	y in.	t_a °F	Δt °F	$h_{ai} \times 10^2$ $\frac{Btu}{sec, ft^2, °F}$	$Nu_{\ell, \lambda, a}$	$(Nu_{\ell, \lambda, a})$ $\Delta t = 50$ °F
			Test 406			
-0.100	0.943	100.78	77.71	7.226	1.3830	1.3699
		100.78	105.60	7.296	1.3962	
-0.100	0.743	101.25	77.30	7.171	1.3713	1.3583
		101.25	105.20	7.240	1.3846	
-0.100	0.643	101.02	77.72	7.224	1.3821	1.3642
		101.02	105.51	7.318	1.4000	
			Test 513A			
-0.100	0.529	114.86	46.40	6.903	1.2929	1.2949
		114.74	66.94	7.091	1.3285	
		114.72	97.24	7.056	1.3219	
-0.100	0.519	125.23	48.10	6.254	1.1533	1.1560
		125.21	66.75	6.376	1.1758	
		125.18	85.89	6.441	1.1879	
-0.100	0.564	100.92	50.94	7.258	1.3888	1.3884 X
		100.74	80.83	7.320	1.4010	
		100.55	110.16	7.385	1.4138	
			Test 537B			
-0.100	0.498	149.75	57.87	4.343	0.7728	0.770
		149.70	51.13	3.765	0.6699 X	
		149.79	68.06	4.386	0.7802	
-0.100	0.505	143.49	44.24	4.431	0.7956	0.797
		143.47	59.85	4.481	0.8044	
		143.51	75.40	4.443	0.7977	
-0.100	0.513	134.34	69.04	5.368	0.9767	0.9796
		134.16	53.25	5.379	0.9789	
		134.24	41.48	5.393	0.9813	
-0.100	0.525	119.59	55.93	6.611	1.2296 X	1.255
		119.49	72.46	6.801	1.2651	
		119.63	92.48	6.850	1.2738	
-0.100	0.538	108.21	49.32	7.018	1.3278	1.3304
		108.29	76.76	7.132	1.3492	
		108.33	106.29	7.196	1.3614	
-0.100	0.550	102.55	54.92	7.136	1.3619	1.3596
		102.55	82.18	7.196	1.3734	
		102.47	112.14	7.263	1.3863	

TABLE V (Continued)

x in.	y in.	t_a ^oF	Δt ^oF	$h_{ai} \times 10^2$ $\frac{Btu}{sec, ft^2, ^oF}$	$Nu_{\ell, \lambda, a}$	$(Nu_{\ell, \lambda, a})$ $\Delta t = 50\ ^oF$
			Test 500			
0.000	0.800	100.20	50.04	7.284	1.3953	1.3952 X
		100.24	80.20	7.321	1.4023	
		100.26	104.81	7.412	1.4197	
0.000	0.640	100.10	62.06	6.692	1.2820	1.3998 X
		100.07	80.68	7.356	1.4093	
		100.21	106.15	7.414	1.4201	
0.000	0.570	113.92	36.69	6.956	1.3047	1.3103
		113.75	68.01	7.060	1.3246	
		113.58	93.70	7.085	1.3297	
0.000	0.540	144.80	25.81	3.222	0.5773	0.5762 X
		144.91	47.91	3.214	0.5759	
		144.99	64.65	3.223	0.5774	
0.000	0.520	146.34	35.89	3.088	0.5521	0.5584
		146.33	46.96	3.115	0.5570	
		146.29	62.26	3.165	0.5660	
0.000	0.508	151.26	29.74	3.418	0.6069	0.6041
		151.38	41.09	3.407	0.6048	
		151.30	57.17	3.405	0.6044	
			Test 502			
0.000	0.530	141.64	51.63	3.518	0.6333	0.6413
		141.71	50.87	3.570	0.6425	
		141.85	60.67	3.622	0.6518	
		141.81	71.72	3.635	0.6542	
0.000	0.540	139.16	46.76	3.985	0.7200	0.7200
		139.07	31.55	4.083	0.7378	
		139.24	64.65	4.024	0.7268	
0.000	0.550	129.56	51.00	5.712	1.0466	1.0410
		129.69	57.24	5.936	1.0875	
		129.57	80.91	5.583	1.0229	
0.000	0.560	124.62	44.27	6.253	1.1542	1.1506
		124.44	57.55	6.165	1.1383	
		125.06	84.37	6.368	1.1746	

TABLE V (Continued)

x in.	y in.	t_a °F	Δt °F	$h_{ai} \times 10^2$ $\frac{Btu}{sec, ft^2, °F}$	$Nu_{\ell, \lambda, a}$	$(Nu_{\ell, \lambda, a})$ $\Delta t = 50$ °F
			Test 518			
+0.101	0.495	151.39	56.14	4.099	0.7276	0.7272 X
		151.51	65.74	4.135	0.7339	
		151.57	75.56	4.156	0.7375	
+0.101	0.499	148.71	58.19	3.578	0.6376	0.6240
		148.57	68.99	3.549	0.6325	
		148.41	78.71	3.575	0.6372	
+0.101	0.505	147.76	55.46	3.318	0.5921	0.5882
		147.11	70.37	3.345	0.5973	
		147.47	78.93	3.393	0.6056	
+0.101	0.511	141.92	52.72	3.191	0.5742	0.570
		141.50	64.65	3.104	0.5589	
+0.101	0.521	135.64	58.27	2.890	0.5243 X	0.5468
		135.89	69.50	3.036	0.5511	
		135.98	80.32	3.049	0.5535	
+0.101	0.541	133.41	51.48	2.931	0.5341	0.5343
		133.41	73.07	2.916	0.5313	
+0.101	0.561	135.34	50.26	3.711	0.6743	0.6762
		135.34	69.63	3.787	0.6880	
		135.45	86.51	3.788	0.6881	
+0.101	0.581	128.71	48.88	5.648	1.0362	1.0372
		128.63	70.19	5.546	1.0176	
			Test 519			
+0.101	0.552	133.35	54.98	3.261	0.5941	0.5941
		133.02	75.61	3.260	0.5943	
+0.101	0.602	115.29	61.53	6.906	1.2928 X	1.29
		115.15	83.83	6.776	1.2687	
		114.78	100.80	6.923	1.2968	
+0.101	0.622	104.47	62.35	7.088	1.3489	1.3424
		104.37	82.68	7.144	1.3598	
+0.101	0.652	100.00	55.86	7.090	1.3586	1.3604
		100.10	87.39	7.214	1.3821	
		100.10	116.32	7.236	1.3864	
+0.101	0.752	100.00	56.02	7.058	1.3524	1.3498
		99.77	87.98	7.124	1.3656	
		99.70	115.55	7.187	1.3778	
+0.101	0.852	99.91	55.38	7.004	1.3423	1.3391
		99.72	85.77	7.082	1.3576	

TABLE V (Continued)

x in.	y in.	t_a ^oF	Δt ^oF	$h_{ai} \times 10^2$ $\frac{Btu}{sec, ft^2, ^oF}$	$Nu_{\ell, \lambda, a}$	$(Nu_{\ell, \lambda, a})$ $\Delta t = 50\ ^oF$
			Test 516			
+0.201	0.462	149.20	43.31	3.659	0.6515	0.656
		148.97	52.77	3.693	0.6579	
		148.71	64.39	3.573	0.6366 X	
+0.201	0.467	144.85	46.54	3.209	0.5749	0.5787
		145.36	56.15	3.259	0.5835	
		145.22	64.92	3.279	0.5871	
+0.201	0.475	139.16	51.00	2.922	0.5279	0.5257
		139.24	64.47	2.776	0.5014 X	
		139.23	69.92	3.040	0.5492	
+0.201	0.485	133.96	46.49	2.803	0.5103	0.519
		133.96	67.21	2.833	0.5157	
+0.201	0.500	125.30	58.15	2.892	0.5332	0.5294
		125.30	74.74	2.803	0.5183 X	
		125.61	87.00	2.966	0.5467	
+0.201	0.520	118.74	42.24	3.620	0.6741 X	0.5561
		118.56	84.29	2.988	0.5565	
+0.201	0.540	117.49	55.88	3.071	0.5730	0.567
		117.49	76.93	3.045	0.5681 X	
		117.67	93.40	3.097	0.5777	
+0.201	0.560	117.02	55.40	2.828	0.5280	0.5226
		117.64	72.15	2.920	0.5446	

TABLE V (Continued)

x in.	y in.	t_a °F	Δt °F	$h_{ai} \times 10^2$ $\frac{Btu}{sec, ft^2, °F}$	$Nu_{\ell, \lambda, a}$	$(Nu_{\ell, \lambda, a})$ $\Delta t = 50$ °F
			Test 517			
+0.201	0.579	122.96	55.16	3.317	0.6138	0.6115
		123.01	73.59	3.388	0.6268	
		123.18	94.10	3.436	0.6357	
+0.201	0.599	126.81	49.97	4.675	0.8602	0.8602
		127.22	71.28	4.758	0.8748	
+0.201	0.619	122.51	55.00	6.290	1.1647	1.1652
		122.51	74.25	6.423	1.1894	
		123.45	95.30	6.451	1.1929	
+0.201	0.634	113.00	54.14	6.732	1.2645	1.2622
		112.23	74.75	6.785	1.2759	
+0.201	0.644	107.89	56.77	6.989	1.3231	1.3224
		107.76	77.92	7.079	1.3403	
		107.62	108.90	7.123	1.3490	
+0.201	0.679	100.32	51.81	7.201	1.3792	1.3762
		100.22	83.26	7.240	1.3868	
		100.40	111.57	7.352	1.4080	
+0.201	0.709	100.13	59.95	6.585	1.2616 X	1.374
		99.96	85.20	7.244	1.3881	
+0.201	0.809	99.90	84.82	7.182	1.3763	1.3708
		100.00	53.03	7.149	1.3699	
			Test 535B			
+0.201	0.800	100.04	73.99	7.100	1.3603	1.3496
		99.93	93.80	7.137	1.3677	
		100.03	122.19	7.212	1.3818	

TABLE VI

Radial Nusselt Number and Air Temperature Distributions Near the Cylinder

$r - r'_o$ inches	Isothermal Nu^{*a}	Nonisothermal Nu^{*a}	t^*_a °F
	at stagnation ($r'_o - r_o = 0.0000$ inches)		
0.0000	0.700[b]	0.718[b]	160.0
0.0050	0.648	0.670	143.9
0.0100	0.6145	0.633	130.7
0.0150	0.6040	0.611	120.4
0.0200	0.6113	0.603	111.9
0.0250	0.6350	0.611	106.4
0.0300	0.6415	0.628	103.0
0.0400	0.6765	0.664	100.4
0.0500	0.707	0.698	100.0
0.0600	0.733	0.731	100.0
0.0700	0.756	0.761	100.0
	15 degrees from stagnation ($r'_o - r_o = 0.0021$ inches)		
0.0000	0.791[b]	0.790[b]	160.0
0.0050	0.842	0.829	145.5
0.0100	0.897	0.876	131.7
0.0150	0.936	0.925	118.7
0.0200	0.955	0.956	109.0
0.0250	0.962	0.963	103.7
0.0300	0.965	0.962	101.3
0.0400	0.9695	0.954	100.1
0.0500	0.973	0.954	100.0
0.0600	0.975	0.962	100.0
0.0700	0.976	0.972	100.0

[a] Based on a wire temperature 50° F above the local air stream temperature.

[b] Extrapolation to this value is questionable.

TABLE VI (Continued)

$r - r_o'$ inches	Isothermal Nu^{*a}	Nonisothermal Nu^{*a}	t_a^* °F
	30 degrees from stagnation ($r_o' - r_o$ = 0.0037 inches)		
0.0000	0.872[a]	0.885[a]	160.0
0.0050	0.967	0.963	146.1
0.0100	1.068	1.056	132.6
0.0150	1.140	1.134	119.5
0.0200	1.173	1.171	110.2
0.0250	1.183	1.189	104.9
0.0300	1.184	1.197	102.8
0.0400	1.180	1.204	100.1
0.0500	1.178	1.202	100.0
0.0600	1.174	1.197	100.0
0.0700	1.166	1.191	100.0
	45 degrees from stagnation ($r_o' - r_o$ = 0.0033 inches)		
0.0000	0.913[a]	0.914[a]	160.0
0.0050	1.030	1.003	147.5
0.0100	1.148	1.106	135.6
0.0150	1.237	1.208	124.4
0.0200	1.283	1.273	114.0
0.0250	1.300	1.303	107.3
0.0300	1.306	1.319	103.4
0.0400	1.303	1.329	100.3
0.0500	1.298	1.322	100.0
0.0600	1.293	1.313	100.0
0.0700	1.288	1.304	100.0

[a]Based on a wire temperature 50° F above the local air stream temperature

[b]Extrapolation to this value is questionable.

TABLE VI (Continued)

$r - r_o'$ inches	Isothermal Nu^{*a}	Nonisothermal Nu^{*a}	t_a^* °F
	60 degrees from stagnation ($r_o' - r_o = 0.0012$ inches)		
0.0000	0.879[b]	0.873[b]	160.0
0.0050	0.976	0.942	150.3
0.0100	1.082	1.036	140.4
0.0150	1.194	1.154	131.6
0.0200	1.285	1.253	121.1
0.0250	1.333	1.315	113.6
0.0300	1.352	1.344	107.2
0.0350	1.356	1.356	103.2
0.0400	1.358	1.362	101.5
0.0500	1.357	1.363	100.1
0.0600	1.355	1.357	100.0
0.0700	1.351	1.350	100.0
	75 degrees from stagnation ($r_o' - r_o = 0.0004$ inches)		
0.0000	0.795[b]	0.792[b]	160.0
0.0050	0.805	0.801	153.2
0.0100	0.842	0.839	146.2
0.0150	0.928	0.920	138.6
0.0200	1.080	1.058	131.3
0.0250	1.206	1.182	124.5
0.0300	1.291	1.270	118.1
0.0350	1.332	1.319	112.4
0.0400	1.363	1.342	108.1
0.0450	1.365	1.357	104.9
0.0500	1.365	1.367	102.6
0.0600	1.360	1.372	100.3
0.0700	1.354	1.374	100.0
0.0800	1.347	1.372	100.0

[a] Based on a wire temperature 50° F above the local air stream temperature.

[b] Extrapolation to this value is questionable.

TABLE VI (Continued)

$r - r_o'$ inches	Isothermal Nu^{*a}	Nonisothermal Nu^{*a}	Nonisothermal t_a^* ^oF
	90 degrees from stagnation ($r_o' - r_o = 0.0000$ inches)		
0.0000	0.725[b]	0.742[b]	160.0
0.0050	0.650	0.643	155.4
0.0100	0.604	0.587	151.7
0.0150	0.582	0.559	148.6
0.0200	0.592	0.557	145.9
0.0250	0.650	0.586	143.4
0.0300	0.731	0.651	141.0
0.0350	0.824	0.732	138.5
0.0400	0.912	0.824	135.9
0.0450	1.008	0.927	132.9
0.0500	1.102	1.034	132.9
0.0600	1.259	1.212	125.3
0.0700	1.3455	1.308	113.1
0.0800	1.366	1.349	106.6
0.0900	1.366	1.366	102.5
0.1000	1.364	1.374	100.7
0.1100	1.361	1.376	100.1

[a]Based on a wire temperature 50^o F above the local air stream temperature.

[b]Extrapolation to this value is questionable.

TABLE VI (Continued)

$r - r_o'$ inches	Isothermal Nu^{*a}	Nonisothermal Nu^{*a}	Nonisothermal t_a^* °F
	105° degrees from stagnation ($r_o' - r_o = -0.0003$ inches)		
0.0000	[c]		160.0
0.0050		0.732[b]	151.0
0.0100		0.616	146.7
0.0150		0.583	142.8
0.0200		0.571	139.6
0.0300		0.559	134.3
0.0400		0.551	129.9
0.0500		0.545	127.2
0.0600		0.535	126.2
0.0700		0.530	126.1
0.0800		0.559	127.2
0.0900		0.628	129.1
0.1000		0.735	131.0
0.1100		0.882	131.6
0.1200		1.033	128.7
0.1300		1.160	123.1
0.1400		1.242	117.2
0.1500		1.298	111.7
0.1600		1.333	107.2
0.1700		1.353	104.3
0.1800		1.363	102.4

[a] Based on a wire temperature 50° F above the local air stream temperature.

[b] Extrapolation to this value is questionable.

[c] Measurements for the isothermal case were not taken in this region.

TABLE VII

Nusselt Numbers in the Air Stream around the Cylinder

x, inches	Isothermal Nu^{*a}	Nonisothermal Nu^{*a}	Isothermal Nu^{*a}	Nonisothermal Nu^{*a}
	y = 0.000 inches		y = 0.101 inches	
-0.500			0.8398	0.8090
-0.600	0.821	0.8428	0.9155	0.9115
-0.700	0.9785	0.9838	1.0155	1.007
-0.800	1.0640	1.0635	1.076	1.074
	y = 0.200 inches		y = 0.300 inches	
-0.500	1.0785	1.082	1.171	1.196
-0.600	1.0505	1.068	1.1410	1.1515
-0.700	1.083	1.083	1.1380	1.143
-0.800	1.102	1.099	1.1350	1.1375
	y = 0.400 inches		y = 0.500 inches	
-0.203			1.3658	1.3625
-0.300			1.3435	1.3415
-0.400	1.292	1.3105	1.2945	1.2895
-0.500	1.225	1.234	1.258	1.2455
-0.600	1.1905	1.197	1.2255	1.229
-0.700	1.1805	1.181	1.2110	1.212
-0.800	1.1695	1.171	1.2013	1.202

[a]Based on a wire temperature 50° F above the local air stream temperature.

TABLE VII (Continued)

x, inches	Isothermal Nu^{*a}	Nonisothermal Nu^{*a}	Isothermal Nu^{*a}	Nonisothermal Nu^{*a}
	y = 0.600 inches		y = 0.700 inches	
+0.201				1.372
+0.101				1.369
0.000	1.3635	1.3745	1.340	1.3615
-0.100	1.3535	1.371	1.3348	1.3505
-0.203	1.342	1.3475	1.3272	1.331
-0.300	1.324	1.317	1.3160	1.312
-0.400	1.2957	1.291	1.298	1.294
-0.500	1.2690	1.258	1.2782	1.278
-0.600	1.2472	1.251	1.2605	1.264
-0.700	1.234	1.2375	1.2485	1.253
-0.800	1.2263	1.227	1.2430	1.2445
	y = 0.800 inches			
+0.201		1.360		
+0.101		1.356		
0.000	1.332	1.3505		
-0.100	1.328	1.3395		
-0.203	1.322	1.3245		
-0.300	1.313	1.3105		
-0.400	1.301	1.2965		
-0.500	1.284	1.284		
-0.600	1.2680	1.274		
-0.700	1.259	1.266		
-0.800	1.2535	1.2585		

[a]Based on a wire temperature 50° F above the local air stream temperature.

TABLE VIII

Experimental Data Taken in the Air Stream Without the Cylinder for the Nusselt Number Correlation with the Reynolds Number

Position[a] x	Position[a] y	Temperatures t_a	Temperatures Δt	Nusselt Numbers $Nu_{\ell,\lambda,a}$	Nusselt Numbers $\frac{Nu_{\ell,\lambda,m}}{\left(\frac{T_m}{T_a}\right)^{0.17}}$	Reynolds Number $Re_m^{0.45}$	Velocity u
inches	inches	°F	°F				ft/sec
			Test 522B (U_∞ = 6.76 ft/sec)				
-0.500	0.000	99.88	71.04	1.2376	1.1609	1.5638	6.780
		99.77	103.41	1.2494	1.1396	1.5290	6.751
		99.83	133.12	1.2584	1.1193	1.4983	6.698
0.000	0.000	99.80	71.04	1.2292	1.1530	1.5639	6.645
		99.83	102.93	1.2497	1.1403	1.5294	6.760
		99.83	131.89	1.2635	1.1250	1.4995	6.787
0.000	0.500	99.94	70.11	1.2373	1.1616	1.5647	6.783
0.000	0.600	99.77	70.65	1.2350	1.1588	1.5644	6.739
		99.94	103.01	1.2509	1.1413	1.5291	6.781
		99.81	132.29	1.2614	1.1227	1.4992	6.751
			Test 521 (U_∞ = 7.87 ft/sec)				
-0.750	0.000	99.84	55.72	1.2941	1.2304	1.6892	7.868
		99.82	86.54	1.3076	1.2101	1.6527	7.873
		99.88	115.02	1.3176	1.1899	1.6204	7.837
-0.500	0.000	99.88	54.69	1.2910	1.2286	1.6903	7.823
		99.73	86.34	1.3037	1.2067	1.6532	7.804
		99.83	114.47	1.3189	1.1917	1.6211	7.862
0.000	0.000	100.02	55.33	1.2830	1.2203	1.6892	7.684
		99.83	86.03	1.3047	1.2079	1.6533	7.827
		99.77	114.31	1.3169	1.1900	1.6215	7.827
10.100	0.000	99.84	54.59	1.2881	1.2259	1.6905	7.772
		99.72	96.32	1.3055	1.1980	1.6418	7.762

[a]Coordinates relative to position of the axis of the cylinder as determined before it was removed from the air stream.

TABLE VIII (Continued)

Position x, inches	Position y, inches	Temperatures t_a, °F	Temperatures Δt, °F	Nusselt Numbers $Nu_{\ell,\lambda,a}$	Nusselt Numbers $\frac{Nu_{\ell,\lambda,m}}{\left(\frac{T_m}{T_a}\right)^{0.17}}$	Reynolds Number $Re_m^{0.45}$	Velocity u, ft/sec
			Test 521 (Continued) (U_∞ = 7.87 ft/sec)				
0.000	0.300	99.95	53.10	1.2904	1.2297	1.6921	7.826
		99.96	85.66	1.3041	1.2078	1.6534	7.823
0.000	0.600	99.90	51.91	1.2846	1.2255	1.6936	7.733
		99.96	85.91	1.3043	1.2077	1.6532	7.824
		100.00	114.44	1.3164	1.1895	1.6208	7.824
-0.500	0.600	99.91	54.36	1.2925	1.2304	1.6906	7.852
		100.06	85.35	1.3049	1.2089	1.6536	7.841
		99.93	54.04	1.3006	1.2384	1.6910	7.997
0.000	0.900	99.93	86.39	1.3067	1.2094	1.6527	7.861
		100.18	114.65	1.3175	1.1903	1.6202	7.846
		99.91	52.93	1.2891	1.2287	1.6924	7.804
-0.750	0.900	99.76	84.27	1.3075	1.2124	1.6555	7.886
		99.85	111.77	1.3185	1.1940	1.6241	7.875
			Test 522A (U_∞ = 9.13 ft/sec)				
0.000	0.600	100.05	67.21	1.3723	1.2916	1.7954	9.153
		99.90	92.92	1.3831	1.2729	1.7636	9.138
		99.92	119.91	1.3948	1.2553	1.7231	9.142
0.000	0.000	100.08	70.84	1.3778	1.2927	1.7907	9.227
		99.89	97.45	1.3841	1.2689	1.7581	9.119
		99.80	123.46	1.3955	1.2513	1.7273	9.116
-0.500	0.000	99.87	71.01	1.3708	1.2859	1.7910	9.087
		100.16	96.75	1.3869	1.2723	1.7583	9.186
		99.87	123.17	1.3944	1.2507	1.7274	9.100

PROPOSITION I

It is proposed that the separation of nitric oxide, NO, from nitrogen, N_2, by a silica gel chromatography column is dependent upon conditioning a "dried" column with small amounts of nitrogen dioxide, NO_2. For reproducible separations, conditioning with nitric oxide is also required.

A. Discussion

These observations are based on the experimental work conducted by the author during the first four months of 1960. Previous presentations of this work are available (1, 2). A brief description of the apparatus and a presentation of the experimental results are presented below.

The equipment used was designed by Sakaida (3) for the separation and quantitative determination of small quantities of nitric oxide in nitrogen. Based on these studies, an 8-foot column of one-quarter-inch stainless steel tubing packed with Davison No. 912 silica gel of 48 to 60 mesh was used in conjunction with a dual-thermistor thermal conductivity cell as a sensing element. The column was heated to about 75° C at the entrance and about 52° C at the exit. The thermistors were in a 30° C air bath. The helium carrier gas was flowing at about 41 cubic-centimeters-per-minute at one atmosphere and 25° C. The pressure drop through the column was maintained at 10 pounds-per-square-inch with the exit at the local air pressure. A more detailed description of the apparatus

is available in the literature (4).

Following a two-day drying period during which the column was heated to 200° C with a low helium flow rate, various samples were passed through each column to determine the conditioning requirements. With the sample introduction procedure used, about two cubic centimeters of air were introduced to the column prior to the 2.8 cubic centimeter samples. Samples from a cylinder labeled 0.5 per cent nitric oxide in nitrogen were introduced to check the nitric oxide separation by the column. The quality of the separation is reported as the ratio of the peak-times of the elution curves for the nitric oxide to that for the nitrogen which passed directly through the column. These peak-times were measured from the introduction of the sample to the column. Separation ratios of less than about 1.4 were not detectable due to the size and tailing of the nitrogen curve. Therefore, when no separation was observed, the separation ratio is reported as being one. A separation ratio of about two is preferred so that an adequate determination of the base line between the two elution curves can be made. These data are presented for the three columns used in Tables I, II, and III as a function of the various other samples which were introduced to effect the separation.

In the conditioning of Column A, it was noted that repeated introduction of nitric oxide samples produced and improved the nitric oxide separation. This will be explained below as resulting from the small amounts of nitrogen dioxide in these samples. A

substantial increase in the separation ratio was still possible after the introduction of 15 such samples when a mixture of nitric oxide with air to produce nitrogen dioxide was added.

With Column B, this mixture of nitric oxide and air produced separation and improved it after three initial samples of nitric oxide. Additional nitric oxide samples were required for reproducible separations, and improved the separation slightly with each addition. After the reproducibility was proved with 0.5, 0.25, and 0.1 per cent nitric oxide in nitrogen samples, the addition of dry air was shown to have no effect on the separation. A few samples of nitrogen dioxide, however, greatly increased the separation ratio and ruined the reproducibility of the separation. An explanation of the excess nitric oxide eluted after over-saturating the column with nitrogen dioxide is given by Morrison (5).

Finally, it was shown with Column C that separation could be produced by the introduction of only nitrogen dioxide.

The continual improvement of the nitric oxide separation ratio by the introduction of only pure nitric oxide samples is explained by the assumed presence of nitrogen dioxide in these samples. Indeed, a second elution curve comprising 0.89 ± 0.04 per cent of the combined areas of the elution curves is observed (1, 2). A mechanism for the separation of this material involving the water on the silica gel is presented in Proposition II.

The separation of nitric oxide and nitrogen dioxide by silica gel is believed (3) to be connected with absorbtion sites on the silica

gel which attract nitric oxide and nitrogen dioxide. Prior to this work, conditioning the column was believed to be dependent upon filling the irreversibly adsorbed sites of the species in question. Separation was then assumed to be produced by the reversible adsorption of the species on the remaining sites. Although the filling of these irreversibly adsorbed sites is necessary before the separation can be quantitatively reproducible, this proposition proposes that the separation of the nitric oxide involves the association with the absorbed nitrogen dioxide. Thus the conditioning with nitrogen dioxide is essential for separation, while the conditioning with nitric oxide is required for reproducibility.

Since these studies, further investigations by Fossard, Rinker, and Corcoran (6) and Morrison (5) have added further credence to this proposition.

B. References

1. Cuffel, Robert F.,
"The Chromatographic Analysis of the N_2-NO-NO_2 System." Unpublished Student Report No. 874, Chemical Engineering Department, California Institute of Technology. (May 27, 1960).

2. Cuffel, Robert F.,
"Part II. Gas Chromatography Separation of NO and NO_2 from N_2." Unpublished Student Report No. 908, Chemical Engineering Department, California Institute of Technology. (March 1, 1961).

3. Sakaida, R. R.,
"Part II. A Chromatographic Apparatus and Technique for the Analysis of Nitric Oxide in Nitrogen." Unpublished Ph. D. Thesis, California Institute of Technology. (1960).

4. Sakaida, Roy R., Robert G. Rinker, Robert F. Cuffel, and William H. Corcoran,
"Determination of Nitric Oxide in a Nitric Oxide-Nitrogen System of Gas Chromatography," Analytical Chemistry, Vol. 33, pp. 32-34. (1961).

5. Morrison, Milton Edward,
"Part I. The Chromatographic Analysis of the N_2-NO-NO_2 System." Unpublished Student Report No. 965, Chemical Engineering Department, California Institute of Technology. (Jan. 25, 1962).

6. Frossard, M., R. G. Rinker, and W. H. Corcoran,
"Gas Chromatographic Determination of Small Quantities of Nitric Oxide and Nitrogen Dioxide in Nitrogen: Preliminary Studies." Unpublished Manuscript No. 5213, Chemical Engineering Department, California Institute of Technology. (August, 1963).

TABLE I

Conditioning for Nitric Oxide Separations
for Column A

Number of intervening 2.8 cc samples of conditioning materials	Ratio of elution curve peak-times for NO to that for N_2 from 2.8 cc samples of 0.5% NO in N_2
Drying for two days	
none	1 (i.e. not detectible)
1 of NO	1
1 of NO	1
1 of NO	1 (10 samples)
1 of NO	1 (11 samples)
1 of NO	1.43
	1.45
	1.49
	1.52
Additional drying for two days	
none	1 (2 samples)
1 of NO	1 (6 samples)
1 of NO	1.47
1 of NO	1.49
1 of NO	1.50
Additional drying for one day	
none	1
1 of NO	1.47
1 of NO	1.59
1 of NO	1.63 (2 samples)
	1.69 (2 samples)
1 of NO	1.73
1 of NO	1.75
1 of NO	
1 of NO + air	2.13
	2.11
	1.91
	2.2 to 2.3 (7 samples)

TABLE II

Conditioning for Nitric Oxide Separations
for Column B

Number of intervening 2.8 cc samples of conditioning materials	Ratio of elution curve peak-times for NO to that for N_2 from 2.8 cc samples of 0.5% NO in N_2
Drying for two days	
none	1 (i.e. not detectible)
1 of NO	1
1 of NO	1
1 of NO	1
1 of NO + air	1.56
	1.73
(3.7 ml) of NO + air	1.82
	1.85
1 of NO	2.0 to 2.3 (10 samples)
1 of NO	2.41
1 of NO	2.5 (3 samples)
1 of NO	2.60
1 of NO	2.70
1 of NO	2.8 (5 samples)
Miscellaneous samples of 0.25% or 0.1% NO in N_2 which checked the reproducibility of the NO separations	
14 of "dry" air	2.7 (3 samples)
1 of NO_2	3.24
	3.26
1 of NO_2	3.49
4 of NO_2	4.24 } about twice the amount
	4.65 } of NO was eluted rela-
	4.73 } tive to that introduced.

TABLE III

Conditioning for Nitric Oxide Separations

for Column C

Number of intervening 2.8 cc samples of conditioning materials	Ratio of elution curve peak-times for NO to that for N_2 from 2.8 cc samples of 0.5% NO in N_2
	Drying for two days
1 of NO_2	1.72
1 of NO_2	1.85
1 of NO_2	2.16
	2.16

PROPOSITION II

It is proposed that some separation of nitrogen dioxide, NO_2, and carbon dioxide, CO_2, by a silica gel chromatography column may result from their reversible association with the small quantities of water absorbed on the silica gel. It is believed that this hypothesis is worthy of experimental investigation.

A. Discussion

The chromatrographic procedures and apparatus of interest to this discussion were presented with Proposition One. This information will not be repeated here. In the previous presentation (1, 2) of this work by the author, reference has been made to an unidentified "third" elution curve. The first elution curve contains the inert materials, such as nitrogen and oxygen, which pass directly through the column. The second elution curve contains the nitric oxide, NO. Morrison (3) has since shown that the nitrogen dioxide separated by chemical and physical adsorption is eluted with the nitric oxide in this second peak. In addition the author noted a single-or double-peaked third elution curve.

For the conditions specified in Proposition I,the orders of magnitude of the times elapsed for the peaks of these curves since the introduction of the sample are: 1) first peak at 105 seconds; 2) second peak at 130 seconds for pure nitric oxide and at 280 to 340 seconds for smaller concentrations of nitric oxide, increasing with decreasing concentration; and 3) the third peak near 500 seconds

or near 550 seconds for "dry" air. The percentage of the total area contained in the third elution curves, each with a fractional deviation of about ± 0.01, were: 0.89 area per cent for the pure nitric oxide samples, 0.016 area per cent for the 0.5 per cent nitric oxide samples, 0.013 area per cent for the 0.25 per cent nitric oxide samples, none detectible for the 0.1 per cent nitric oxide samples, and 0.051 area per cent for the "dry" air samples.

These third elution curves are assumed to be due to nitrogen dioxide in the nitric oxide samples, or carbon dioxide in the "dry" air samples. The separation of these materials to produce this curve is proposed to result from their reversible association with the water adsorbed on the silica gel packing. Therefore, a mechanism for such a separation process is developed.

It is believed that water is very strongly adsorbed on silica gel, so strongly that even a drying period of a day or two at 200° C is probably not sufficient to completely dry the column. In addition some moisture would be added to the column in the air purged from the lines after connecting the sample tube. Therefore, the possible presence of water is a reality, and it only remains to show that this water can aid in the elution.

The resonance structures for carbon dioxide may be represented as follows:

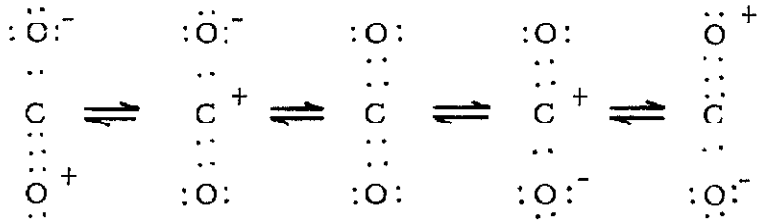

(1)

Similarly, half of the resonance structures for nitrogen dioxide may be written as follows:

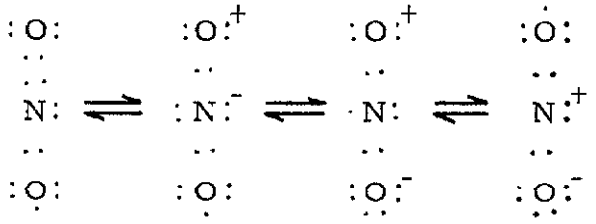

(2)

The other half of these nitrogen dioxide resonance structures are obtained by interchanging the positions of the oxygen atoms. Since nitrogen dioxide is in practically instantaneous equilibrium with nitrogen tetroxide, the latter must also be considered. Its possible resonance structures are the following:

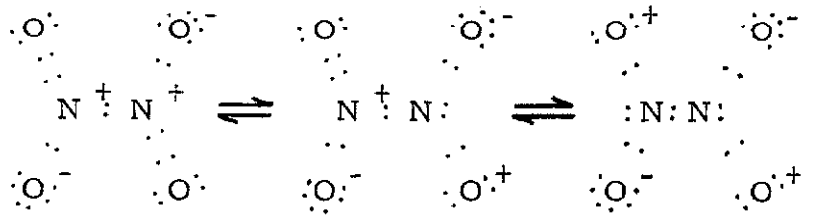

(3)

It is realized that all these resonance structures undoubtedly do not contribute equally to the character of the particular molecule. They are useful, however, when looking for possible reactive properties.

One striking similarity between these structures is the negatively charged oxygen end. This could possibly associate with the silica gel, and should be investigated. The purpose of this discussion, however, is to look for the possibility of association with water. This oxygen end could easily be associated with the water by hydrogen bonding. Furthermore, the central atom of structures 1 and 2 can be positively charged and surrounded by only six electrons. This would allow the formation of a second bond with water.

The following representation indicates the resonance structures which are reactive in this manner:

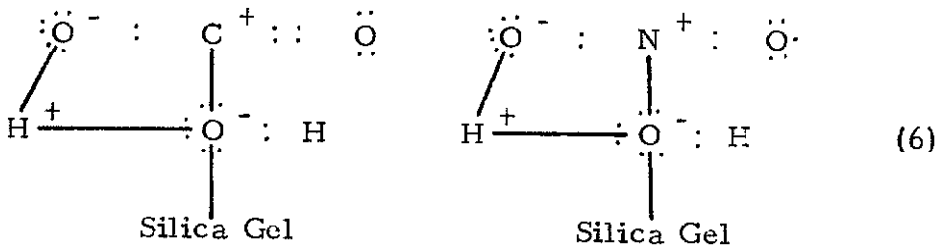

(6)

The solid lines in the above structures indicate the additional associations and bond formations possible from this configuration.

A reaction of nitrogen tetroxide and water would require the breaking of a bond within the molecule. This does not seem as probable as the associations indicated above.

In conclusion, the hypothesis has been proposed that carbon dioxide and nitrogen dioxide are separated by association with the water adsorbed on the silica gel. As an argument the high probability of the presence of adsorbed water was shown, and theoretical adsorbed

structures were proposed. The unidentified third elution curve which has been observed could easily be the result of this proposed separation mechanism. Further experimental work may provide additional insight regarding this process.

B. References

1. Cuffel, Robert F.,
"The Chromatographic Analysis of the N_2-NO-NO_2 System." Unpublished Student Report No. 874, Chemical Engineering Department, California Institute of Technology. (May 27, 1960).

2. Cuffel, Robert F.,
"Part II. Gas Chromatography Separation of NO and NO_2 from N_2." Unpublished Student Report No. 908, Chemical Engineering Department, California Institute of Technology. (March 1, 1961).

3. Morrison, Milton Edward,
"Part I. The Chromatographic Analysis of the N_2-NO-NO_2 System." Unpublished Student Report No. 965, Chemical Engineering Department, California Institute of Technology. (May 25, 1962).

PROPOSITION III

It is proposed that in their analysis of longitudinal diffusion in a catalyst bed Hougen and Watson (1) assumed the simple case of $\delta = 0$ in which the total number of moles is constant rather than the more general case for variable δ. Furthermore, to determine the necessity to consider longitudinal diffusion they improperly compare the maximum diffusional flux of component A with the change in the flux from gross motion within an initial reactor increment rather than the relative magnitudes of the fluxes.

A. Discussion

The simple case of $\delta = 0$ was probably assumed in order to eliminate the non-linear terms. This should either have been stated, or the complexities of the more general case developed. The equations resulting from the general case will be shown.

As written, the criterion for the necessity to consider longitudinal diffusion is a function of the size of the initial increment chosen. This inconsistency arises from the error noted. This can be corrected by comparing the maximum diffusional flux of component A with the flux of A from the initial gross motion, Fn_{Ao}. This improved procedure will be described after the corrected equations have been developed.

The analysis is based on the isothermal, isobaric, plug flow of ideal gases through a catalyst bed. Resistances to diffusion to and from the catalyst surfaces are neglected, and the general

reaction, $aA + bB \rightleftarrows rR + sS$, takes place at the surface of the catalyst. The nomenclature used is defined in Section C.

Under the conditions described, the material balance for component A in an element of unit cross-sectional area and differential length, dZ, at steady state is given as follows:

Net flow of A into the element =

$$Fn_A - \frac{D_{Am}\pi^2}{RT(\pi + \delta p_A)} \frac{d\left(\frac{n_A}{n_T}\right)}{dZ} = Fn_A - \frac{D_{Am}\pi}{RT\left(1 + \frac{\delta n_A}{n_T}\right)} \frac{d\left(\frac{n_A}{n_T}\right)}{dZ} \qquad \text{(XX-74')}$$

Net flow of A out of element =

$$F\left(n_A - \frac{dn_A}{dZ}\,dZ\right) - \frac{D_{Am}\pi^2}{RT}\left\{\frac{1}{\pi + \delta p_A}\frac{d\left(\frac{n_A}{n_T}\right)}{dZ} + \frac{d}{dZ}\left[\frac{1}{\pi + \delta p_A}\frac{d\left(\frac{n_A}{n_T}\right)}{dZ}\right]dZ\right\}$$

$$= F\left(n_A + \frac{dn_A}{dZ}\,dZ\right) - \frac{D_{Am}\pi}{RT}\left\{\frac{1}{1 + \frac{\delta n_A}{n_T}}\frac{d\left(\frac{n_A}{n_T}\right)}{dZ} + \frac{d}{dZ}\left[\frac{1}{1 + \frac{\delta n_A}{n_T}}\frac{d\left(\frac{n_A}{n_T}\right)}{dZ}\right]dZ\right\} \qquad \text{(XX-75')}$$

Noting that the reaction creates a sink and the accumulation is zero, the combined material balance equation follows:

$$- F\,dn_A + \frac{D_{Am}\pi}{RT}\ \frac{d}{dZ}\left[\frac{1}{1+\frac{\delta n_A}{n_T}}\ \frac{d\left(\frac{n_A}{n_T}\right)}{dZ}\right] dZ = r_A \rho_B\, dZ \qquad \text{(XX-76')}$$

The following equation is obtained by expanding Equation XX-76' to more clearly show the complexities involved:

$$- F\,dn_A + \frac{D_{Am}\pi}{RTn_T}\left[\frac{d^2 n_A}{dZ^2} + \frac{\delta n_A (1+n_T)}{n_T(1+\delta n_A)}\left(\frac{dn_A}{dZ}\right)^2\right] dZ$$

$$= r_A \rho_B\, dZ \qquad \text{(XX-76")}$$

Under the same conditions, the material balance for component A from a section before the inlet of the reactor, which is upstream from all diffusional effects, to any section Z within the reactor is given as follows:

$$Fn_A - \frac{D_{Am}\pi}{RT\left(1+\frac{\delta n_A}{n_T}\right)}\ \frac{d\left(\frac{n_A}{n_T}\right)}{dZ} = Fn_{Ao} - \int_0^Z r_A \rho_B\, dZ \qquad \text{(XX-73')}$$

The method stated below is proposed to replace that developed by Hougen and Watson to determine the necessity to consider longitudinal diffusion. Equation XX-73' is approximated as follows for a small increment at the inlet of the reactor in which the longitudinal diffusion has been neglected:

$$\frac{\Delta n_A}{\Delta Z} = - \frac{r_A \rho_B}{F} \qquad \text{(XX-77')}$$

The initial concentration gradient is then approximated by the ratio of Δn_A to ΔZ obtained from Equation XX-77'. Then the relative magnitudes of the first two terms in Equation XX-73' are compared for the inlet region of the reactor to determine the necessity to consider longitudinal diffusion.

B. Reference

1. Hougen, Olaf A. and Kenneth M. Watson, Chemical Process Principles, Part Three, Kinetics and Catalysis. New York: John Wiley and Sons. Equations XX-73 to XX-77, pp. 1003-1005. (1947).

C. Nomenclature

d	Differential operator.
D_{Am}	Mean Maxwell diffusion coefficient, sq ft/sec.
F	Feed rate, (lb-mass of feed)/(sec, sq ft).
n_A	Moles of A per unit mass of feed at section Z, (lb-moles of A)/(lb-mass of feed).
n_{Ao}	n_A at the inlet, (lb-moles of A in feed)/(lb-mass of feed).
n_T	Total number of moles per unit mass of feed at section Z, (lb-moles total)/(lb-mass of feed).
p_A	Partial pressure of A = $\pi n_A/n_T$, atm.
r_A	Rate of reaction of A, (lb-moles of A reacted)/(lb-mass of catalyst, sec).
R	Natural gas constant, (cu ft, atm)/(lb-mole, ^oR).

T	Absolute temperature, $^{\circ}R$.
Z	Distance from the inlet of the reactor, ft.
π	Total pressure, atm.
δ	$(r + s - a - b)/a$ for the reaction $aA + bB \rightleftharpoons rR + sS$.
Δ	Change over a finite increment of length.

PROPOSITION IV

It is proposed that a platinum resistance glass tube thermometer is not an adequate temperature measuring device for an air stream if exposed to surroundings which are not maintained at about the temperature of the air stream being measured. The air temperature measurement can be substantially improved by mounting a gold foil radiation shield over the glass tube of the resistance thermometer.

A. Discussion

During the experimental investigations presented in Part II of this thesis, it was noted that the normal platinum resistance thermometer did not indicate the same air stream temperature when held above the jet opening as it did when placed in the air stream flowing within the ducts below the jet opening. This was subsequently shown to be a function of the radiant energy loss to the surroundings. This effect was no longer noticeable after a gold foil radiation shield was mounted over the glass tube around the sensing end of the thermometer. A simplified energy balance is presented for each of these two situations to show the effect of the radiation.

The resistance thermometer consisted of a two-inch-long coil of platinum wire as the sensing element, mounted in the end of a one-foot-long, three-eights-inch-diameter glass tube filled with an inert atmosphere of helium. It is reasonable to assume that the conduction through the glass and helium maintained the platinum

sensing element at the temperature of the glass tube. Therefore, a steady state energy balance for the thermometer would equate the heat loss by radiation with the heat input by convection to the surface of the glass tube. Therefore, if the effects of the hemispherical end of the glass tube are neglected, the energy balance for the glass thermometer tube may be approximated to that for an infinitely long cylinder.

The air flow was normal to the thermometer. For the normal flow of gases past cylinders at Reynolds numbers greater than 44, Collis and Williams (1) present the following correlation for the Nusselt number:

$$Nu_m \left(\frac{T_m}{T_\infty} \right)^{-0.17} = 0.48 \, (Re_m)^{0.51} \qquad (1)$$

The 7.81-foot-per-second, 100° F air stream from the jet opening past the three-eighth-inch-diameter thermometer tube could be characterized by a Reynolds number of 1712.5. Assuming that the thermometer temperature will be maintained sufficiently close to the air stream temperature so that the temperature correction and adjustment of the fluid properties to a mean temperature will not be necessary for the use of Equation 1, a Nusselt number for the thermometer tube of 18.68 is obtained.

The steady state energy balance between the convection to and the radiation from a unit length of an infinitely long cylinder follows:

$$Nu_m k_a (T_\infty - T_t) = \epsilon_t b d_t (T_t^4 - T_s^4) \qquad (2)$$

For Equation 2, the air thermal conductivity, k_a, at 100° F was evaluated as 4.049×10^{-6} Btu-per-foot-per-second-per-degree-Fahrenheit, and the temperature of the surroundings, T_s, at 544.69° R (85° F).

For the glass tube with an emissivity, ϵ_t, of 0.937 (2), the temperature of the glass tube from Equation 2 is 98.34° F. This measurement error of 1.66° F results from the radiation loss to surroundings only 15° F below the air stream temperature.

If a gold foil with an emissivity, ϵ_t, of 0.02 (3) covers the glass tube, the temperature of the tube from Equation 2 is 99.96° F. This is only 0.04° F below the air stream temperature.

When the temperature of the surroundings is maintained at the air stream temperature, there is no longer a driving force to lower the thermometer temperature, and it will be at that of the air stream.

It has been shown that a sizable error in the measurement of the air stream temperature resulted from radiation losses from the unshielded resistance thermometer glass tube. A calculated correction would be difficult for such a case due to the difficulty in assessing an effective temperature for the surroundings. The addition of a gold foil radiation shield over the glass tube of the thermometer has been shown to be one method of reducing the error to an acceptable level.

B. References

1. Collis, D. C. and M. J. Williams, "Two-Dimensional Convection from Heated Wires at Low Reynolds Numbers," Journal of Fluid Mechanics. Vol. 6-III, pp. 357-384. (1959).

2. Perry, John H., editor, Chemical Engineers' Handbook. 3rd ed. New York: McGraw-Hill Book Company, Inc., pp. 484-485. (1950).

3. Hodgman, C. D., R. C. Weast, and S. M. Selby, editors, Handbook of Chemistry and Physics. 37th ed. Cleveland, Ohio: Chemical Rubber Publishing Co., p. 2700. (1955).

C. Nomenclature

b — Stefan-Boltzmann constant = 0.173×10^{-8} Btu/(sq ft, hr, $^{o}R^{4}$).

d_t — Outside diameter of the thermometer tube, ft.

h — Heat transfer coefficient from the outside thermometer surface by convection and conduction to the air stream, Btu/(sq ft, hr, ^{o}F).

k_a — Thermal conductivity of the air, Btu/(ft, hr, ^{o}F).

Nu_m — Nusselt number for the thermometer cylinder in the air stream based on the fluid properties evaluated at the mean film temperature = hd_c/k_a, dimensionless.

Re_m — Reynolds number for the air flow around the thermometer cylinder based on the fluid properties evaluated at the mean film temperature = $d_c U_\infty/\nu$, dimensionless.

T_m — Mean absolute temperature for the air film about the thermometer cylinder, ^{o}F.

T_s — Absolute temperature of the surroundings radiating to the temperature, ^{o}F.

T_t — Absolute temperature of the thermometer, ^{o}R.

T_∞ — Absolute temperature of the air stream, ^{o}R.

U_∞ — Bulk velocity of the air stream, ft/sec.

ϵ_t Emissivity of the outside thermometer surface, dimensionless.

ν Kinematic viscosity for the air stream, sq ft/sec.

PROPOSITION V

It is proposed that the long-half-lived radioactive wastes, for which disposal is difficult, may be used as a heat source in producing oil wells to reduce the viscosity of heavy oils near the well-bore and thus increase the production of these wells.

A. Discussion

Radioactive wastes are produced as fission products in nuclear reactors. They are separated and concentrated during the processing of the fuel elements. Most of the isotopes have half-lives of less than one year, and their disposal is relatively easy. Strontium-90 and cesium-137 have half-lives of 28 years and 26.6 years, respectively. Therefore they are separated from the others and their aqueous waste solutions must be stored for more than 600 years. Such storage is also complicated during its initial stages by the transformation of the radioactivity released into heat. This has prevented their being stored in abandoned oil wells.

It is therefore proposed that these wastes be injected into producing oil wells where the heat source can be useful. The aqueous waste solution would be injected into the oil sands around the producing wells and followed by a water pusher. The clay in these sands produces some cation exchange action so that the isotope front will lag behind the water front. A good share of the isotopes will be eluted off the clays in the back flush of the injection water. More will be eluted when breakthrough occurs if a water flood is being used.

Nevertheless, some isotopes are fixed onto the clays and cannot be removed. These are sufficient to form a significant heat source around the producing well bore. The oil flowing through this section is therefore heated. The hotter oil has less resistance to flow in this critical section of the oil well. Therefore the flow rate is increased.

There are many points which must be considered in such an operation. One of these is the possibility of contaminating ground water and thus introducing the isotopes into the human life cycle. Since the oil remains trapped in the sands, however, one may assume that it has little contact with the ground water. The well bores, however, do provide contact with the ground water and adequate casings would be required.

The elution of the isotopes is another problem. The returned injection water would probably be concentrated and the solution used for another oil well. The contaminated breakthrough water would be re-injected via the water flood, using the exchange capacity of the reservoir for its disposal. The heat which they will produce may require the operation of the water flood beyond its normal termination, however. The amount and shielding of the above ground processing equipment will mainly affect the economics of the process. Also the problem, if any, with the elution of the isotopes in the oil must be investigated.

Thus a useful method for the disposal of the radioactive wastes with long half-lives has been proposed. If the process can

be developed to meet the safety requirements of the Atomic Energy Commission, the economics of the process would govern its use.